SURFACE EFFECTS ON CLEAN AND CONTAMINATED ZINC OXIDE $(000\bar{1})$ FOLLOWING THE ADSORPTION OF HYDROGEN SULPHIDE AND CHLORINE

by

P.E. CHANDLER B.Sc.

A thesis presented for the degree of

Master of Philosophy

of the

University of Southampton

Department of Physics

September 1976

To My Parents

CONTENTS

ABSTRACT

FACULTY OF SCIENCE
PHYSICS

Master of Philosophy

SURFACE EFFECTS ON CLEAN AND CONTAMINATED ZINC OXIDE ($000\bar{1}$)
FOLLOWING THE ADSORPTION OF HYDROGEN SULPHIDE AND CHLORINE

by Peter Edmond Chandler

This thesis reports on the behaviour of zinc oxide ($000\bar{1}$) surfaces following the adsorption of hydrogen sulphide and chlorine. The state of the crystal surface was determined by Auger electron spectroscopy, low energy electron diffraction and work function measurements. All the experiments were performed under conditions of ultra high vacuum.

The adsorption of hydrogen sulphide onto the clean surface appeared to involve the dissociation of the impinging gas molecules. After saturation was achieved, electron beam dissociation of the gas enabled multi-monolayer coverages to be deposited.

The surface reactivity was greatly reduced by the presence of calcium and carbon impurities and the behaviour of the contaminated ($000\bar{1}$) surface to chlorine adsorption resembled, in some respects, that of the clean neutral prism surface of zinc oxide. The de-activation of the ($000\bar{1}$) surface to chlorine and hydrogen sulphide adsorption was attributed to at least partial charge stabilisation by calcium.

CHAPTER 1

INTRODUCTION

Surface physics is the study of the chemical composition and atomic arrangements at the surface of solids and the theory and observation of their mechanical, electronic and chemical properties. Thus, the ultimate objective of surface studies would be to establish an understanding of the relationship between the properties of surfaces and their composition and structure. Recently ($\sim$ 1960), several useful surface probes have been developed, which include Auger Electron Spectroscopy (A.E.S.), used to determine surface chemistry, and Low Energy Electron Diffraction (LEED), used to measure surface structure. Although these techniques have provided much information, their use imposes certain fundamental restrictions on the type of system used for investigation. A clean, well defined surface is necessary and experiments are best performed in conditions of ultra high vacuum (u.h.v.). These technical constraints have meant that, in general, surface physics has not yet been extended to the problems of more complex industrial situations where many technically important processes employ solid surfaces, e.g. in catalysis, semiconductor devices etc. Thus, at present, most research is limited to "simple" surfaces and the study of their interaction with highly controlled environments.

The work reported in this thesis is concerned with the adsorption of hydrogen sulphide on ZnO-$(000\bar{1})$ and with the effects of certain surface contaminants on the adsorption characteristics of both hydrogen sulphide and chlorine. A.E.S. and LEED were used as surface probes and all the experiments were performed in conditions of u.h.v.

Synopsis of the thesis:

Chapter 2 deals with the attainment of u.h.v. and with the experimental apparatus used. Chapters 3 and 4 outline, respectively, some of the theoretical and experimental aspects of the surface probes. Chapter 5 reviews some of the bulk and surface properties of zinc oxide. Chapters 6, 7 and 8 present the results obtained in the present study and discusses some pertinent results of other workers. Finally, Chapter 9 draws some conclusions from the previous three chapters and suggests further experiments and improvements.

CHAPTER 2

VACUUM TECHNOLOGY

This chapter discusses the importance of ultra high vacuum (u.h.v.) conditions in surface studies, together with the techniques and "hardware" necessary for its attainment. A description of the crystal mount is also included.

2.1 THE NEED FOR U.H.V.

For clean surface study it is essential to control the rate of re-contamination of a clean surface from the ambient gas. Clearly vacuum conditions are necessary, but it becomes apparent from a consideration of the Kinetic theory of gases that even the use of high vacuum ($\sim 10^{-7}$ torr) is insufficient. It can be shown (Dushman and Lafferty, 1962) that the number of gas molecules incident on unit surface area per unit time is given by the expression,

$$N = 3.52 \times 10^{22} \times \frac{P}{(MT)^{\frac{1}{2}}} \text{ cm}^{-2} \text{ sec}^{-1} \qquad 2.1$$

where P is the gas pressure (torr), M the molecular weight and T the temperature (K). Thus, in high vacuum (10^{-7} torr) at room temperature (300 K) with M = 28 (since the residual gas is largely CO) equation 2.1 yields an incident flux of $\sim 5 \times 10^{13}$ molecules cm^{-2} sec^{-1}. Comparing this result with the number of substrate atoms, typically 10^{15} cm^{-2}, suggests "monolayer" coverage will take place within 30 seconds (assuming a unity sticking coefficient). Hence, only pressures of $< 1 \times 10^{-9}$ torr (u.h.v.) will provide realistic ($\sim$ 1 hour) experimentation times, at room temperature. However, pressures in the low 10^{-10} torr region are normally used, not only to reduce the rate of re-contamination during an experiment

but also to enable the use of relatively low gas pressures in adsorption studies without loss in purity of the added gas due to the residual component.

Much of the present work was conducted in a torral pressure of 1×10^{-9}. This was perfectly adequate for ZnO since the sticking coefficient of CO is much less than unity (Campbell et al, 1969). Also, in the gas exposure studies relatively high pressures, between 10^{-8} and 10^{-7} torr were used so that the high purity of the added gases was maintained.

2.2 U.H.V. EQUIPMENT

The main limitation in the attainment of pressures below 10^{-8} torr, apart from leaks, is outgassing from the interior walls of the system. All substances desorb gas when placed in vacuo and the choice of materials with a low outgassing rate is therefore important in u.h.v. chamber construction. A common method for 'in situ' reduction of the outgassing rate involves a bake to $\sim$ 500 K. This thus precludes the use of plastics, rubber, greases and other such fabrics frequently used in high vacuum systems. With the above limitations in mind, u.h.v. chambers are mainly constructed from glass or stainless steel, both of which have favourable characteristics (see for comparison Hopkins, 1968). The main advantage of stainless steel is its strength, allowing much more equipment to be mounted onto the work chamber.

A commercial stainless (EN58B) steel chamber, manufactured by Varian Ltd., was used in the present study, photograph fig. 2.1. It was built in two sections, fig. 2.2, with a division between the work chamber and the pumps. The pumps could be isolated by means of a gate valve. Since the work chamber could be let up to air independently of the pumps, a fast recycling time could be achieved. The gate valve was also used during gas exposure studies to prevent excessive gas flow through the

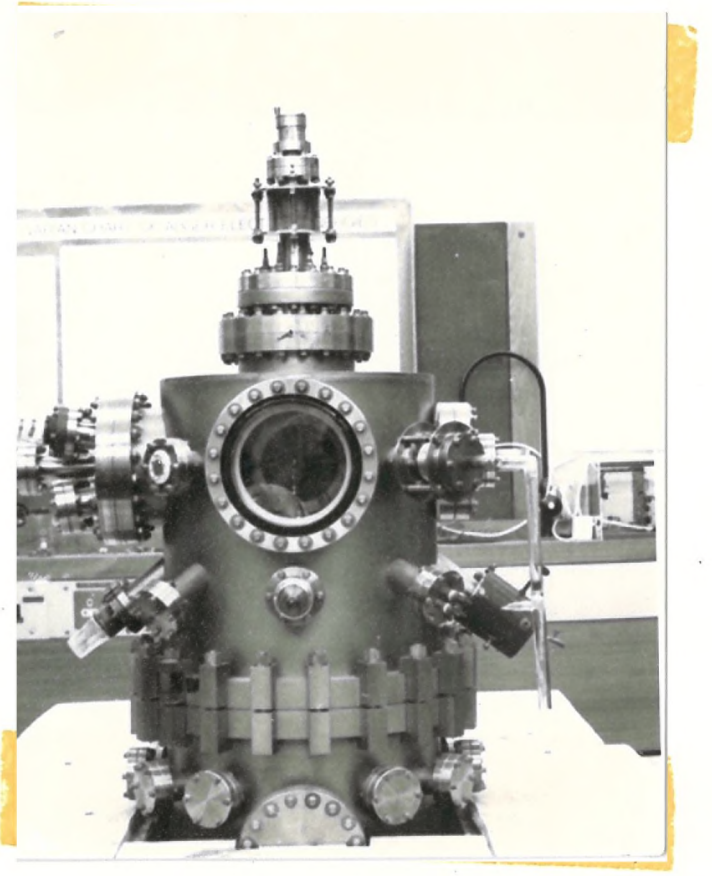

Figure 2.1 Photograph of work chamber.

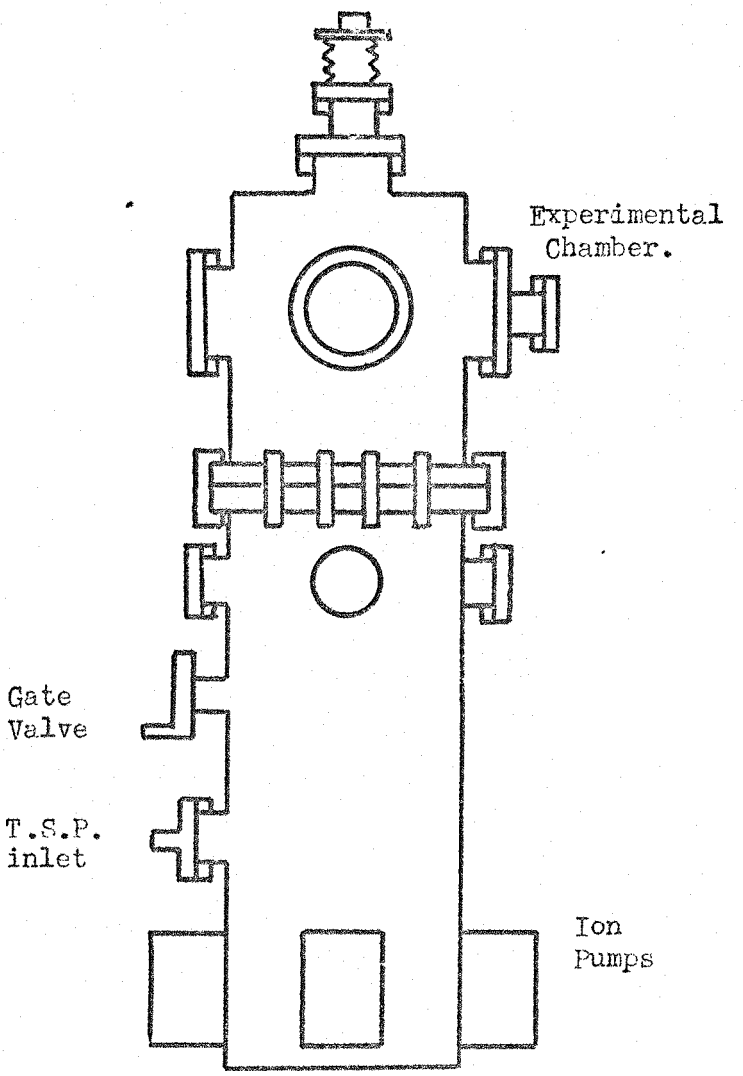

Figure 2.2 Schematic of vacuum system.

system.

Standard bolt-on "conflat" flanges were provided on the work chamber to house the necessary experimental equipment. This type of flange produces a seal by bringing together two knife edges placed either side of a ring copper gasket. A schematic of the work chamber, fig. 2.3, shows the relative positions of the components used in the present study.

2.3 THE PUMPS

Varian ion pumps, backed by a liquid nitrogen cooled sorption pump were used to obtain u.h.v. conditions. Pumping speed, at low pressures, was increased by the use of a titanium sublimation pump (t.s.p.). The sorption pump contained a zeolite molecular sieve which pumps by physical adsorption of gas molecules. Four standard Varian 30 litres s^{-1} sputter ion pumps, housed in the lower chamber, pumped by ionising the gas in a cold cathode discharge (see Redhead et al, 1968). A disadvantage associated with ion pumps is the presence of large field magnets necessary for their operation. In this system, with the use of small volume pumps and with a large separation between the pumps and the work chamber, the effects of these magnetic fields were greatly reduced. The t.s.p. pumps by the deposition of titanium onto the chamber walls. Here the titanium forms stable compounds with active elements and"buries" inert ones.

Pressure measurement was made with a commercial Bayard-Alpert gauge, which had a quoted X-ray limit of 5×10^{-11}torr. Partial pressures of the component gases were determined using an E.A.I. Quadrupole 250 gas analyser.

2.4 ATTAINMENT OF U.H.V.

To prevent unnecessary outgassing care was taken to ensure the cleanliness of all internal assemblies. Tungsten components were chemically

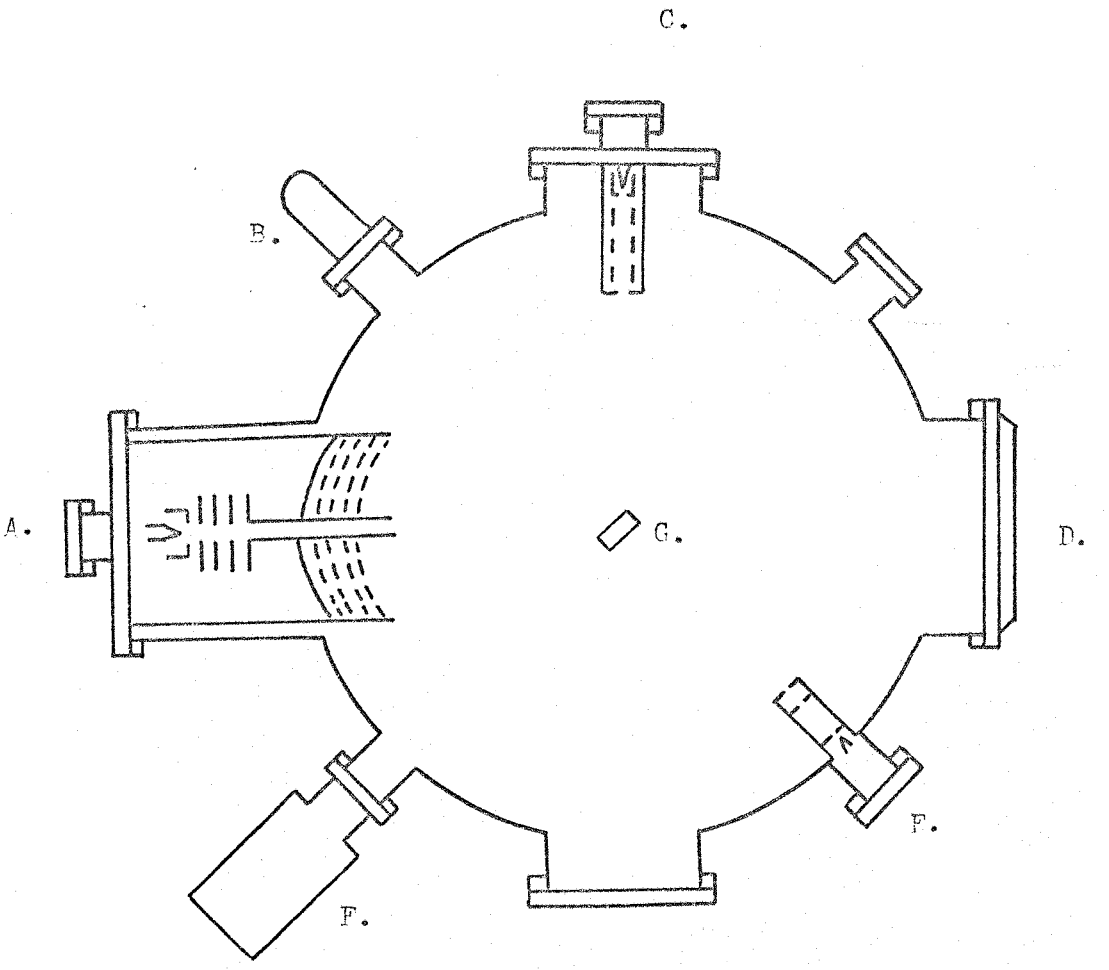

A: LEED OPTICS.

B: LEAK VALVE.

C: AUGER ELECTRON GUN.

D: VIEWING PORT.

E: ARGON ION GUN.

F: MASS SPECTROMETER.

G: SPECIMEN.

Figure 2.3 Schematic of work chamber.

etched in sodium hydroxide solution and thoroughly washed in distilled water. Ultrasonic cleaning in research grade isopropyl alcohol was used for other materials. Prior to installation, hand contaminated parts were wiped with a lint free cloth soaked in acetone, to remove finger grease etc.

When construction was complete, the system was opened to the vacsorb pump. Cycling of this pump, by re-baking and liquid nitrogen cooling, was necessary before the ion pumps could be started. Once the ion pumps were in operation, the pressure quickly fell to the 10^{-7} torr range. At this stage leak testing was carried out. The ionisation gauge was used to monitor the effect of acetone painted around all newly fitted flanges. All filaments were then tested and given a preliminary outgas. The system would now be baked for $\sim$ 48 hours, the upper chamber kept at a slightly higher temperature to produce a thermal gradient into the pumps, situated in the lower section. On cooling,this procedure results in a pressure drop to the mid 10^{-10} torr range and after filament outgassing a further decrease to the low 10^{-10} torr range. In the present study a complete bake was not possible because two zinc evaporators had been mounted in the upper chamber. Instead, only the lower pump section was baked, to $\sim$ 500 K for $\sim$ 48 hours. On cooling and with the use of the t.s.p., the pressure fell to the low 10^{-9} torr range and ultimately, after filament outgassing, was $< 1 \times 10^{-9}$ torr.

2.5 CRYSTAL MOUNT AND MANIPULATION

Bearing in mind the criteria for the choice of materials used in construction, the crystal mount was built from tungsten and molybdenum. An all metal structure was chosen to prevent charge build-up from incident electron beams. The mount, fig. 2.4, consisted of a tungsten heater filament sprung around the crystal and coiled onto two tungsten support rods.

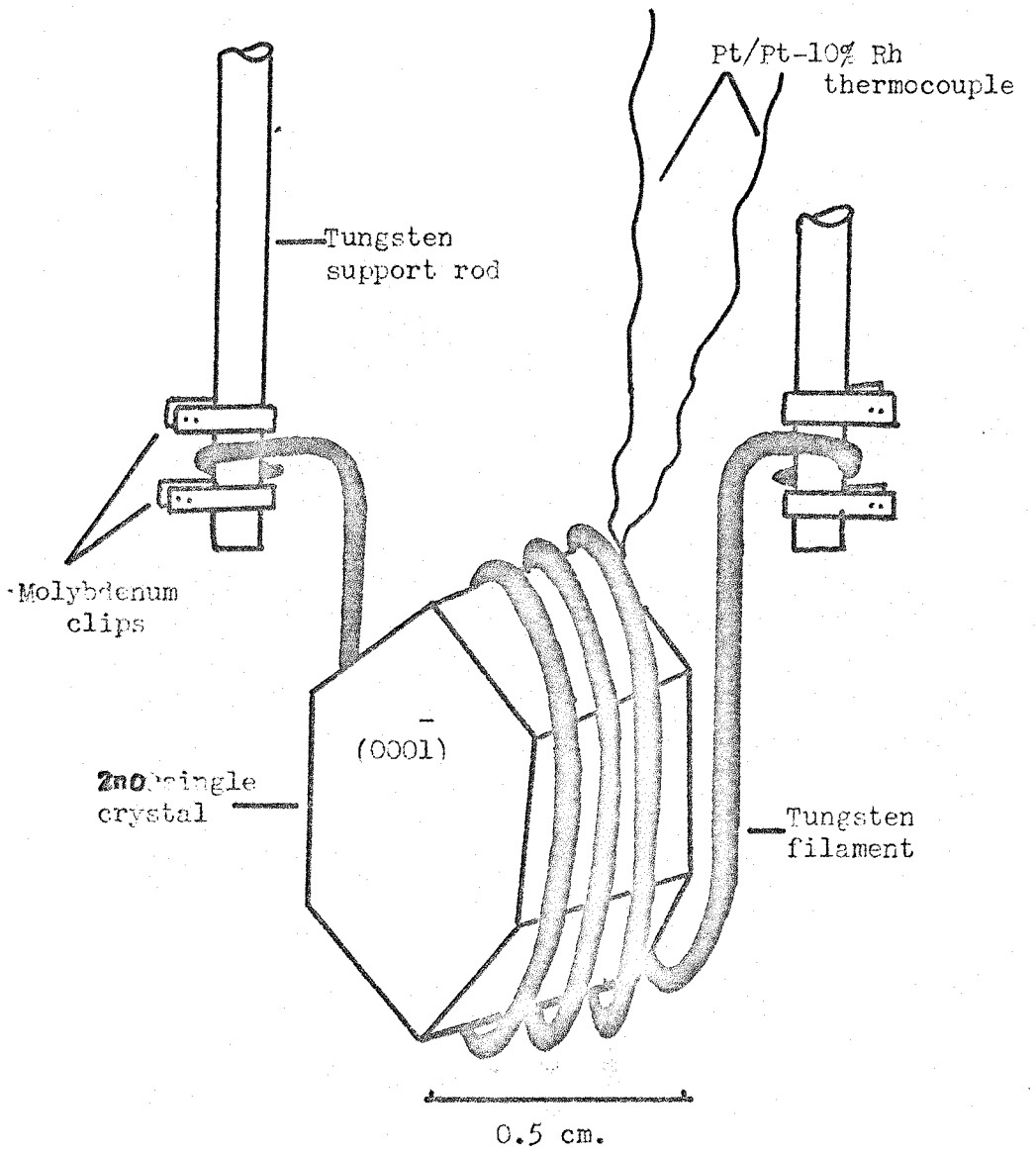

Figure 2.4 Schematic of crystal mount.

Molybdenum clips, spot welded onto the supports, kept the filament in place. An A.C. current was used to heat the filament which then heated the crystal by conduction. While direct resistive heating of the crystal would have been more even, its small size made it difficult to make the necessary connections. A Pt/Pt-10% Rh thermocouple was wedged between the filament and the crystal. Since this could not give the $(000\bar{1})$ surface temperature, see fig. 2.4, temperature readings taken during the course of this work were later compared to measurements made with a second thermocouple sprung onto the $(000\bar{1})$ surface.

The crystal mount was fixed to a two dimensional manipulator fitted with electrical feedthroughs. Flexible bellows (Palatine Precision Ltd.) were used to control the vertical position of the crystal and by tilting the bellows, movement in the horizontal plane was accomplished. A wobble drive (Torvac Ltd.) gave rotation of the crystal through 360^{o}.

2.6 GAS HANDLING

The high purity research grade argon, used for sample cleaning, was supplied in a 1 litre pyrex flask by British Oxygen Co. Ltd. This was attached via a glass to metal seal to a Varian leak valve (Model 951-5100), which was bolted onto the main chamber. The intermediate glass gas line was roughed out using a water cooled oil diffusion pump. At a pressure of $\sim 10^{-6}$ torr the pump was removed and the gas line was finally pumped through the chamber to $\sim 10^{-9}$ torr. At this pressure the "pigstail" seal on the argon bottle was broken using external magnetic manipulation of an iron slug.

The chamber incorporated a second gas line to handle the gases used in adsorption studies. However, only one gas could be used at a time and this limitation should be removed in future work. The gases used were chlorine and hydrogen sulphide. The high purity research grade chlorine was

supplied by Cambrian Chemicals Ltd., again in a 1 litre pyrex flask. The hydrogen sulphide was suppled by British Drug Houses Ltd. in a pressurised stainless steel "lecture bottle" and the high pressure made it impracticable to connect this directly to the system. The gas was therefore transferred to pyrex glass ampoules in a separate glass vacuum chamber, fig. 2.5. Two 80 ℓs^{-1}, liquid nitrogen trapped mercury diffusion pumps, backed by a rotary pump, evacuated this sytem. The pumps were isolated from the ampoules by a stainless steel valve. To eliminate displacement effects from the ampoule walls, which had previously been flamed to remove water vapour, the system was flushed several times with 900 torr of H_2S. The H_2S pressure was given by an A.E.I. diaphragm gauge. With an ampoule pressure of 2×10^{-7} torr, measured by a Bayard-Alpert gauge, 500 torr of H_2S was admitted into the system and the ampoules were then sealed. The ionisation gauge was switched off before H_2S admission to avoid dissociation of the gas. The glass ampoules were then transferred to the U.H.V. gas inlet.

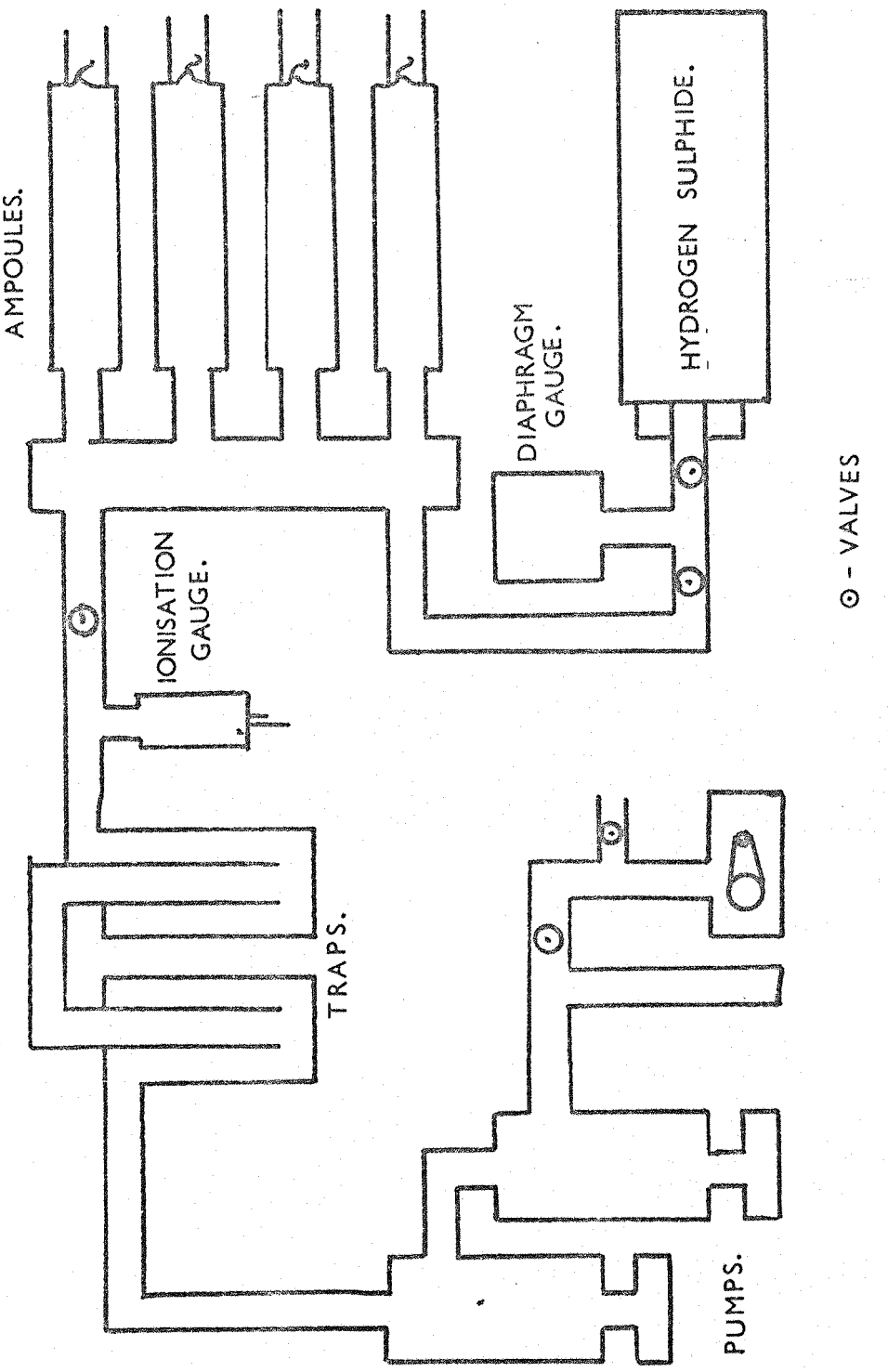

Figure 2.5 Schematic of apparatus used for transfer of H_2S.

CHAPTER 3

SURFACE PROBES - THEORETICAL

This chapter discusses some of the theoretical aspects of the experimental techniques used in the present study for the determination of surface chemistry and structure. A method used for continuous measurement of work function is also reviewed.

3.1 INTRODUCTION

All the techniques used in this work employed a monoenergetic electron beam as the surface sensitive probe. The interaction of this primary beam of electrons with a solid surface results in a secondary electron energy distribution of the form shown in fig. 3.1. The curve may be divided into three distinct regions.

Region I, consists of the true secondary electrons which, as a result of multiple inelastic collisions in the bulk, have lost most of their energy.

Region II, is a further region of inelastic secondaries and exhibits a slowly varying background on which is superimposed a series of peaks. Some of these are characteristic loss peaks due to the excitation of bulk or surface plasmons or interband transitions (Page, 1973). Others, fixed in energy, are characteristic of the surface constituents and are known as Auger electrons (Auger, 1925).

Region III, is a sharp, well defined peak which occurs at the primary energy, E_p. These are the elastically scattered electrons which produce the diffraction features in LEED.

3.2.1. AUGER ELECTRON SPECTROSCOPY (A.E.S.)

The emission of a $KL_1\ L_{23}$ Auger electron from an oxygen atom

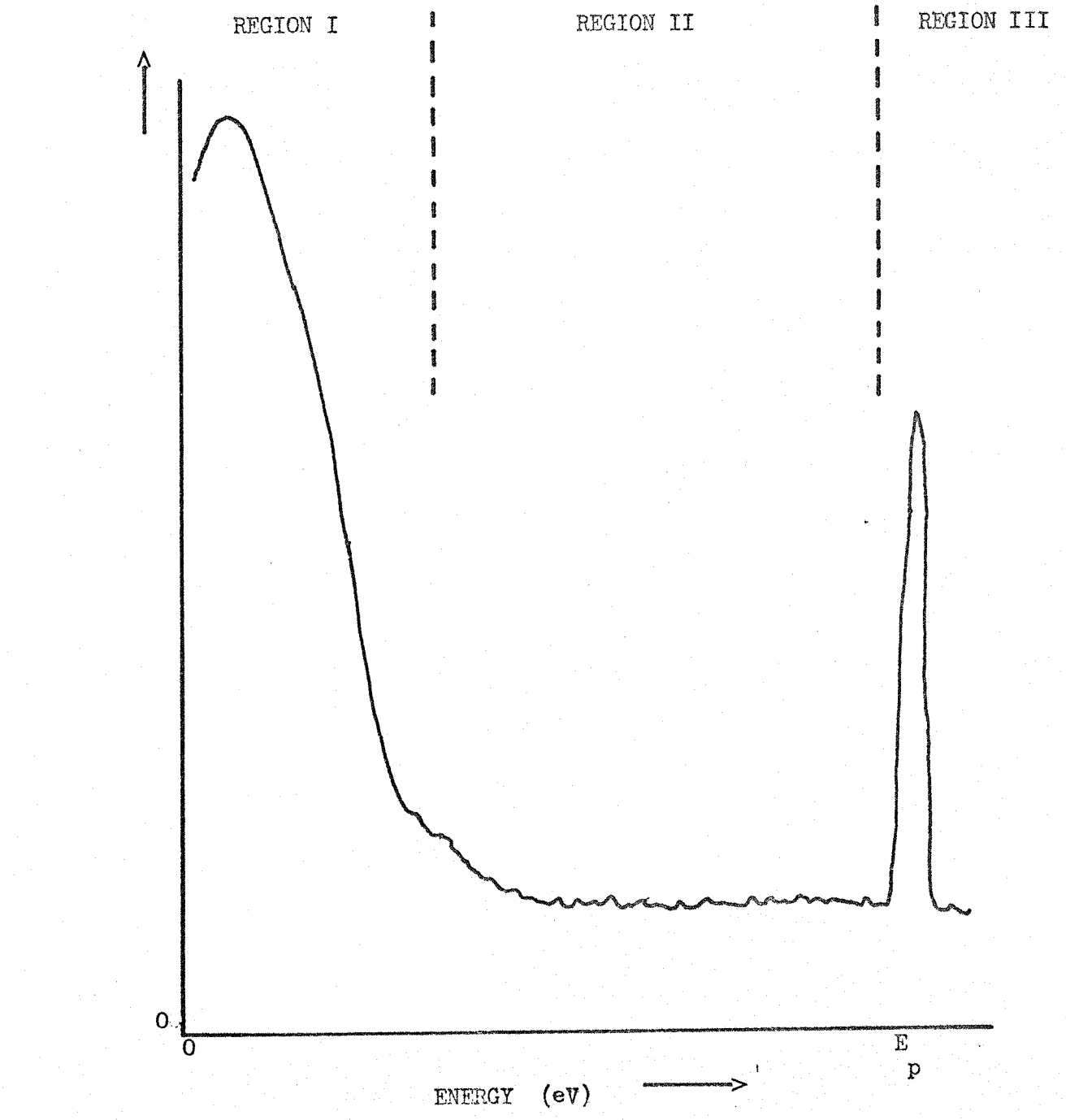

Figure 3.1 The secondary electron energy spectrum.

is shown schematically in fig. 3.2. Initially, the atom is ionised by an incident primary electron and the vacancy produced (in the K shell) is filled from a less tightly bound shell (in this case from level L_1). The excess energy ($E_K - E_{L_1}$) may then appear as a photon or alternatively may be given to another electron which is subsequently ejected from the atom as an Auger electron. The kinetic energy of the Auger electron shown in fig. 3.2 is thus given by:

$$E = E_K - E_{L_1} - E_{L_{23}} \qquad 3.1$$

and can be seen to be equal to 501 eV. Two other transitions which are immediately obvious from fig. 3.2 are $KL_1\ L_1$ (484 eV) and $KL_{23}\ KL_{23}$ (518 eV). These three transitions account for the triplet-like appearance of oxygen in A.E. spectra (see for example fig. 6.4).

Although oxygen has particular significance in the present study, all elements, except hydrogen and helium, have at least one possible Auger transition. A comprehensive chart of the theoretically possible transitions and those observed experimentally has been compiled by Varian Associates Ltd..

3.2.2 Production of A.E. Spectra

Auger transitions occur as small peaks in region II of the secondary electron distribution curve of fig. 3.1. The current associated with any transition is typically only about 2×10^{-11} amp (Rivière, 1968) and thus an extremely sensitive electronic detection system is required. The current collected is given by the expression,

$$I = \int_{E_1}^{E_p} N(E)\,dE \qquad 3.2$$

where the lower limit, E_1, is set by the experimental system E_p is the energy

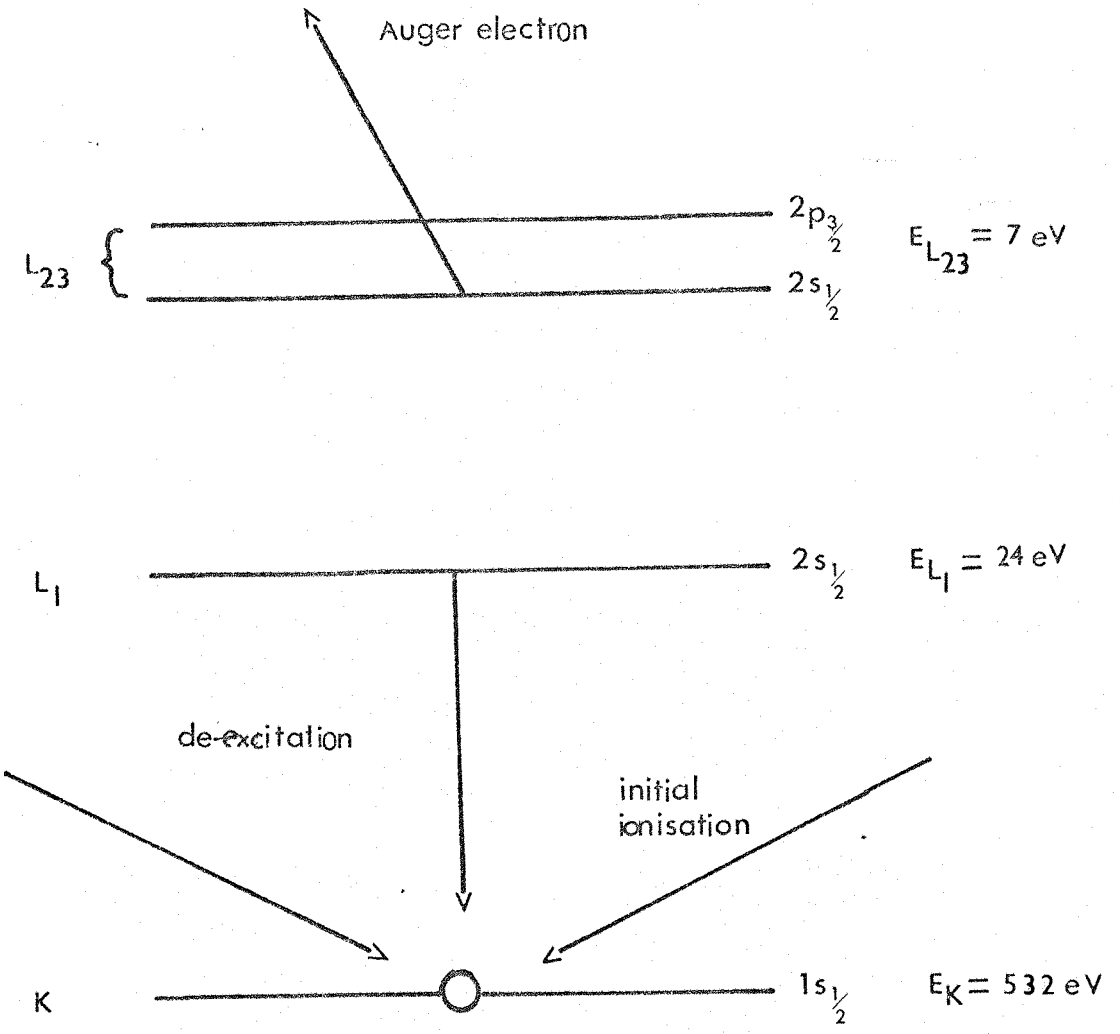

Figure 3.2 The oxygen electronic shell configuration indicating the KL_1L_{23} Auger transition.

of the primary electron beam and N(E) is the number of electrons collected of energy E. It can be seen, from equation 3.2, that the number of electrons may be obtained by differentiation of the current with respect to energy and in the case of a R.F.A., used in the present study, this is affected by use of an external electronic detection system.

The external differentiation mechanism is best described by consideration of the sample and collector acting as a diode, the current-voltage characteristics of which are shown in fig. 3.3. Application of a D.C. ramp to the equipotential analyser grids permits the voltage to be swept along the x-axis. Onto this swept voltage is superimposed a small A.C. modulation of the form $V = K \sin \omega t$. The frequency (ω) is considerably larger than the time taken for a single ramp cycle and this high frequency signal can be thought of as fixing the D.C. voltage at an arbitrary value E_1 while the A.C. oscillates between $E_1 \pm \Delta E/2$ (see fig. 3.3). The A.C. signal received at the collector is then detected synchronously with the modulation frequency. The peak to peak voltage (V_{ptp}) will be proportional to the change in current due to the modulation i.e. $V_{ptp} = I_1 - I_2 = dI$. Thus, dI/dE as a function of E is obtained. Harris, 1968, has shown that detection is greatly enchanced by a second electronic differentiation. In practice this is achieved by using a frequency of twice that of the modulation voltage to detect the collector signal. It can be shown, Chang, 1971, that,

$$I = I_o + \frac{dI}{dE} K \sin \omega t + \frac{d^2I}{dE^2} \frac{K^2}{4} \cos 2 \omega t \qquad 3.3$$

and thus d^2I/dE^2 may be obtained by the use of a filter to remove the first harmonic term (see chapter 4). As shown in fig. 3.3, the size of the signal is dependant on the modulation amplitude. However, although an increase in the signal may be affected, resolution is decreased since dE

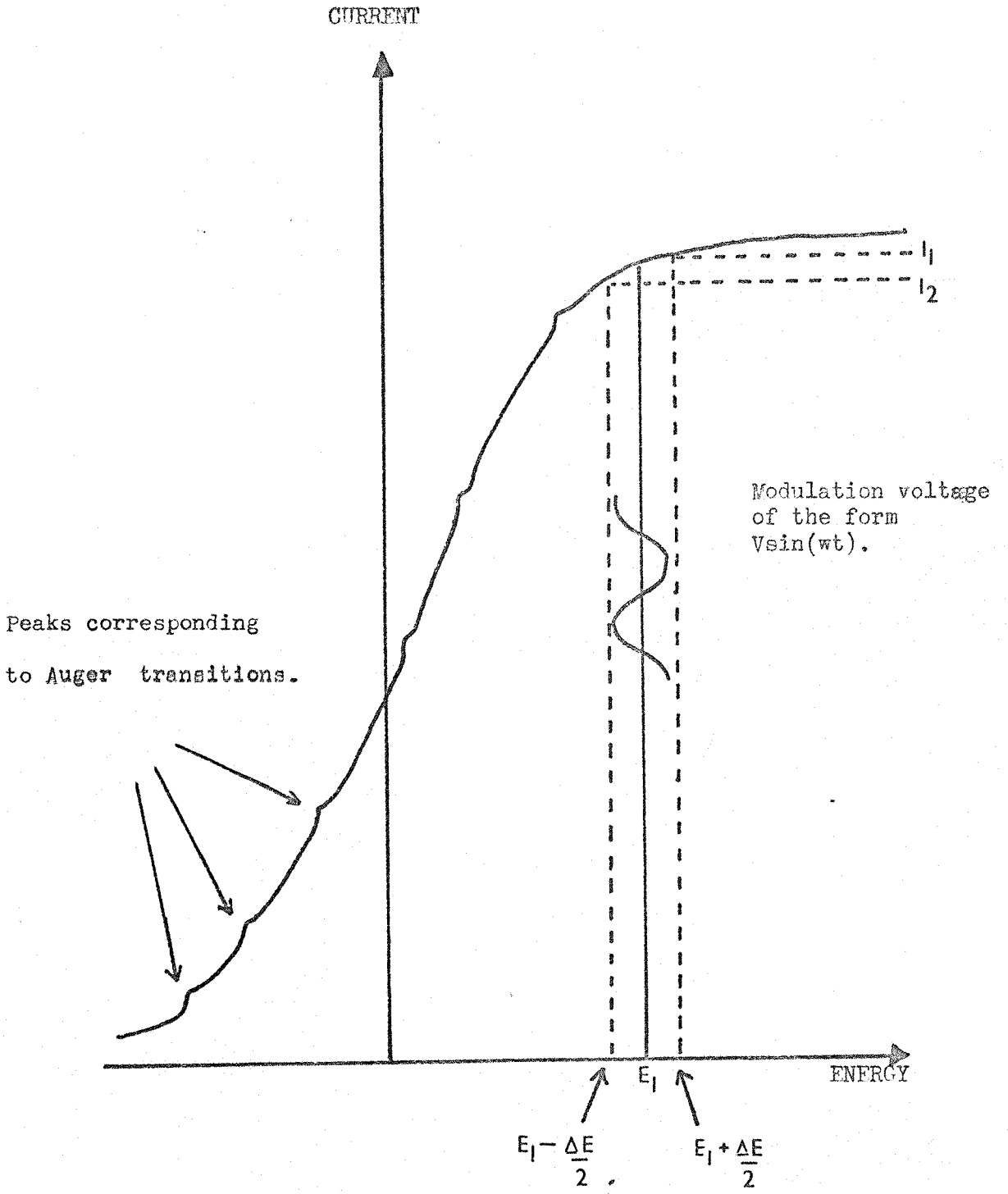

Figure 3.3 The current-energy characteristics for the Auger diode arrangement.

becomes larger. Thus in practice a compromise between resolution loss and signal gain is achieved.

3.3 LOW ENERGY ELECTRON DIFFRACTION (LEED)

Diffraction features arise from the elastically reflected electrons in region III of the secondary electron energy distribution curve, fig. 3.1.

There exist two models for the interpretation of diffraction events. One, the Kinematic theory, assumes negligible multiple scattering of the incident electron beam by the ion core potentials while the other, the Dynamical theory, makes no such a priori assumptions. A comprehensive review of this subject has recently been published (Pendry, 1974) and as such only a brief outline of the two approaches is given in the following sections.

3.3.1 Kinematic Theory

A useful concept employed in LEED analysis is that of the reciprocal lattice which is a translation of the real lattice into Fourier space. The vectors associated with the lattice in Fourier space have the dimensions of $(\text{length})^{-1}$. Vectors defining the reciprocal lattice unit cell are $\underline{a}^*$, $\underline{b}^*$ and $\underline{c}^*$ and satisfy the relations (for orthorhombic, tetragonal and cubic lattices):

$$\underline{a}^* . \underline{a} = \underline{b}^* . \underline{b} = \underline{c}^* . \underline{c} = 1 \qquad 3.4$$

$$\underline{a}^* . \underline{b} = \underline{b}^* . \underline{c} = \underline{c}^* . \underline{a}$$

$$= \underline{a}^* . \underline{c} = \ldots\ldots\ldots = 0 \qquad 3.5$$

The reciprocal lattice vector $\underline{g}_{hk\ell} = h\underline{a}^* + k\underline{b}^* + \ell\underline{c}^*$ is perpendicular to the lattice plane defined by the Miller indices $(hk\ell)$ of length:

$$|g_{hk\ell}| = \frac{1}{d_{hk\ell}} \qquad 3.6$$

where $d_{hk\ell}$ is the separation of the lattice planes in real space.

If the diffraction is considered in terms of a plane wave $\psi_o = \psi_s = \{f(\theta) \exp(2\pi i k^1 r)\}/r$, the total wave function at a distance r from the scattering centre is given by the sum $\psi_s + \psi_o$,

$$= \exp(2\pi i k r) + \{f(\theta) \exp(2\pi i k^1 r)\}/r \qquad 3.7$$

where $k = 1/\lambda$ and $f(\theta)$ is the atomic scattering amplitude. It can be shown (Hirsch et al, 1965) that $f(\theta)$ is of the form

$$f(\theta) = \frac{Me^2}{2h^2} \left(\frac{\lambda}{\sin \theta}\right)^2 (z - fx) \qquad 3.8$$

where z is the atomic number, θ is the angle of incidence and fx is the X-ray scattering factor. The term $(\lambda/\sin\theta)^2$ is a contribution from Rutherford scattering and (z-fx) is due to scattering from the electron cloud.

This approach can be extended through scattering from the unit cell up to scattering from the N such cells which make up the crystal surface. The amplitude of the wave scattered in this way is given by:

$$\phi = \sum_N F_n \exp(-2\pi i \Delta\underline{k}.\underline{r}_n) \qquad 3.9$$

where F_n is the structure factor of the n^{th} unit cell, $\underline{r}_n = n_1\underline{a} + n_2\underline{b} + n_3\underline{c}$ (n_1, n_2 and n are integers and $\underline{a}$, $\underline{b}$ and $\underline{c}$ are the primitive translation vectors of the crystal in real space) and $\Delta\underline{k}$ is the change in wave vector = $\underline{k}^1 - \underline{k}$ (see fig. 3.4).

If $\Delta\underline{k}$ is now written in terms of reciprocal lattice co-ordinates

$$\Delta\underline{k} = u\underline{a}^* + v\underline{b}^* + w\underline{c}^* \qquad 3.10$$

then

$$\Delta\underline{k}.\underline{r}_n = (u\underline{a}^* + v\underline{b}^* + w\underline{c}^*) \; . \; (n_1\underline{a} + n_2\underline{b} + n_3\underline{c})$$

$$= un_1 + vn_2 + wn_3 \qquad 3.11$$

Thus the scattering amplitude becomes

$$\phi = \sum_N F_n \exp\{-2\pi i(un_1 + vn_2 + wn_3)\} \qquad 3.12$$

from which it can be seen that ϕ is a maximum (strong diffraction) when $(un_1 + vn_2 + wn_3)$ is integer. This condition is satisfied when $\Delta\underline{k} = h\underline{a} + k\underline{b} + \ell\underline{c}$, i.e. when $\underline{k}$ coincides with the reciprocal lattice vector $\underline{g}_{hk\ell}$. From fig. 3.4 it can be seen that $|\Delta\underline{k}| = (2 \sin\theta)/\lambda$, in addition $|\Delta\underline{k}| = |\underline{g}_{hk\ell}| = 1/|d_{hk\ell}|$ (equation 3.7), the conbination of which gives the expression for the Bragg condition for strong reflection

$$\lambda = 2d_{hk\ell} \sin\theta \qquad 3.13$$

As the diffraction process is elastic two selection rules result; $|\underline{K}| = |K^1|$ and $\Delta\underline{K} = \underline{K}^1 - \underline{K}$. These two rules have a geometrical signficance shown in fig. 3.5. The magnitude of the vector k^1 (length CO) will be equal to that of $\underline{k}$ (length CP) if $\underline{k}^1$ is terminated on a spherical surface of radius $k \equiv 1/\lambda$. Any reciprocal lattice point intersected by the sphere will then satisfy the second selection rule and a strong diffraction condition will result. The construction is known as the Ewald sphere which is also used in X-ray and neutron diffraction.

In LEED the crystal surface may be considered as just a two dimensional plane (Watts, 1974). The reciprocal lattice now becomes a series of rods, extending out from the surface, each of which represents

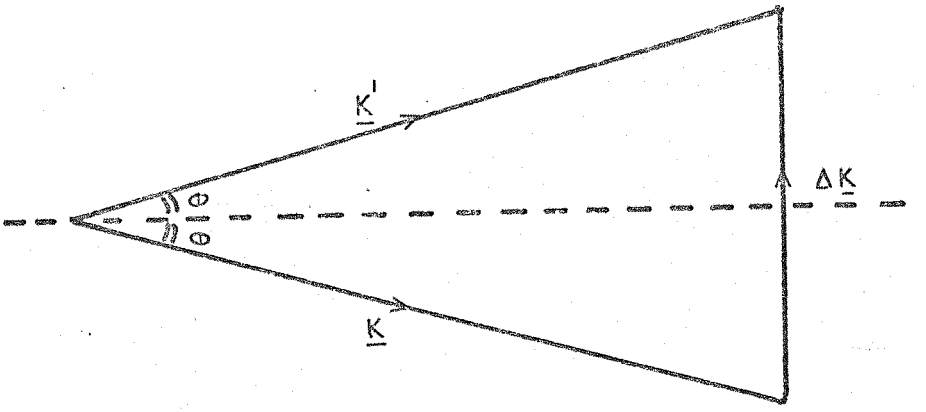

Figure 3.4 Definition of the scattering vector $\Delta\underline{K}$ where $\Delta\underline{K} = \underline{K}' - \underline{K}$

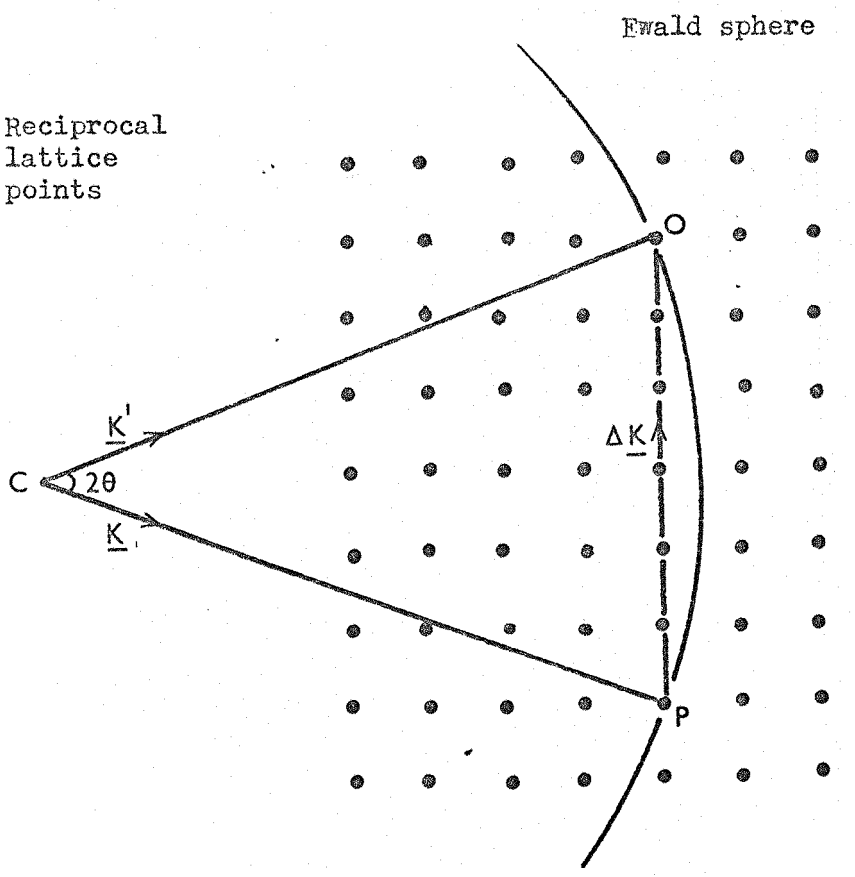

Figure 3.5 The Ewald Sphere construction.

a crystal plane. The strong diffraction condition is met when the Ewald sphere intersects with one of these rods. Thus surface symmetry is immediately made available for study, the separation of the spots enabling determination of the unit mesh of either the substrate or an ordered adlayer.

3.3.2 Dynamical Theory

At the low incident electron energies (0-300 eV) used in LEED studies, the scattering cross sections of the ion cores in the lattice, for electrons, are high. Although this ensures that the majority of the backscattered intensity comes from the surface layers, the probability that an electron will only undergo a single scattering event is very small. Thus diffraction features are often observed which have not been predicted by the Kinematic theory and these may only be interpreted by consideration of multiple scattering and inelastic events. This is the basis of the Dynamical theory but its use means that the surface can no longer be simplified to a two dimensional plane. The inclusion of a third dimension introduces intensity variations into the reciprocal lattice rods which may be probed by varying the incident electron energies. This has the effect of altering the wave length and hence the diameter of the Ewald sphere, its intersection point with the rods then moves along their length. In the case of ZnO however, intensity plots have shown (Taylor 1976) that it is essentially Kinematic in nature which may be accounted for by its comparatively large unit cell (Pendry, 1974).

3.4 WORK FUNCTION TECHNIQUE

Changes in work function of a surface accompanying the formation of an adlayer were monitored in the present study by using an A.C. retarding field technique developed in this laboratory. The method used, which is a variation of technique by Anderson (1935) is fully described by Nathan

and Hopkins (1974) and consequently only a brief outline is given below.

The technique is based on the fact that the peak position in the energy distribution curve (e.d.c.) of the electron beam depends only on the work function (ϕ_c) of the collector, provided that the filament temperature (T_c) and the beam energy (Ea) are constant. The differential of the e.d.c. with respect to energy has a cross-over point on the energy axis and it is this feature which is utilised as an error signal in a feed back loop to maintain the analyser on the e.d.c. peak and hence track its position. The magnitude of this feedback voltage can be shown to be a measure of the change in work function ($d\phi_c$) of the collector under high gain conditions (Nathan and Hopkins).

The main advantage of this technique is that a stable reference surface is not required and also that a more reliable estimate of gas exposure at the surface can be made. Further, this method is not prone to drift problems associated with D.C. techniques. Finally, the electron beam used has little effect on the adsorbate, compared with A.E.S., since the energy of the electrons striking the surface is $\sim$ 5 eV whereas a typical threshold energy for desorption is $\sim$ 20 eV (see Madey and Yates, 1971).

CHAPTER 4

SURFACE PROBES - EXPERIMENTAL

This chapter describes the experimental methods and instrumentation used to exploit the techniques discussed theoretically in the preceding chapter.

4.1 A.E.S. INSTRUMENTATION

The principle components of any Auger spectrometer (which uses electron induced Auger emission) are an electron gun, an electron energy analyser and an external electronic detection system. Spectrometers may be divided into two broad categories, depending on the type of energy analyser used, but because several recent reviews of this subject are available (Steckelmacher, 1973 and Wanneberg et al, 1974) this section will be confined to an outline of the A.E.S. detection system used in the present study.

The basic apparatus was similar to that described by Palmberg and Rhodin (1968) and consisted of a 4-grid LEED optics, manufactured by Varian Associates Ltd. The primary electron beam was provided by an adapted Superior Electronics SE5KU gun, mounted on a $2\frac{3}{4}$" conflat flange. Mu-metal was used to shield the gun from stray magnetic fields and the incorporation of "X-Y" deflector plates facilitated positioning of the electron beam onto the sample. Using the laboratory built Auger gun power supply, fig. 4.1, the gun was capable of beam currents up to 50 μA at 2.5 KeV, although it was normally operated at $\sim$ 10 μA. The high primary energy is an advantage in A.E.S. measurements since, the maximum Auger yield for a particular transition energy, ε, occurs at a primary excitation energy of 2 to 5ε (Peria, 1969). Gun voltages were supplied by a Fluke (4.15B) power supply and the deflection voltages were provided from a

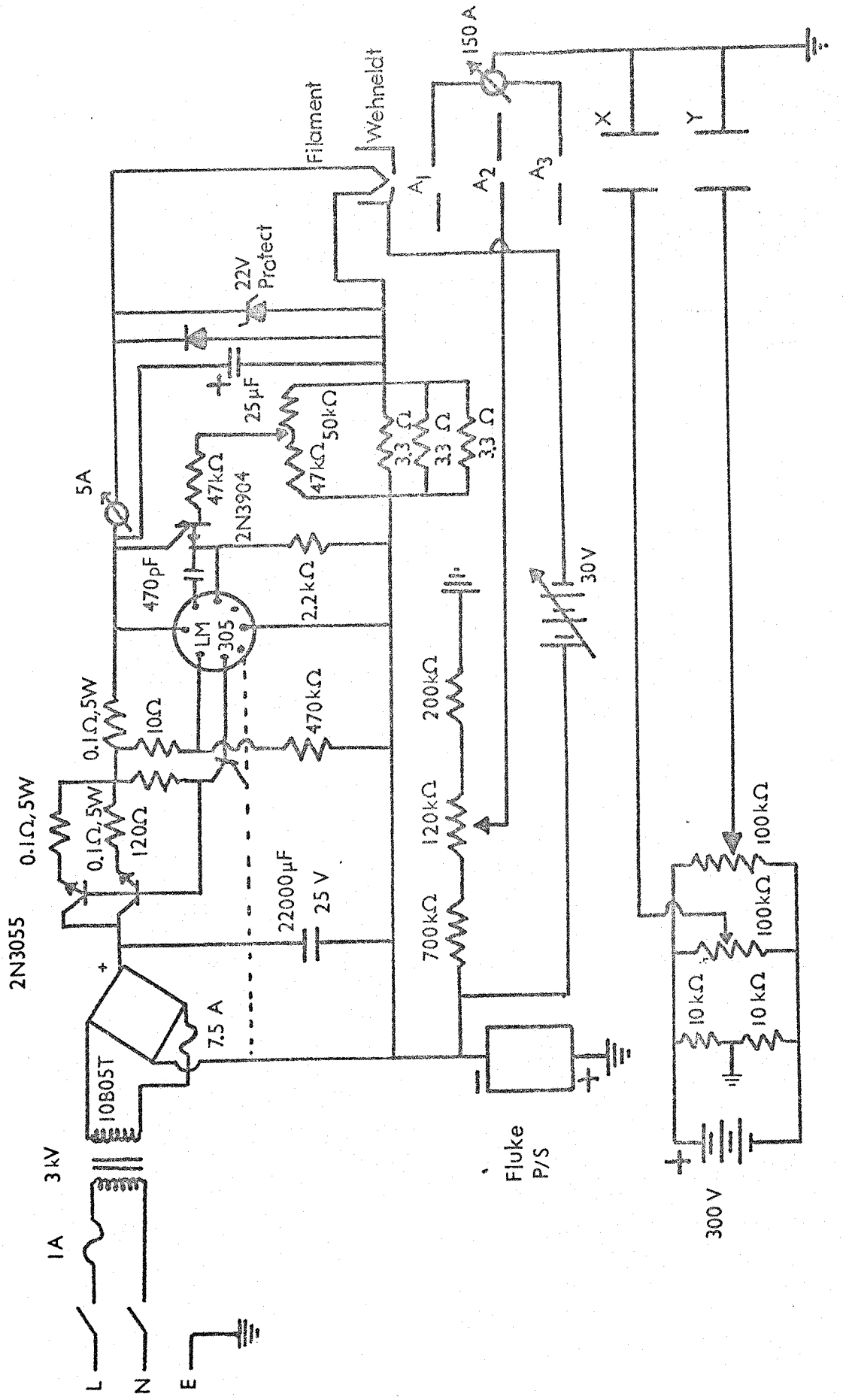

Figure 4.1 Auger gun power supply.

separate ± 300 V D.C. supply.

The LEED optics, as used for A.E.S., were connected to the external detection system as shown in fig. 4.2. The outer grids (G_1 and G_4), together with the specimen were earthed, which maintained a field free region between the sample and the two inner grids (G_2 and G_3). G_2 and G_3 were coupled together and driven by a 0 to - 1.5 KV ramp generator which had a small A.C. modulation superimposed. Two retarding grids were used to improve on the resolution of the analyser by increasing grid spacing (Taylor, 1969). The screen was held at a high positive potential, several kilovolts, which not only increased collection efficiency but also minimised the effect of non-radial electron trajectories, resulting from imperfections in grid symmetry. The detection system was standard with the exception of the pre-amplifier stage and the oscillator, which were designed and built in this laboratory (Nathan and Hopkins, 1973). Essentially the pre-amplifier consisted of a narrow band impedance converter with a high transimpedance of $\sim 10^8\Omega$. This had the advantage of reducing noise at the first detection stage but required an extremely stable reference oscillator with small harmonic content. The complete system resulted in a reduction in the amplifier noise to a level comparable with the shot noise from a 1 μA electron beam. Further the improvement in the Auger signal to noise allowed the use of a reduced time constant enabling fast scan rates to be used.

4.2 LEED INSTRUMENTATION

The use of a fluorescent screen and post accelerating grids for the display of electrons diffracted from solids was first discussed by Ehrenberg (1934). Development of the original system led ultimately to the use of grids of spherical symmetry and the 2-grid optics of Lander et al (1962) became standard. In the present study commercial Varian optics

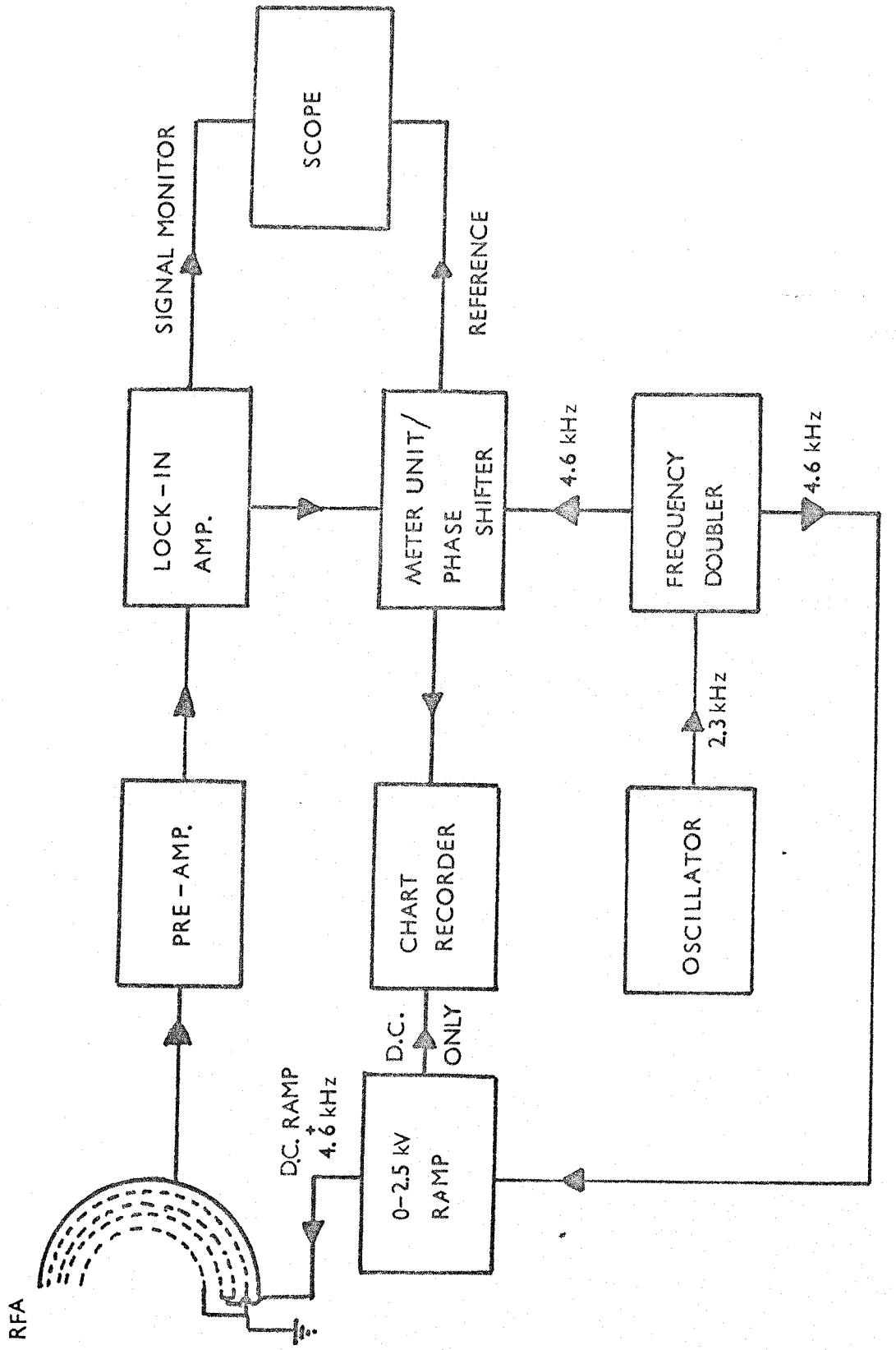

Figure 4.2 Auger detection system.

were used which incorporated two extra grids, however, these were only necessary for operation in the A.E.S. mode. The hemispherical grids were made from 80% transmission 100 mesh nickel coated tungsten. The collector was a hemispherical stainless steel backplate dusted with P11 phosphor. The 4-grid optics were connected into the external LEED electronics as shown in fig. 4.3. The first two grids (G_1 and G_2) were earthed, as was the crystal, to form a field free region. The remaining two grids (G_3 and G_4) are then held at a potential of a few volts below the energy of the primary beam, which excludes the collection of inelastic secondaries. The elastic secondaries are collected by the screen which is biased at + 5 KV to excite the phosphor. The primary electron beam was provided by an indirectly heated bariated nickel cathode contained in a gun positioned at the centre of the optics. This integral gun was capable of giving up to 1 μA beam current and was normally operated at energies between 40 and 150 volts. Thus with this system the whole diffraction pattern could be displayed simultaneously.

4.3 WORK FUNCTION INSTRUMENTATION

In the present study work function changes were measured using the A.C. retarding field technique of Nathan and Hopkins (1974). This method employs the crystal itself as the energy analyser and the external electronics, shown schematically in fig. 4.4, incorporates a low noise detection system similar to that used for A.E.S. The electron beam was provided by the LEED gun. The electrons from the gun filament are accelerated and focussed on the collector (the sample), the beam energy being defined from the accelerating voltage (ε_a) applied to the gun. The incident beam is energy modulated by superimposing an A.C. voltage on ε_a and is retarded at the collector by a suitable bias voltage (ε_b). The true retarding potential, ε_r, between the gun filament and the collector

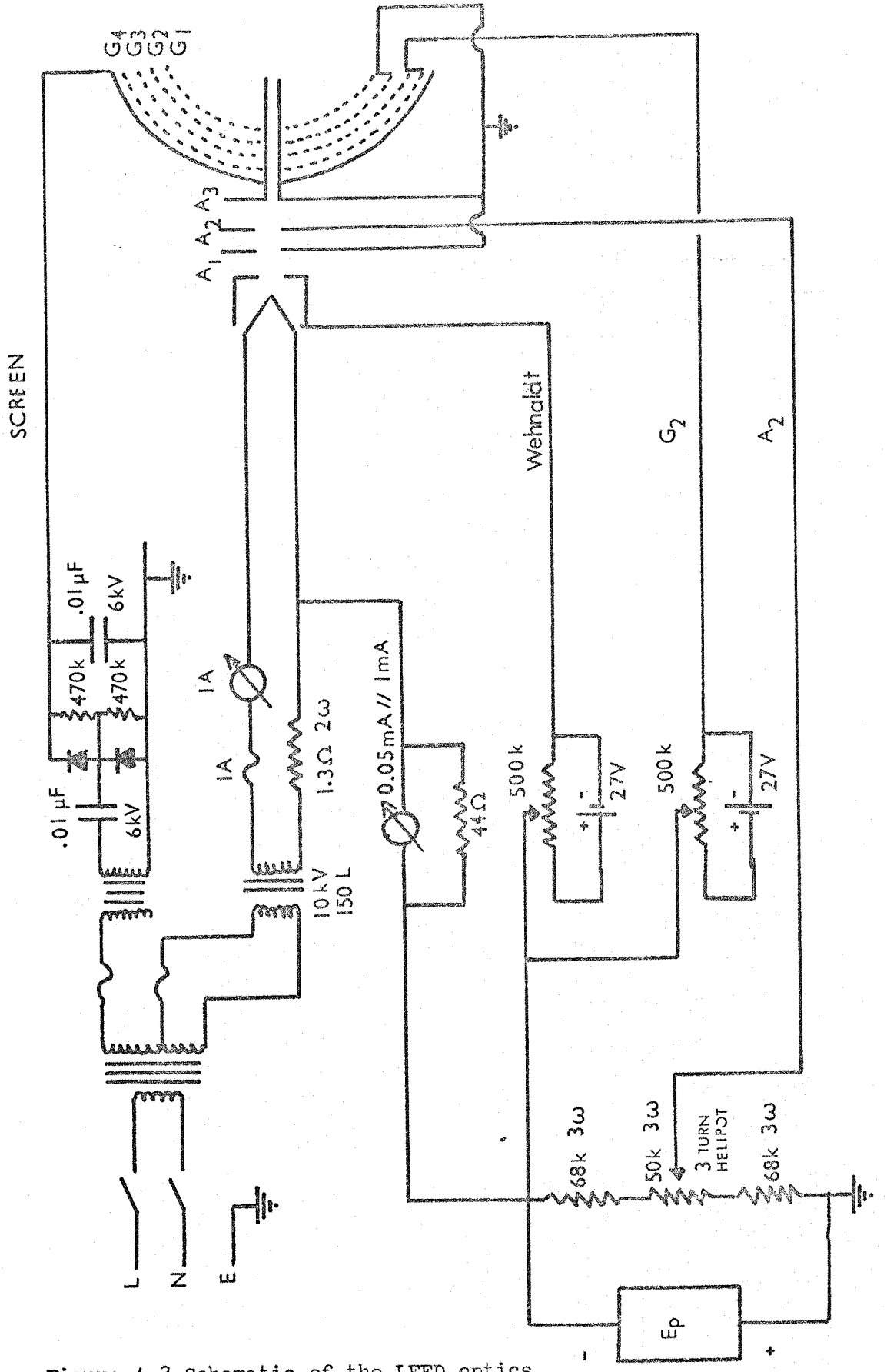

Figure 4.3 Schematic of the LEED optics and power supply.

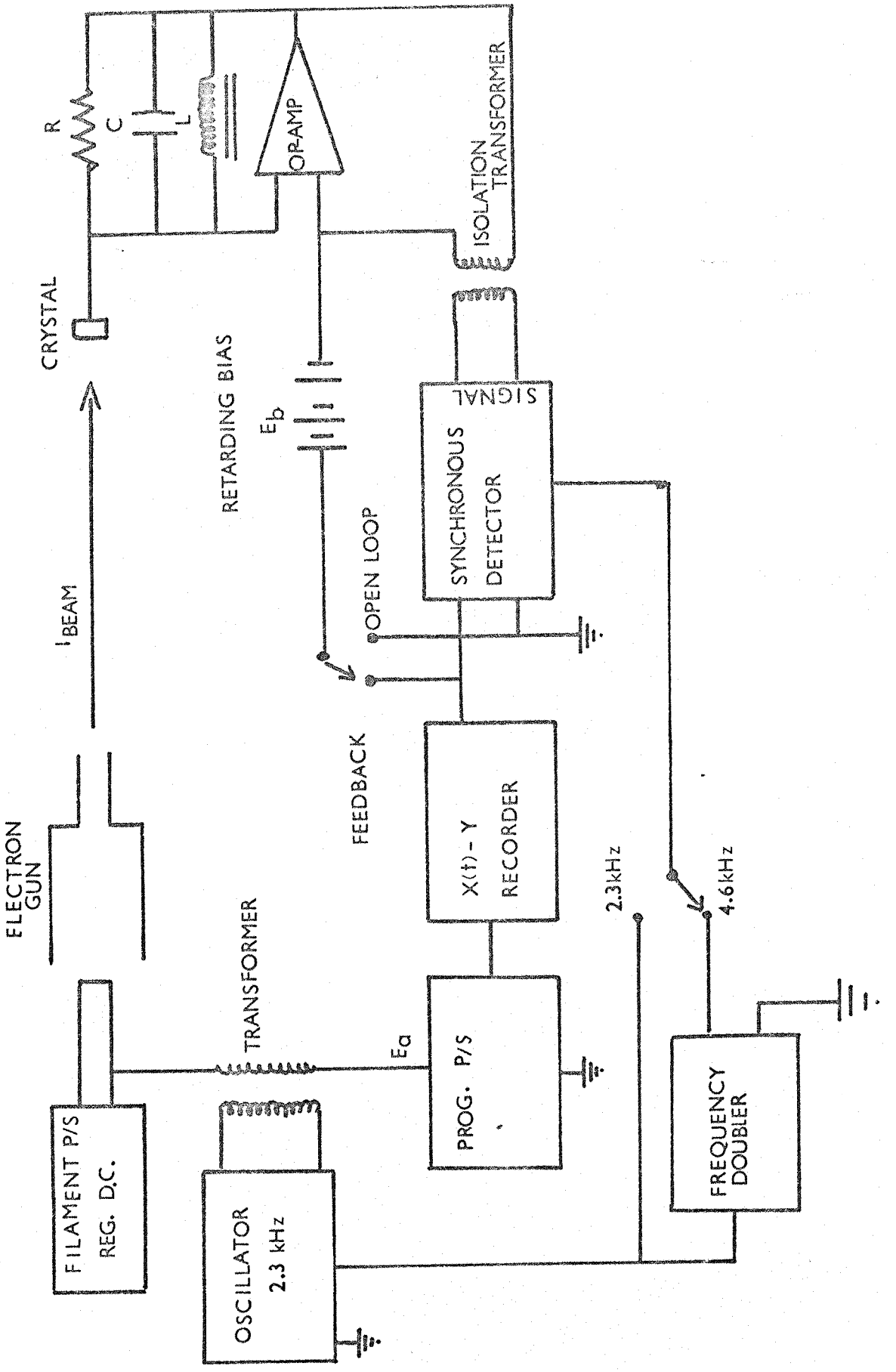

Figure 4.4 Experimental arrangement for the retarding field method for measuring work function.

is then;

$$\varepsilon_r = (\varepsilon_a - \varepsilon_b) - \phi_c \qquad \text{equation 4.1}$$

where ε_c is the work function of the sample which, by a suitable choice of ε_b lies in the vicinity of the edc peak. The system of fig. 4.4 has three modes of operation:

(i) First derivative $[N(\varepsilon)]$ mode, with the synchronous detector tuned to the modulation frequency (ω).

(ii) Second derivative $[dN(\varepsilon)/d\varepsilon]$ mode, with the synchronous detector tuned to 2ω.

(iii) Work function mode, with the synchronous detector to 2ω and the feedback loop closed.

The $[N(\varepsilon)]$ and the $[dN(\varepsilon)/d\varepsilon]$ modes are shown in fig. 4.5(a) and (b). From these figures it can be seen that the second derivative curve has a crossover point at which it changes polarity. It is this feature which is used as an error signal in the feedback mode to maintain the analyser on the peak and track its position. The magnitude of this feedback signal is then a measure of the change in collector work function.

Initially with the feedback loop closed, the linearity of the system was examined by ramping the beam energy and observing the output of the synchronous detector. A family of X-Y recorder traces for various modulation voltages is shown in fig. 4.6. These curves indicate that the tracking range depends on the modulation potential and must be set for the particular experiments being performed. Once the parameters have been established the ramp voltage was disconnected and replaced with a potential, which lay in the linear region of the "lock-in" curve, from a high stability power supply. The chart recorder could then be calibrated to give a direct readout of work function change.

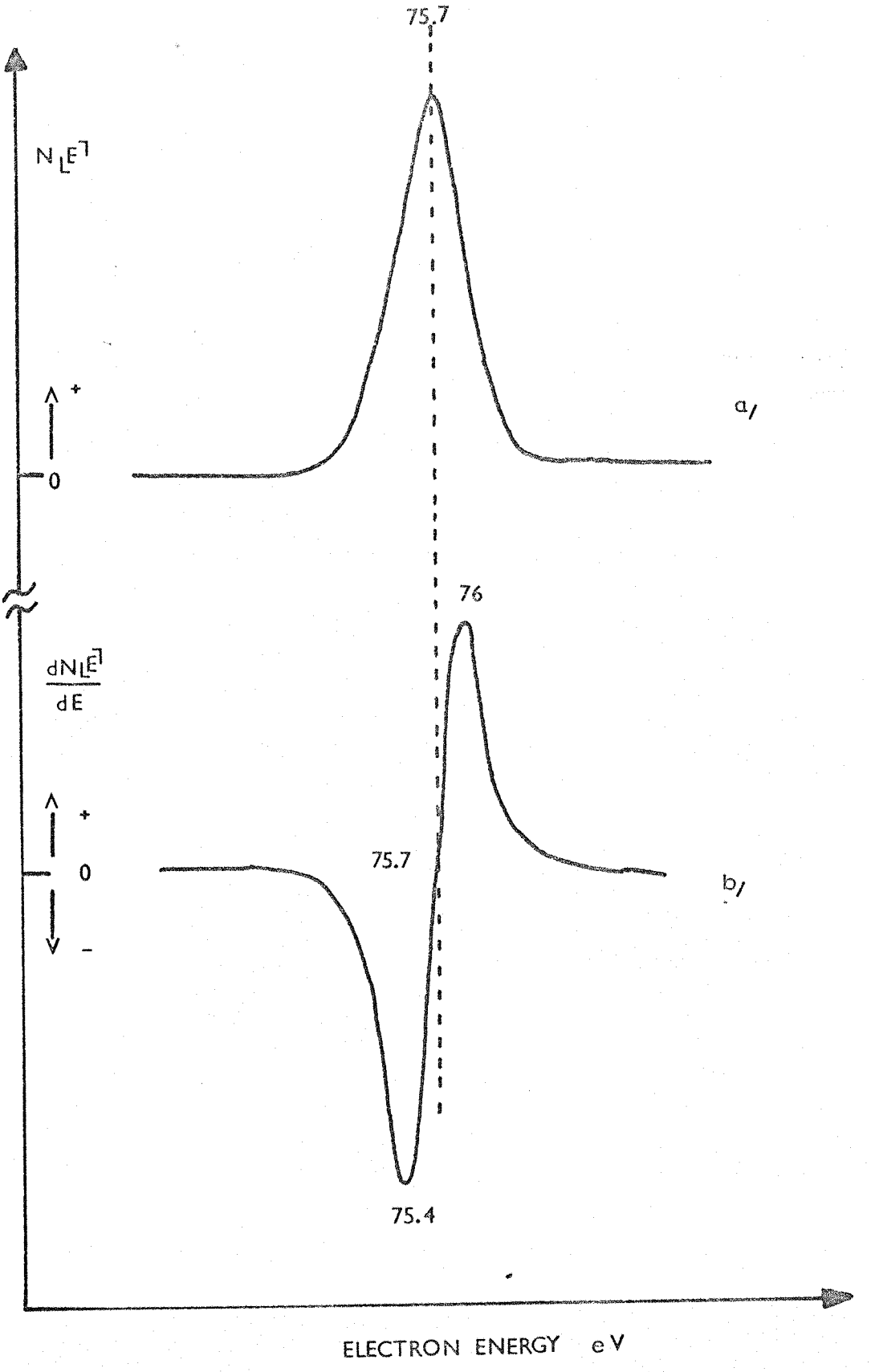

Figure 4.5 a). Energy distribution N(E)
b). Derivative of a), dN(E)/dE.

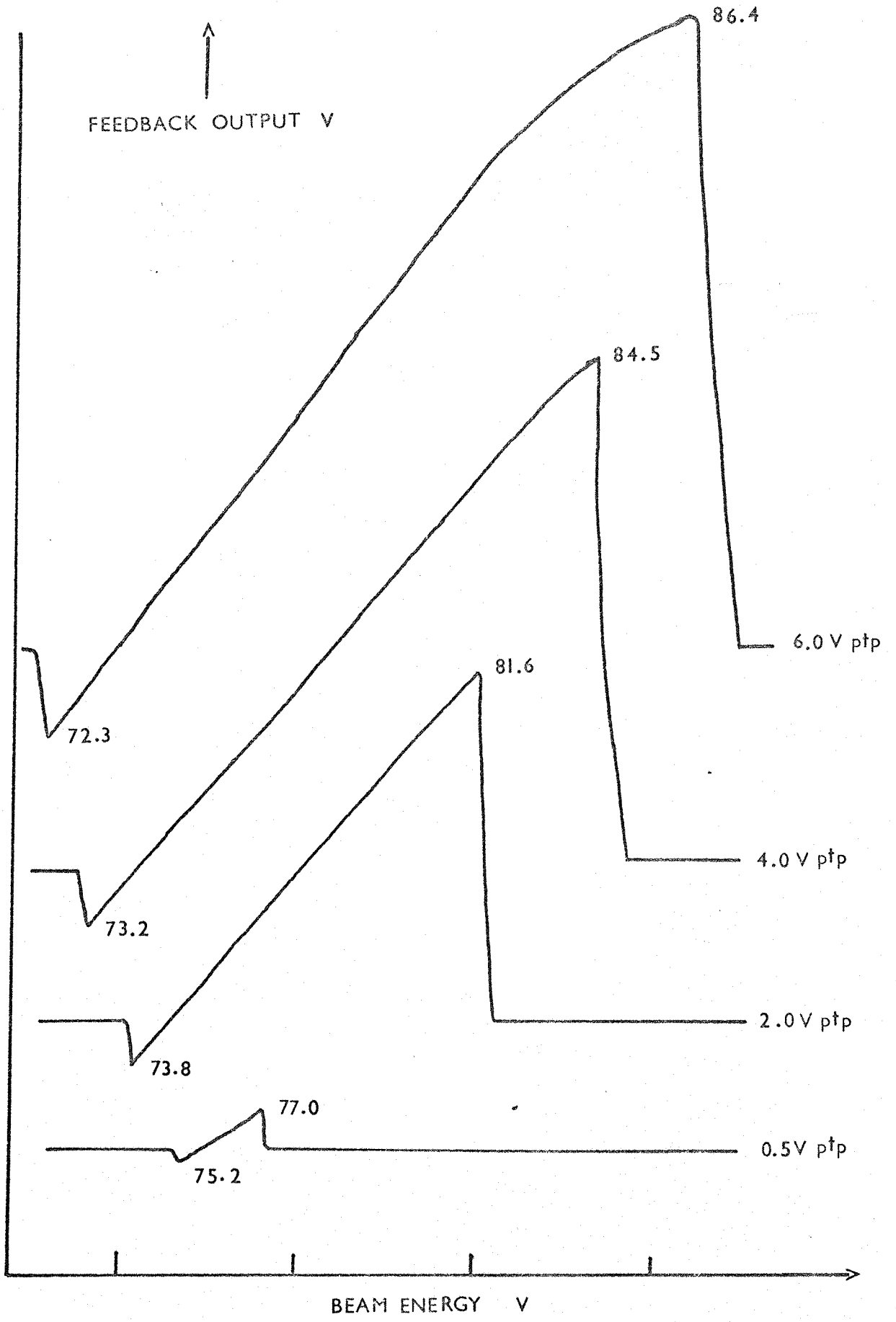

Figure 4.6 A family of lock-in curves for various modulation voltages.

CHAPTER 5

ZINC OXIDE - BULK AND SURFACE PROPERTIES

Zinc oxide (ZnO) occurs naturally as the mineral zincite and it is used in a diverse range of processes which include; vulcanisation of rubber, acoustic transducers, photographic duplication, catalysis and gas detection. This chapter outlines some of the bulk and surface properties of this material, together with some theoretical models developed.

5.1 BULK PROPERTIES

ZnO cannot be melted at atmospheric pressure, as it dissociates and sublimes, but single crystals may be grown by reaction of zinc vapour with oxygen (Heiland, Mollwo and Stockmann, 1959) or by a hydrothermal method (Laudise et al, 1964). The single crystals exhibit a hexagonal wurtzite structure (fig. 5.1) and, as shown, it is a layered material. The zinc ions occupy half of the tetrahedral interstitial positions and have the same relative arrangement as the oxygen ions. The Zn-O bond arises, to a first approximation, from the empty 4s levels of Zn^{++} and the filled 2p levels of O^{--}. There are three low index surfaces; the prism $(10\bar{1}0)$ and the polar (0001) faces. The prism surfaces have the lowest surface energy and are formed preferentially during crystal growth. The (0001)-Zn and the $(000\bar{1})$-O polar surfaces may be exposed by cleavage perpendicular to the c axis. ZnO single crystals are always n-type, due to a stoichiometric excess of Zn which gives rise to donor levels (Heiland, 1974). It has a band gap of $\sim$ 3 eV.

The bulk band structure of ZnO has been investigated both experimentally and theoretically. Two theoretical approaches have been made which to a large extent agree except for the width of the valence band. In the first treatment (Rossler, 1969) it was calculated to be

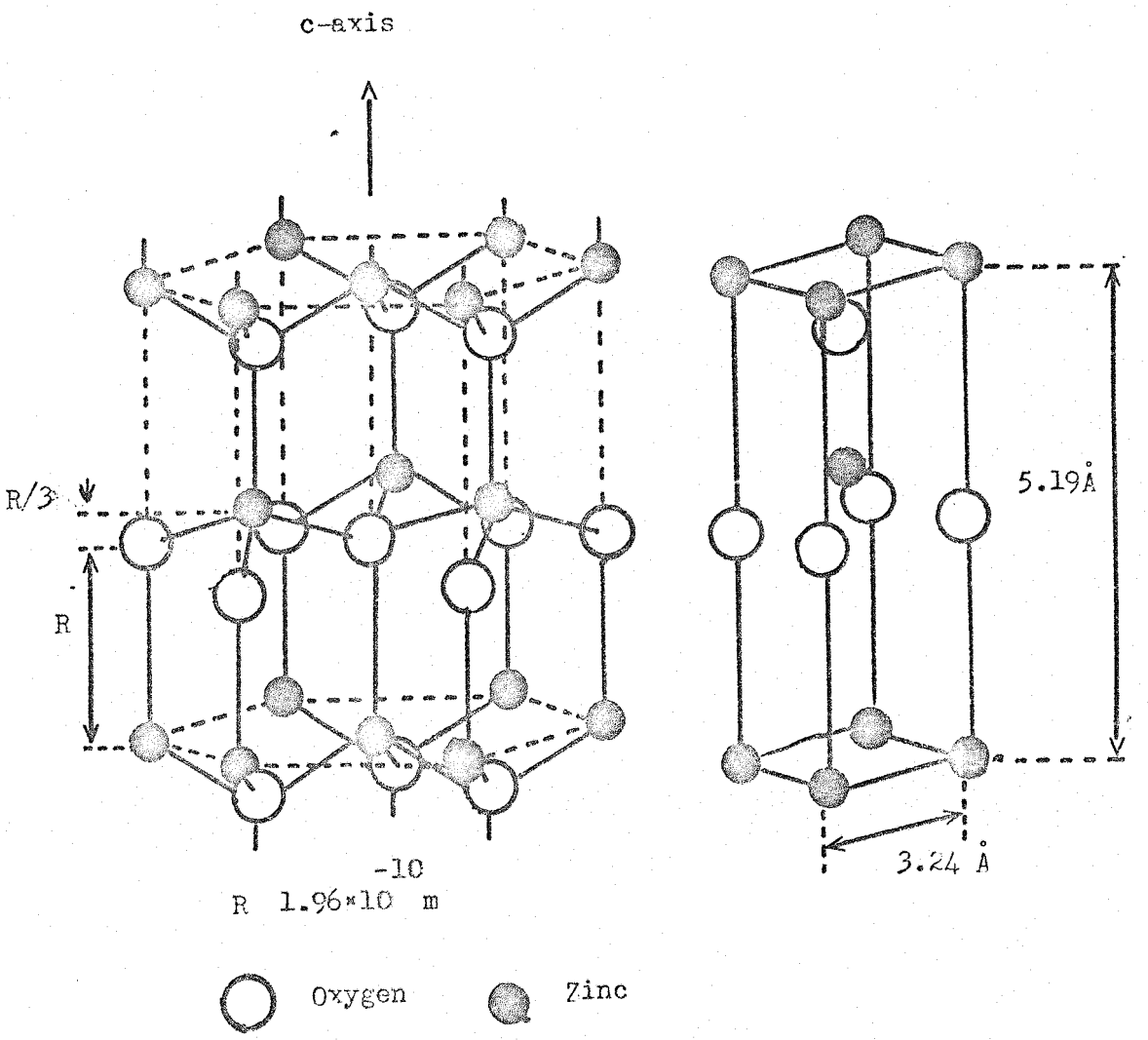

Figure 5.1 Schematic diagram of the ZnO wurtzite structure.

3.5 eV while in the second (Bloom et al, 1973) a value of 5 eV was found. The valence band width is much larger than for other II-VI compounds which may be explained since it is largely dependent on the overlap of the VIA atoms. The O-O separation for ZnO is much smaller than for VIA atoms such as Te or Se in other II-VI compounds. The wave function overlap is therefore greater and so correspondingly is the valence band width. Much experimental data has been compiled on the band structure of ZnO, particularly by Swank (1967) using photoemission, contact potential and surface photovoltage and also by Powell et al (1972). However, a comprehensive review of both the theoretical and experimental results may be found elsewhere (Taylor, 1976).

5.2 SURFACE STATES

Since the surface structure of a crystal determines its interaction with other materials it is clearly necessary to understand any changes that take place in the band structure at the surface by virtue of there being a lattice discontinuity or by the interaction of the surface with an adsorbate. Theoretical evidence for the existence of surface states stems from the work of Tamm (1932). He applied the then recent Kronig-Penny model which consists of a one-dimensional array of delta-function potential barriers. It was known that for an infinite array the allowed energy levels fell into bands and the corresponding wave functions had the Bloch form. Tamm's contribution was to consider a "semi-infinite" array, terminated at one of the lattice points by a constant finite potential. The result was a discrete level in each energy gap, corresponding to a wave function that was localized near the surface. Later, Fowler (1933) showed that the levels should occur in pairs in a finite lattice because of the two surfaces. Rijanow (1934) and Maue (1935) confirmed the possible existence of surface states in three-dimensional

crystals using the nearly-free electron approximation. Goodwin (1939) applied a tight binding approximation to both one and three dimensions. In all cases, surface states were found with energies lying in the forbidden gaps between the bands of "volume states". For each surface state that appeared, one volume state disappeared from one of the bands. The surface state energies were found to depend on parameters involving the potential, namely the Fourier component with wave vector normal to the surface in the nearly-free electron model and the overlap integrals involving the surface atoms in the tight binding case. A more general treatment of the subject was made by Shockley (1939) who dealt with a potential that was perfectly periodic throughout the crystal, including the outermost unit cells. Although much information was obtained from these early studies, the Tamm model cannot be applied to ionic crystals such as zinc oxide, since it assumes only a positive-going potential, compared with the alternate positive and negative poles located at cation and anion sites of an ionic crystal. Several theories have subsequently been developed to deal with "ionic surface states", one of which is the Madelung (electrostatic) model of Levine and Mark (1966).

The Madelung model was an extension of the classical electrostatic approach of Seitz (1940). The theory was applied to ionic crystals of the form M_nX_m where M is a metallic cation and X a non-metallic anion. In the bulk crystal the anions and cations interacted to form the valence band and conduction band respectively which were idealised as discrete levels with a 100% ionic character. Surfaces of MX crystals fall into two categories, the prism or MX(C) surfaces (C for checkerboard) which have equal numbers of anions and cations present and the polar or MX(L) surfaces (L for layer) which have only anions or cations at the boundary. The electronic energy levels M and X^- for an ionic crystal as a function of interionic distance, R, are shown in fig. 5.2. These levels are

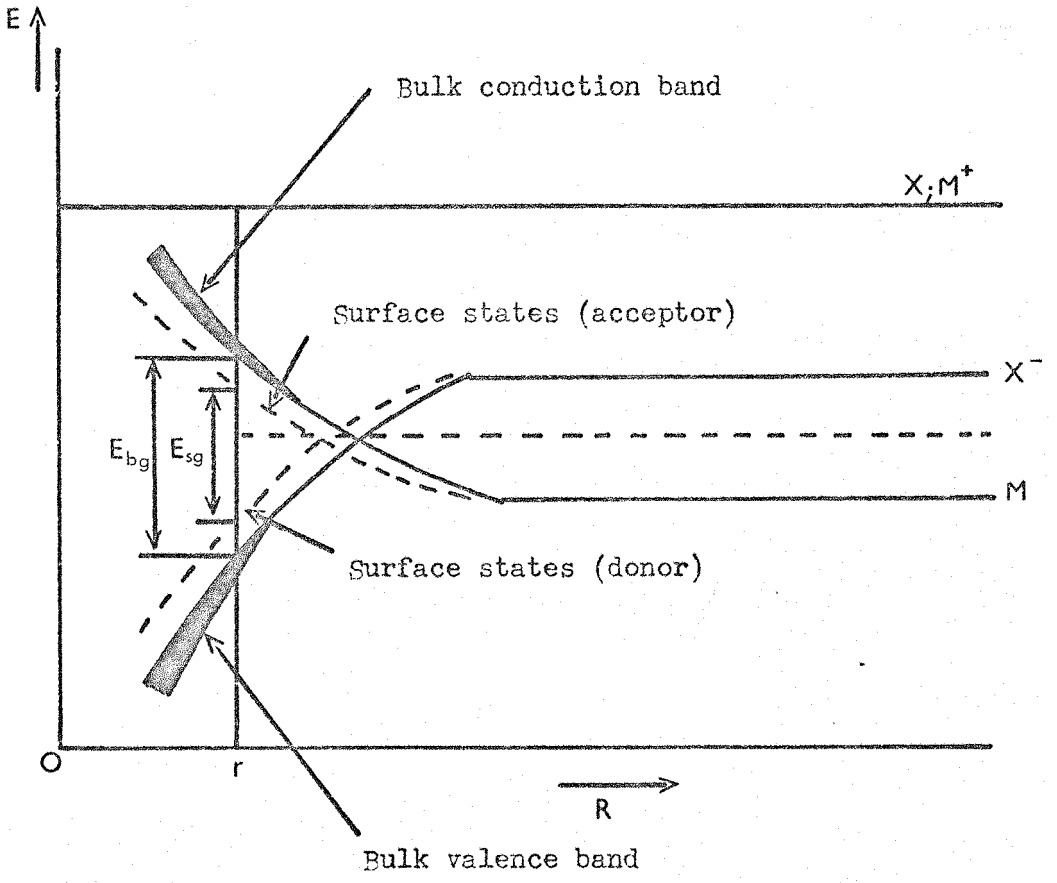

Figure 5.2 Energy levels as a function of ion separation.

referred to a zero of potential X and M^+. In the limit $R \to \infty$ the lower state is M, indicating that the most stable situation is one in which M and X atoms exist. As R is reduced toward the equilibrium separation, r, the change in Madelung potential inverts the M, X levels and the crystal prefers the ionic state of M^+ and X^- ions. The theory predicts two bands of surface states, as shown in fig. 5.2. One set appears in the upper half of the band gap and are derived from cation-like orbitals. As such they are acceptor states or electron traps which are neutral when empty and negatively charged when filled. The second set of states occurs in the lower half of the band gap. These are derived from anion-like orbitals and are doner states or hole traps, neutral when filled and positively charged when empty. The separation of these states, E_{sg}, is a function of the ionicity of the compound, as is the width of the band gap, E_{bg}.

The electrostatic model predicts in addition to surface stability of the MX(C) boundaries that the polar MX(L) surfaces will be more reactive and require either atomic rearrangement or electrostatic compensation for stability. The theory also predicts that the smaller the band gap, the deeper the surface states. More explicit models for the MX(L) polar surfaces are described in section 5.3.

The surface state theories described above only deal with intrinsic states. However, extrinsic surface states arise following the adsorption of material which forms localised energy levels at the substrate/adsorbate interface. Experimental evidence (Swank, 1967, Luth and Heiland, 1972 and Luth, 1973) exists for both intrinsic and extrinsic surface states and it would seem that they play an important role in substrate/adsorbate interactions. Of particular interest, for the case of the polar surfaces, is that it has been suggested (van Hove and Leysen, 1972) that a transfer from intrinsic to extrinsic states occurs on

adsorption of material which gives rise to a lowering of surface energy.

5.3 POLAR SURFACE MODELS

The polar (0001) surfaces of layered materials tend to be highly reactive and have associated with them a net electrostatic dipole. The dipole exists because of the duo-layer nature of the crystal lattice which terminates in a mono-ionic plane which exhibits uncompensated charge. The zinc and oxygen atoms of zinc oxide have significantly different electronegativities leading to an overall electron transfer from zinc to oxygen. The resulting Zn-O bond is thus largely (60%) ionic and as a result electrostatic models may be applied. Two such theories have been developed, one using the idea of dangling bonds, the other based on Madelung potential calculations. The following sections will summarise both of these approaches paying particular attention to their application to zinc oxide.

5.3.1 The Dangling Bond Model

This was originally conceived (Gatos and Lavine, 1960) to explain the different reactivities of the (111) polar surfaces of III-V compounds. It considered the bulk atoms as if they were entirely covalently bonded while the surface atoms retained the bulk tetrahedral configuration. It was assumed that on creation of the (111) surfaces the group V atoms captured both electrons from the original III-V bond to form the surfaces shown in fig. 5.3 (a). Thermodynamically this is more favourable than single electron capture. When applied to ZnO and assuming complete covalent bonding, each of the tetrahedral bonds has a contribution of $\frac{2}{4}$ electrons from the zinc and $\frac{6}{4}$ from the oxygen atoms. If however, due to the highly ionic nature of ZnO, an ionicity of one electron per bulk atom is assumed (Mariano and Hanneman, 1963) the electron contribution becomes $\frac{1}{4}$ and $\frac{7}{4}$ respectively, fig. 5.3 (b). It thus follows that these

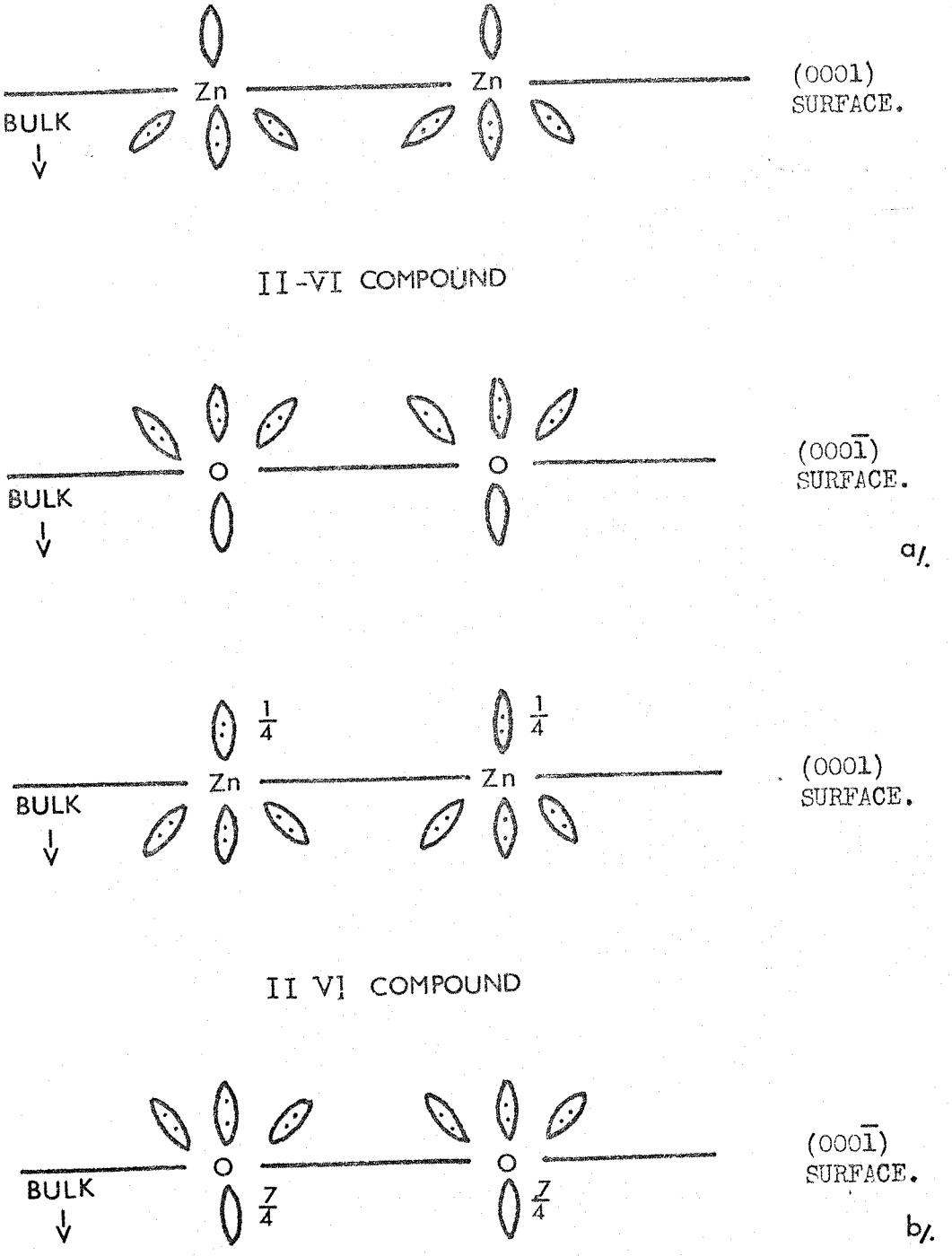

Figure 5.3 Schematic representation of the formation of zinc and oxygen polar surfaces;
a/. Covalent bonding
b/. 50% ionic bonding.

surfaces will have an overall electrostatic charge and that this is equivalent to an excess of one quarter of a monolayer of unit positive charge for the (0001)-Zn surface and an equal but negative charge on the $(000\bar{1})$-O face.

Although this model accounts for the reactivity differences of the two polar surfaces found experimentally it does not take into account quantum mechanical aspects or the possible existence of surface states.

5.3.2 Madelung Potential Model

This second model was proposed by Nosker et al, 1970 and is based on the calculation of Madelung potentials along the (0001) wurtzite axis. These calculations are adequately described by the authors and will not be presented here. The model treats the wurtzite lattice as a series of neutral double layers, each of which may be replaced, to a first approximation, but two charged discs of uniform charge density. The theory assumes that, firstly, there is no perturbation of the bulk atomic periodicity and secondly, the effective charge of all like atoms is the same throughout the material. A knowledge of the exact magnitude of the charge transfer in ionic solids is not a prerequisite for this approach. Again the excess $\frac{1}{4}$ of a monolayer of surface charge is the main result of this model but, as in the theory of Gatos et al, the role of surface states is omitted. From calculations of polar surface energies for stabilisation by reconstruction, by the addition of charge, by impurities or through the existence of facets; the facetted surface was found to be the most stable. However, this is an over simplification since the history of the substrate and a detailed calculation of surface energy for particular surface impurities must be made.

Experimental evidence supporting these models will be discussed in later chapters.

CHAPTER 6

PREPARATION AND CLEANING OF ZINC OXIDE SINGLE CRYSTALS

The presence of physical and chemical irregularities at crystal surfaces can clearly lead to difficulty in the interpretation of gas-surface interactions. The practical requirement of uncontaminated surfaces which also have only a small number of physical imperfections has led, in the case of zinc oxide, to a comprehensive study of surface preparation and cleaning. This chapter reviews previous work and outlines the results obtained in the present study during cleaning of the $(000\bar{1})$ polar surface.

6.1 INTRODUCTION

ZnO crystals grown from the vapour phase (Heiland et al, 1959) take the form of needles with a hexagonal cross-section. They grow from a substrate culminating at a steep point which has been shown to correspond to the <0001>-Zn direction (Mariano and Hanneman, 1963). Cleavage parallel to the (0001) plane exposes both types of polar surface, which are distinguishable from the relative position of the zinc point, fig. 6.1. It is thus possible by cleavage in u.h.v. conditions to produce polar surfaces which are free from both etchant and atmospheric contamination. Such surfaces have been studied by Müller, 1969, van Hove and Leysen, 1972 and Kohl et al, 1974. Initial inspection with LEED showed in all cases a very stable (1 x 1) pattern for both faces. While this pattern reflects bulk symmetry, it is not conclusive evidence of cleanliness. However, A.E.S. spectra by Kohl et al contained only zinc and oxygen transitions.

While cleavage in u.h.v. produces clean surfaces it is technically difficult and it is probably for this reason that most studies have used mechanically polished and chemically etched "real" surfaces. "Real" polar surfaces may be prepared by spark cutting the crystal perpendicular to the

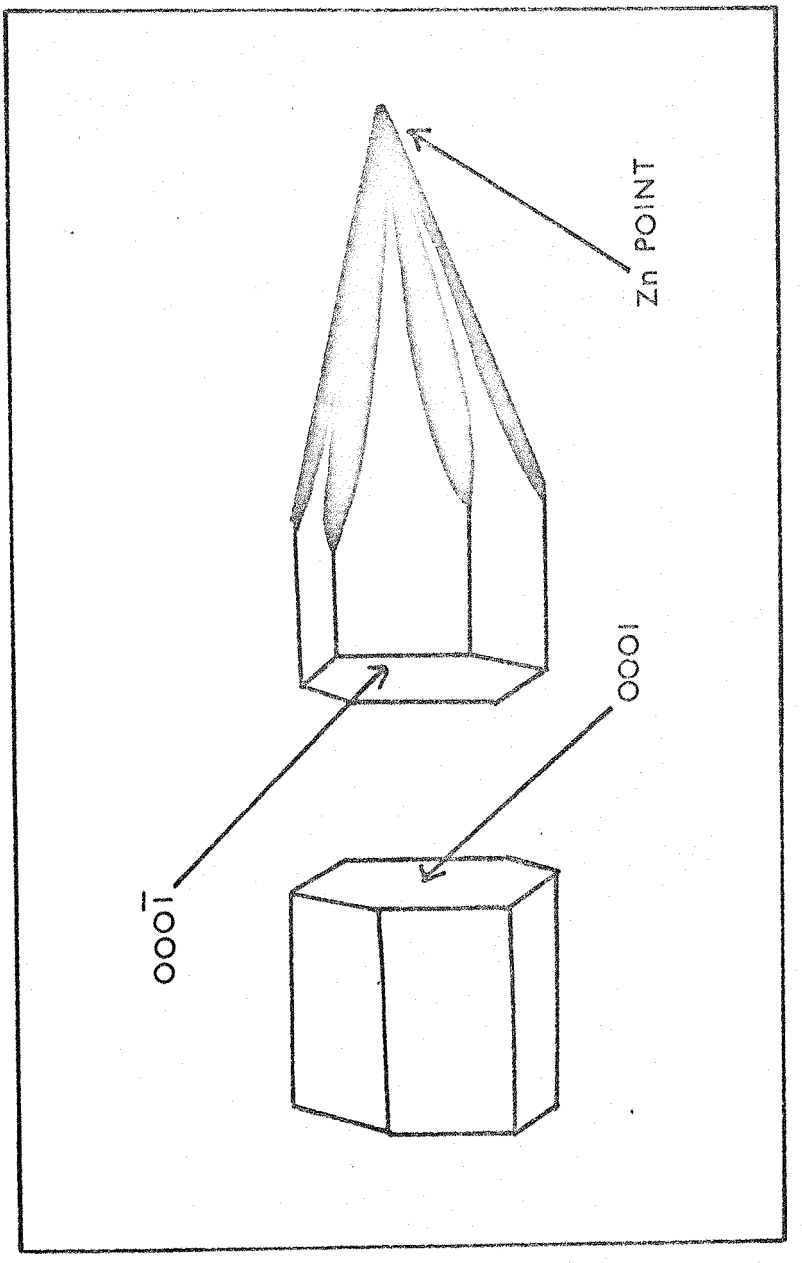

Figure 6.1 Relative position of the zinc point to the cleaved polar surfaces.

c-axis, followed by polishing in successively finer grades of diamond paste. Standard chemical etching techniques (Heiland et al, 1963 and Mariano and Hanneman, 1963) are then used to determine the polarity of the faces. In order to obtain "atomically" flat surfaces after the above procedure, the crystals are chemically polished in HCl and H_3PO_4 (Leysen and van Hove, 1972). The faces then exhibit a "mirror-like" quality and appear smooth even in scanning electron microscope pictures at a magnification of 10,000 x (Levine et al, 1972). However, LEED exhibits a high intensity background which indicates that the first few atomic layers are in disarray and also A.E.S. reveals the presence of chemisorbed impurity species. The formation of clean, well ordered surfaces has been achieved by argon ion bombardment (a.i.b.) and anneal cycles, the results of which are reviewed in the next section.

6.2 PREVIOUS WORK

Early studies by Campbell et al, 1969, Chung and Farnsworth, 1970 and van Hove and Leysen, 1972, used LEED to determine the behaviour of "real" ZnO surfaces during cleaning. Following argon ion bombardment and anneal to 1000 K, Campbell et al reported the formation of (1 x 1) patterns for both polar surfaces. After similar treatment of the Zn-face, Chung and Farnsworth discovered the presence of "extra" spots at $(\frac{1}{2}, \frac{1}{2})$ and $(\frac{1}{2}, 0)$. The failure to observe these beams in the previous work was attributed to the resistivities of the crystals used. Van Hove and Leysen, on the other hand, found that annealing the O-surface to 900 K resulted in the formation of a $(\sqrt{3} \times \sqrt{3})$ superstructure which on further heating disappeared to leave a (1 x 1) pattern. They also found that the Zn-face required bombardment/anneal cycles before even a weak (1 x 1) pattern formed.

More recent studies incorporated A.E.S. as an additional surface

probe. Levine et al, 1972, reported the presence of Cl, S and C in A.E. spectra of as-mounted crystals, carbon persisting even after an anneal to 1400 K. Again, as in the work of Chung and Farnsworth, spots at $(\frac{1}{2}, \frac{1}{2})$ were present in LEED patterns, but in this study they were associated with the carbon contamination. Fiermans et al, 1971 and 1973, used signal-averaged A.E.S. and surface contamination by Ca and P, together with the previously reported Cl, S and C, was found. They also noted that the Cl and S signals were stronger on the Zn-surface, while the P peak was more pronounced on the O-surface. After an anneal to 600 K a $(\sqrt{3} \times \sqrt{3})$ superstructure formed on the O-face, which gave way to a (1 x 1) pattern on further heating and argon ion bombardment. A corresponding clean surface was shown by A.E.S. The Zn-surface was found to be still partially reconstructed. Fiermans et al also suggested a possible correlation between the $(\sqrt{3} \times \sqrt{3})$ structure and the presence of calcium at the surface. Chang and Mark, 1974 and Magoninski and Kirby, 1975, both observed clean polar faces and (1 x 1) LEED structures after bombardment and an anneal to below 900 K. Annealing the Zn-surface to higher temperatures resulted in a $(\sqrt{3} \times \sqrt{3})$ reconstruction (Magoninski) and a combination of $(\sqrt{3} \times \sqrt{3})$ and (2 x 2) (Chang). Magoninski and Kalman, 1974, using X-ray techniques, showed that the half integral order beams observed by Levine et al in fact form a $\sqrt{3} \times \sqrt{3}$ (and not a (2 x 2)) superstructure, in agreement with more recent work. It is also possible that Levine's identification of carbon was in error. Since the Auger peaks for carbon and calcium are adjacent (at 272 eV and 291 eV respectively) it is possible that calcium was present, however no Auger spectra were published. Hopkins et al, 1975, again reported the formation of a $(\sqrt{3} \times \sqrt{3})$ superstructure on the O-surface following an anneal to 1000 K which removed all surface contaminants except K and Ca. The A.E. spectra also exhibited zinc peak shifts of 3-4 eV, further indication of the strong contaminant-adsorbate interaction.

It was also concluded that the K/Ca interaction was not as great on the Zn-face since no zinc peak shifts were present. After repeated bombardment/anneal cycles, clean A.E. spectra were obtained for both faces and LEED gave a stable (1 x 1) pattern.

6.3 SUMMARY OF PREVIOUS WORK

Although production of clean, well ordered polar surfaces by cleavage in u.h.v. was achieved by several authors, most studies have used more conventionally prepared "real" surfaces. These, however, were found to be initially highly disordered and contaminated. In most cases annealing alone removed only some of the contamination and left the polar faces either partially or completely reconstructed. Only after repeated bombardment/anneal cycles were clean, (1 x 1) faces obtained. The most commonly observed superstructures, together with previous treatment are shown in table 6.1. Of the surface contaminants reported, Cl and P were clearly associated with previous chemical preparation. K also was traced (Hopkins et al) to the HCl etch. C and S were shown (Levine et al) to be present as a result of exposure to the atmosphere. It was suggested that the presence of calcium, on the other hand, was due to the out diffusion of a bulk impurity.

6.4 PRESENT STUDY

The crystal used in the present study was an undoped, twin-free sample obtained from Erlangen University, Germany. It had a resistivity of 5-10 Ω cm and had a prism length of ∿ 0.5 cm with a hexagonal cross-section of ∿0.3 cm^2. One end had been previously cleaved to expose the $(000\bar{1})$-O surface, which was prepared using a chemical etch of HCl (30%) for 15 seconds, followed by a polish in H_3PO_4 (85%) for 60 minutes. After

Table 6.1

SURFACE	PREPARATION	OBSERVED LEED STRUCTURES	IMPURITIES FROM AE SPECTRA
$(000\bar{1})$	a. Cleaved	(1x1)	None
	b. 'Real" as mounted	High background	Cl,C,S,P & Ca
	600K	$(\sqrt{3}x\sqrt{3})$	Cl,S & Ca
	> 1000K	$(\sqrt{3}x\sqrt{3})$* & (1x1)	Cl,S & Ca
	Ar^+	(1x1)* & $(\sqrt{3}x\sqrt{3})$	None
(0001)	a. Cleaved	(1x1)	None
	b. 'Real' as mounted	High background	Cl,C,S,P & Ca
	> 900K	Local $(\sqrt{3}x\sqrt{3})$	Cl,S & Ca
	Ar^+	Weak (1x1)* (2x2) & $(\sqrt{3}x\sqrt{3})$	None
	Ar^++>900K	(2x2) + $(\sqrt{3}x\sqrt{3})$	None

* denotes most commonly observed structure.

a thorough wash in distilled water the sample was mounted in the vacuum chamber which was then pumped down to the low 10^{-9} torr range.

Subsequent to a preliminary anneal to 500 K, A.E.S. indicated the presence of both calcium and carbon, fig. 6.2(a). Also, as previously reported by Fiermans et al and Hopkins et al, two of the zinc transitions at 106 and 118 eV were replaced by peaks at 95 and 112 eV. Fiermans attributed this to a loss mechanism caused by the presence of calcium in the first few surface layers. The remaining zinc and oxygen transitions were as in appendix I. LEED at this stage produced only a high intensity background. Displacement effects (see chapter 8) from the chamber walls resulted in a large increase in CO and CO_2 partial pressures. A growth in the carbon peak was also noted. Previous work, in u.h.v. conditions, on the interaction of CO/CO_2 with ZnO surfaces has shown (see for example Campbell et al, 1969) that only limited, if any, adsorption takes place. However, in this study the 7 μA, 2.5 KV Auger gun electron beam was incident on the sample and perhaps electron stimulated adsorption resulted. Reduction of the carbon peak was achieved by annealing to ∿ 600 K, although successive annealing increased the calcium signal, which eventually reached a maximum level. Subsequent removal of the Ca and residual C was only accomplished by using argon ion bombardment/anneal cycles. After the first cycle of bombardment (2 hours: 5 μA, 400 V) and an anneal to 600 K, the Zn transitions at 106 and 118 eV appeared. Only a slight reduction of Ca was obtained but successive cycles reduced the level considerably. The growth and removal of both calcium and carbon are shown schematically in fig. 6.3. The diagram plots $^{C}/_{O}$ and $^{Ca}/_{O}$ ratios against sample treatment. After a further anneal to 600 K potassium was detected with A.E.S., fig. 6.2(b). Aproximately $\frac{1}{15}$ of a monolayer (P.A. Taylor, private communication) was present, which again required bombardment for removal. Ultimately, after a total of 20 two-hour cleaning cycles, the impurity

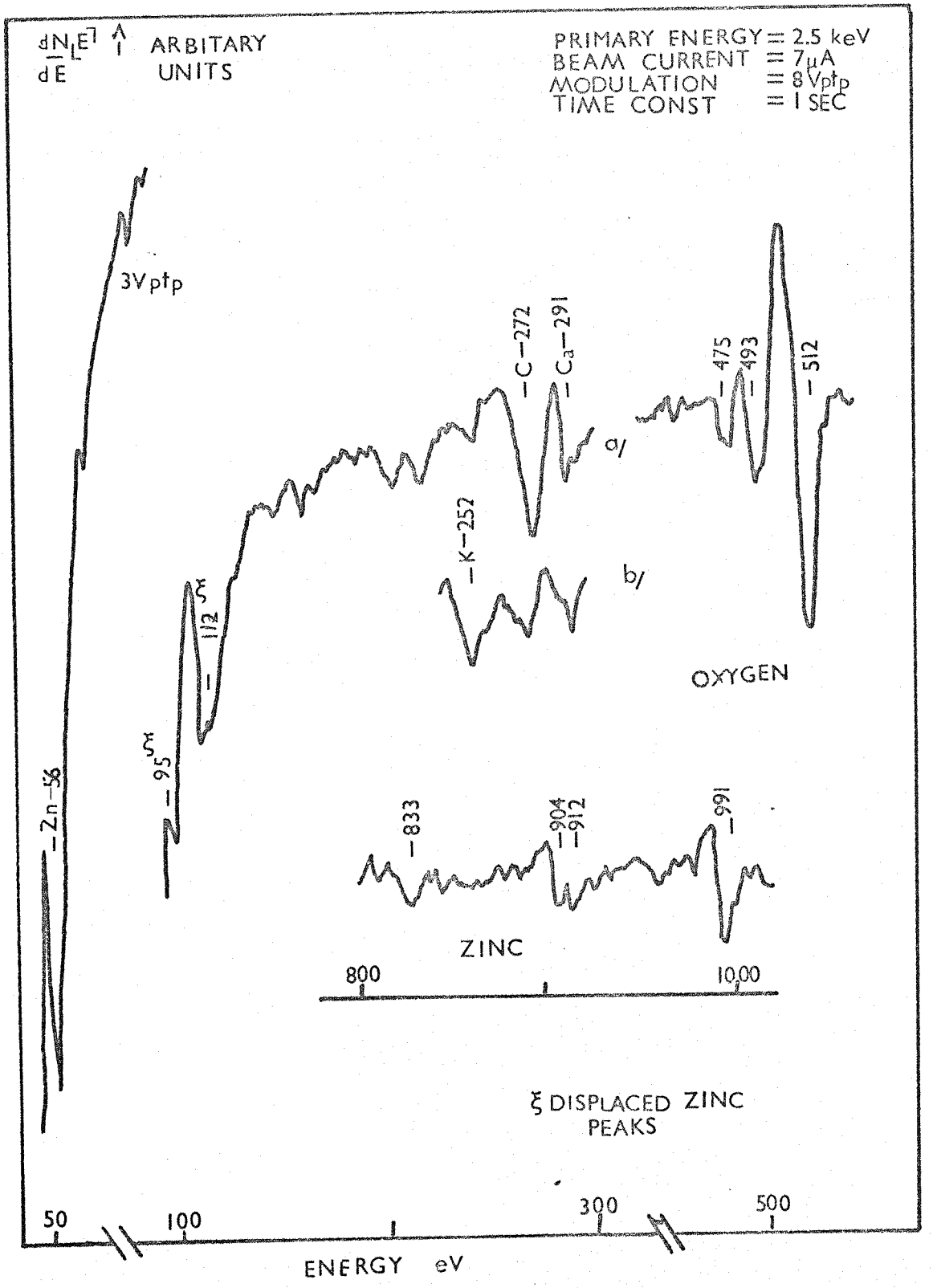

Figure 6.2 A.E. spectra of a/. 'as-mounted' O-polar surface and b/. K-contaminated surface. (For transition identification see Appendix I.).

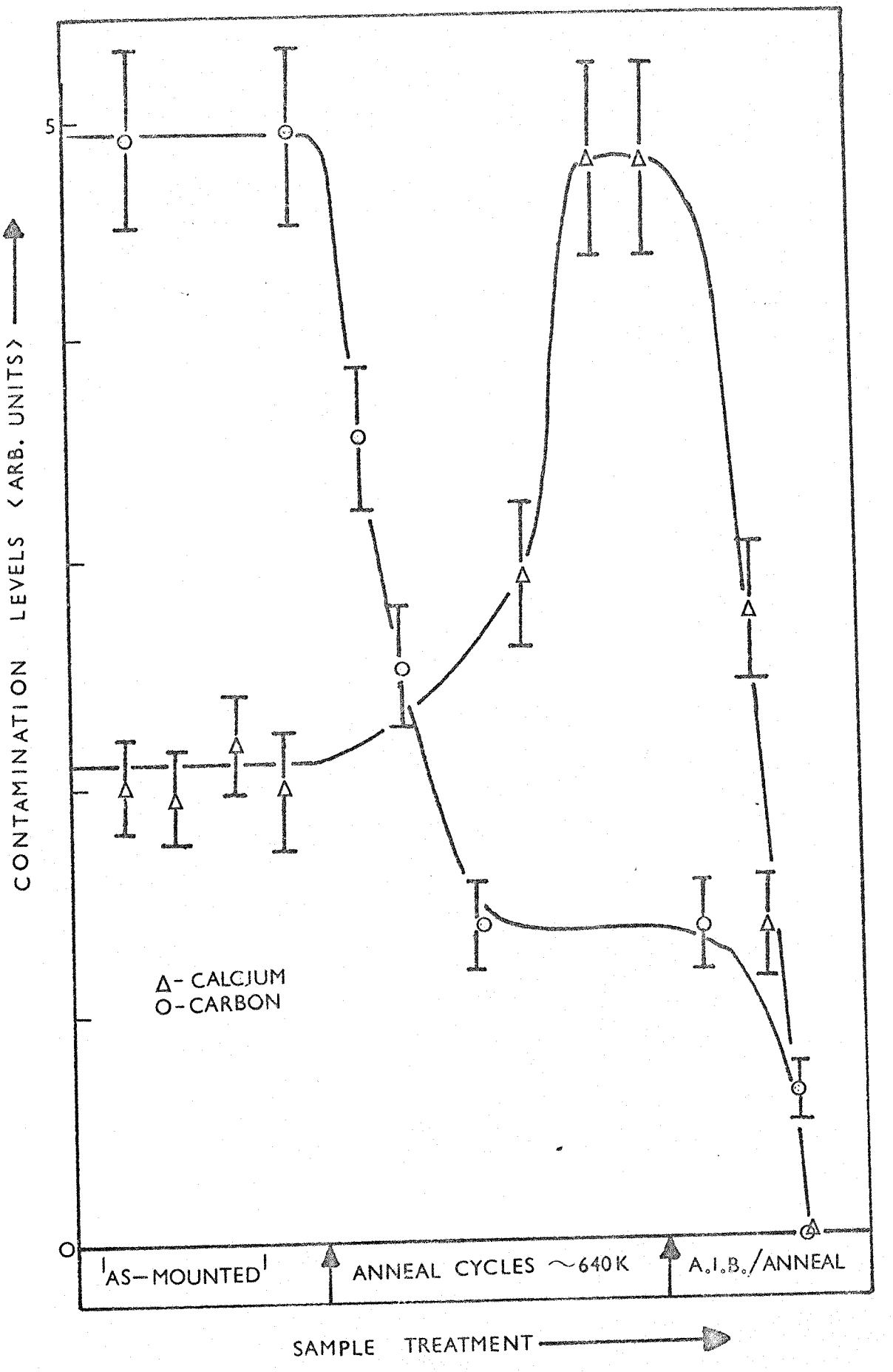

Figure 6.3 Variation of the calcium and carbon levels during cleaning.

peaks disappeared below the noise level, fig. 6.4. A corresponding LEED pattern showed a clear (1 x 1) structure, fig. 6.5. The presence of potassium must, in this study, be associated with segregation of an impurity from tungsten (which was used to support the crystal). Previous work by Hopkins et al, 1975, have, however, related this contaminant with preparatory chemical treatment of the sample.

6.5 SUMMARY AND DISCUSSION

There was a strong indication that calcium was present at the surface due to the outward diffusion of a bulk impurity. Also the anomalous low energy zinc peaks were found to disappear as soon as the calcium, having fully segregated to the surface, was partially removed. These results agree well with the proposal by Fiermans that a loss mechanism, caused by calcium in the first few surface layers, was responsible for the peak shifts. However, the details of the calcium interaction with the near surface layers of the lattice is not known. As with previous results, it was found that both calcium and potassium were tenaciously bound to the O-surface, which again indicated the importance of electropositive material necessary for charge stabilisation of this face. It was also interesting to note that carbon adsorption was achieved, presumably from the gas phase, although further work is required, especially on the effects of electron beams during exposure. As with the more recent results, an unreconstructed clean $(000\bar{1})$-O surface was obtained.

Although attempts have been made, particularly by Hopkins et al, 1975, to investigate the role of impurities on the polar faces of ZnO, it is impossible to determine accurately the effects of individual contaminants when several are present at the same time. For this reason a study of the interaction of electropositive and electronegative material with clean surfaces has been made. This work is reviewed in the next two chapters.

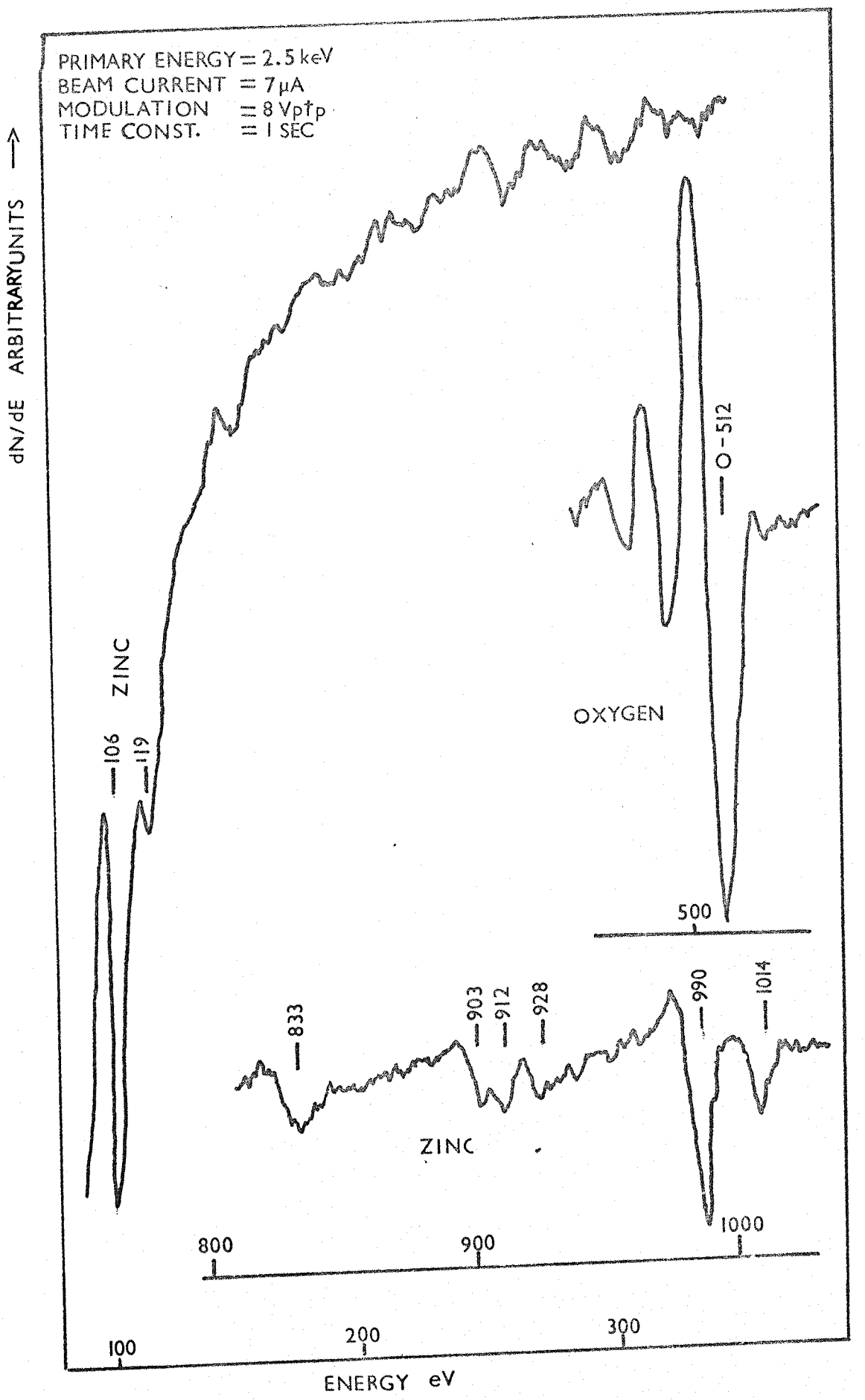

Figure 6.4 A.E. spectra of a clean oxygen polar surface.

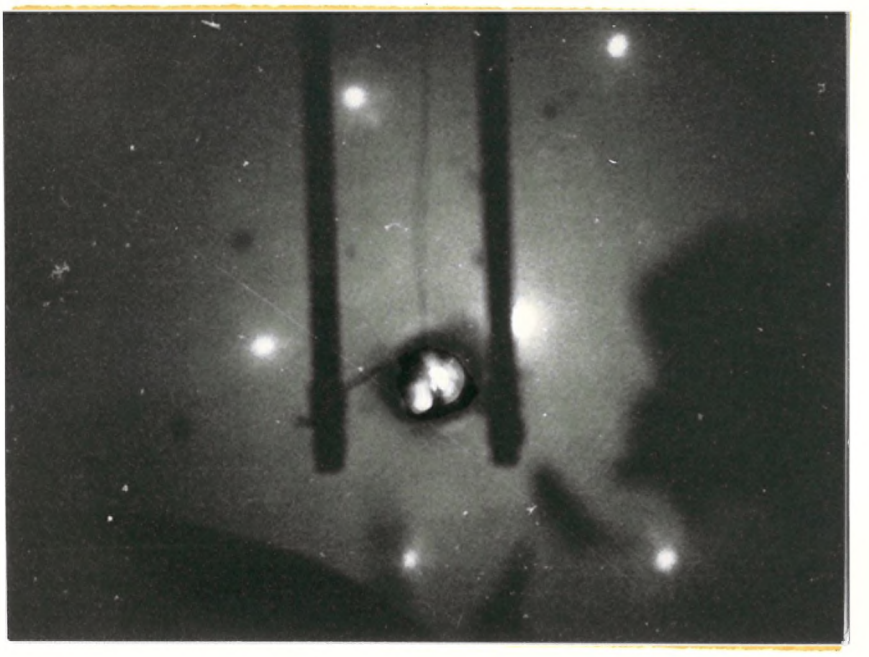

Figure 6.5 (1×1) LEED pattern of the oxygen polar surface.
80 eV

CHAPTER 7

H_2S ADSORPTION ON THE $(000\bar{1})$-O POLAR SURFACE OF ZnO

The adsorption of a slightly more complex molecule such as H_2S is, to some extent, a continuation of previous work, particularly since sulphur (together with carbon) has been shown to adsorb preferentially during exposure of clean ZnO surfaces to the atmosphere (Levine et al, 1972). While quantitative studies of residual sulphur present on "as-mounted" crystals are difficult, exposure of clean surfaces to H_2S provides a convenient and controlled method of re-deposition. Technical ZnO polycrystalline surfaces, e.g. powders,presumably also have an adsorbed carbon-sulphur layer and information concerning the effect of these contaminants on bulk and surface properties is again of interest. This chapter reviews previous work and presents the results obtained in the course of the present study.

7.1 PREVIOUS WORK

Although clean, (1 x 1) polar surfaces have been achieved by cleavage in u.h.v. or after ion bombardment, it is thought (van Hove and Leysen, 1972) that these faces are self-stabilised by charge transfer into surface states. Following Nosker's electrostatic predictions Leysen et al, 1975, calculated that impurity compensation was energetically more favourable and they investigated experimentally the interaction of caesium with a clean, (1 x 1) oxygen surface. They found that caesium adsorption was rapid and gave rise to Auger peak shifts of two of the high energy zinc transitions. (A similar effect was observed by Hopkins et al, 1975, when calcium was present at the surface). Initially LEED showed only a high intensity background, but after an anneal to 900 K a $(\sqrt{3} \times \sqrt{3})$ superstructure formed. The strong interaction of the caesium, suggested by the Auger peak shifts, was confirmed by the stability of the $(\sqrt{3} \times \sqrt{3})$ structure

which persisted even after severe heating to 1100 K for 1 hour. Its subsequent removal, together with the Cs-Auger signal, was only achieved by ion bombardment. The formation of a ($\sqrt{3}$ x $\sqrt{3}$) superstructure more than satisfies electrostatic stability requirements as it corresponds to $\sim \frac{1}{3}$ of a monolayer coverage. It was proposed that a change from a (1 x 1), surface state compensated to a ($\sqrt{3}$ x $\sqrt{3}$), caesium compensated surface had been observed. It was also found that after caesium deposition and an anneal to lower temperatures ($\sim$ 650 K), a (2 x 2) superstructure formed which on further heating transformed into a combined (2 x 2) + ($\sqrt{3}$ x $\sqrt{3}$). The presence of a (2 x 2) was of particular interest since it fulfils exactly the compensation criterion of a $\frac{1}{4}$ of a monolayer of unit positive (Cs^{1+}) charge. However, electrostatic surface energy calculations give a lower surface energy for the (2 x 2) which tended to contradict the experimental evidence that the ($\sqrt{3}$ x $\sqrt{3}$) was at least as stable. Taylor et al, 1975, suggested a possible refinement to the electrostatic model to take into account the bonding characteristics of the surface adions. For the ($\sqrt{3}$ x $\sqrt{3}$) structure all sp^3 dangling orbitals of the oxygen atoms can be saturated by making appropriate bonds with the vacant orbitals of the Cs-ions, whereas only $\frac{3}{4}$ of the available surface bonds are utilised with a (2 x 2) configuration. The remaining $\frac{1}{4}$ of a monolayer of oxygen atoms would then have a surface state-like bonding energy which gives the (2 x 2) structure an overall higher surface energy, comparable to that of the ($\sqrt{3}$ x $\sqrt{3}$). Experimentally, a saturated Cs-covered surface always favours the ($\sqrt{3}$ x $\sqrt{3}$) configuration.

The interaction of electronegative material with the O-surface, which requires positive charge for stabilisation, has been investigated mainly through the adsorption of oxygen. The disadvantage of using the same element as the substrate was particularly noticeable in A.E.S. where changes in existing Auger peaks are difficult to determine. Magoninski

and Kirby, 1975, reported large changes in the O/Zn ratio on exposure to oxygen, but large dosages were used, 15 hours at $\sim 10^{-1}$ torr. Work by Taylor, 1976, using much lower exposures, 2 hours at $\sim 10^{-8}$ torr, found only a 10% change in the O(513): Zn (991) ratio and no change in the (1 x 1) LEED pattern was observed. Work function measurements were more informative and after exposure to $\sim$ 10 L of O_2 an increase of 160 meV was seen. This increase was thought to result from dissociative adsorption - in agreement with conductivity measurements by Heiland et al, 1969. Heiland showed that exposure to atomic oxygen produced a depletion region resulting in upward bending of the band structure at the surface i.e. a positive work function change.

Further studies were made using chlorine and again both dissociative adsorption and a positive work function change were observed. A detailed review of this work will be left until the next chapter. A comparison of the relative activities of oxygen and chlorine with the O-surface indicates that the halogen was far more reactive. It was suggested that this reflected the difference in molecular bond energies [119 K cal mol^{-1} ($\sim$ 5.1 eV) and 58 K cal mol^{-1} ($\sim$ 2.5 eV) for Cl_2]. It was also suggested that the interaction of these two elements with the surface was dictated by the availability of sufficient surface energy to dissociate the incident molecule. It is thus interesting to note that the bond strengths of H_2S [90 K cal mol^{-1} ($\sim$ 3.9 eV) for HS-H and 82 K cal mol^{-1} ($\sim$ 3.5 eV) for S-H] are intermediate to those of Cl_2 and O_2. However, in this case both electropositive and electronegative material is present.

7.2 PRESENT STUDY

The results presented here are divided into sections corresponding, as far as possible, to the A.E.S., LEED and work function techniques used. The A.E.S. results are further divided to discuss supplementary experiments

performed on an initially contaminated surface. All the work was conducted at room temperature ($\sim$ 300 K) in vacuum conditions of $< 1 \times 10^{-9}$ torr.

7.2.1 A.E.S. Results - Contaminated Surface

Although the presence of surface impurities complicates the study of gas-surface interactions, preliminary work was carried out on a calcium-carbon contaminated sample. Calcium has a particular significance in the case of ZnO since it is a bulk impurity and as such may be an integral part of many technical ZnO substrates. H_2S adsorption studies were made at two stages during sample cleaning (which provided two contaminated states) and the corresponding A.E. spectra of the surface are shown in figs. 7.1(a) and 7.1(b). It was not possible to determine exactly the amount of the contaminants present, but because of the high purity of the crystal used and since there is no evidence for preferential diffusion of calcium to the O-surface, it is unlikely that there was enough bulk calcium to produce "monolayer" coverage. The calcium level of "state (1)" was, however, sufficient to produce a highly stable ($\sqrt{3} \times \sqrt{3}$) LEED superstructure and caused low energy Zn peak changes, as discussed in chapter 6. The ($\sqrt{3} \times \sqrt{3}$) structure would, assuming that the calcium was not confined to islands or domains, correspond to $\sim \frac{1}{3}$ of a monolayer coverage. From previous work in this laboratory and from a comparison with precleaning A.E. spectra, it is estimated that carbon contamination was slight. Thus, the main difference between the two "states" was the quantity of calcium present, "state (1)" having appreciably more than "state (2)", as indicated by the Ca/O Auger peak height ratios of 0.48 ± 0.05 and 0.15 ± 0.01 respectively.

Admission of H_2S to pressures of between 5×10^{-9} and 2×10^{-8} torr resulted in the adsorption profiles of fig. 7.2. Since hydrogen could not be detected, having no Auger process, H_2S coverage was plotted using the 150 eV sulphur transition (see for example fig. 7.4). To minimise

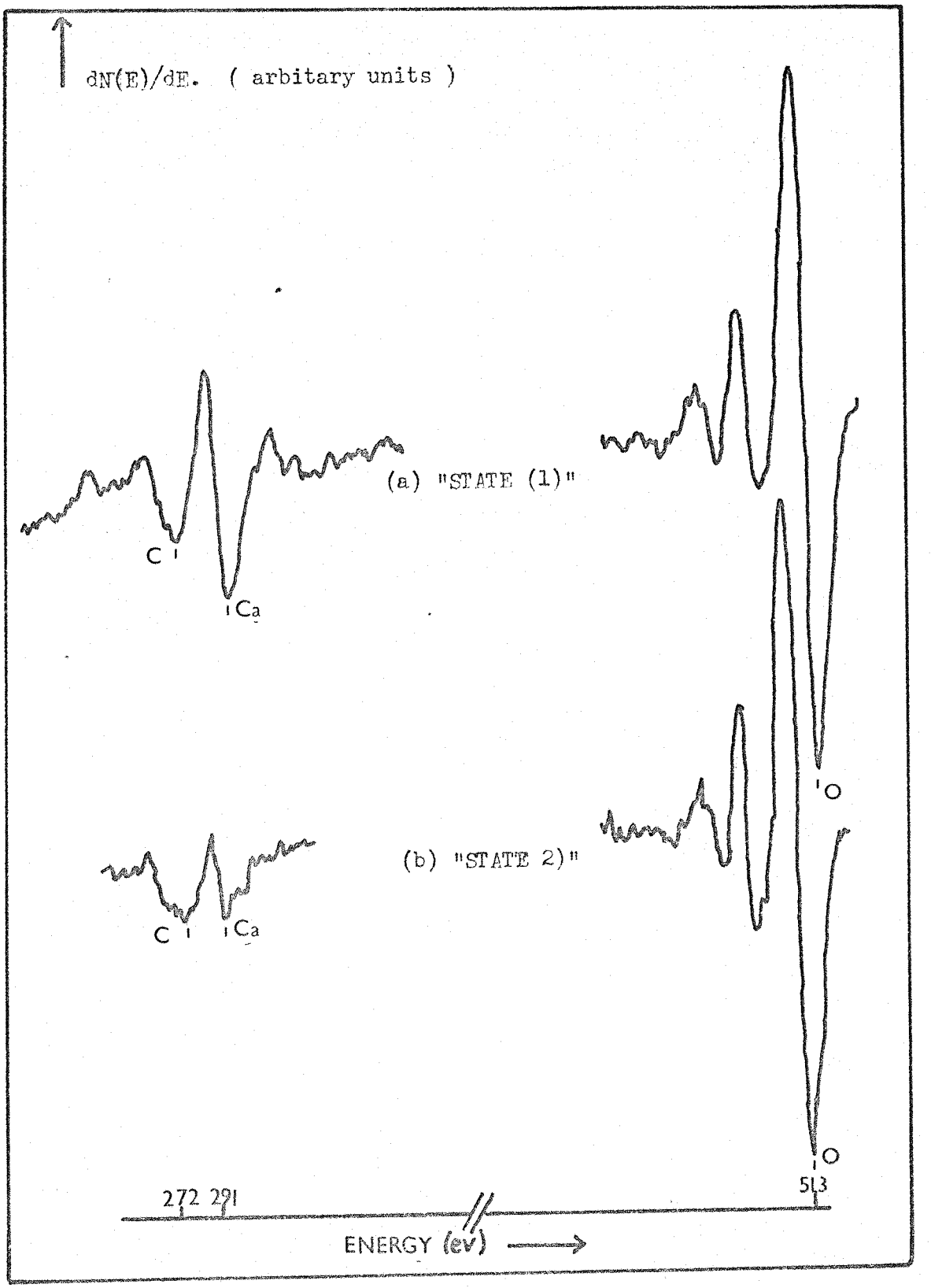

Figure 7.1 A.E. spectra of the $(000\bar{1})$ surface under two "states" of contamination.

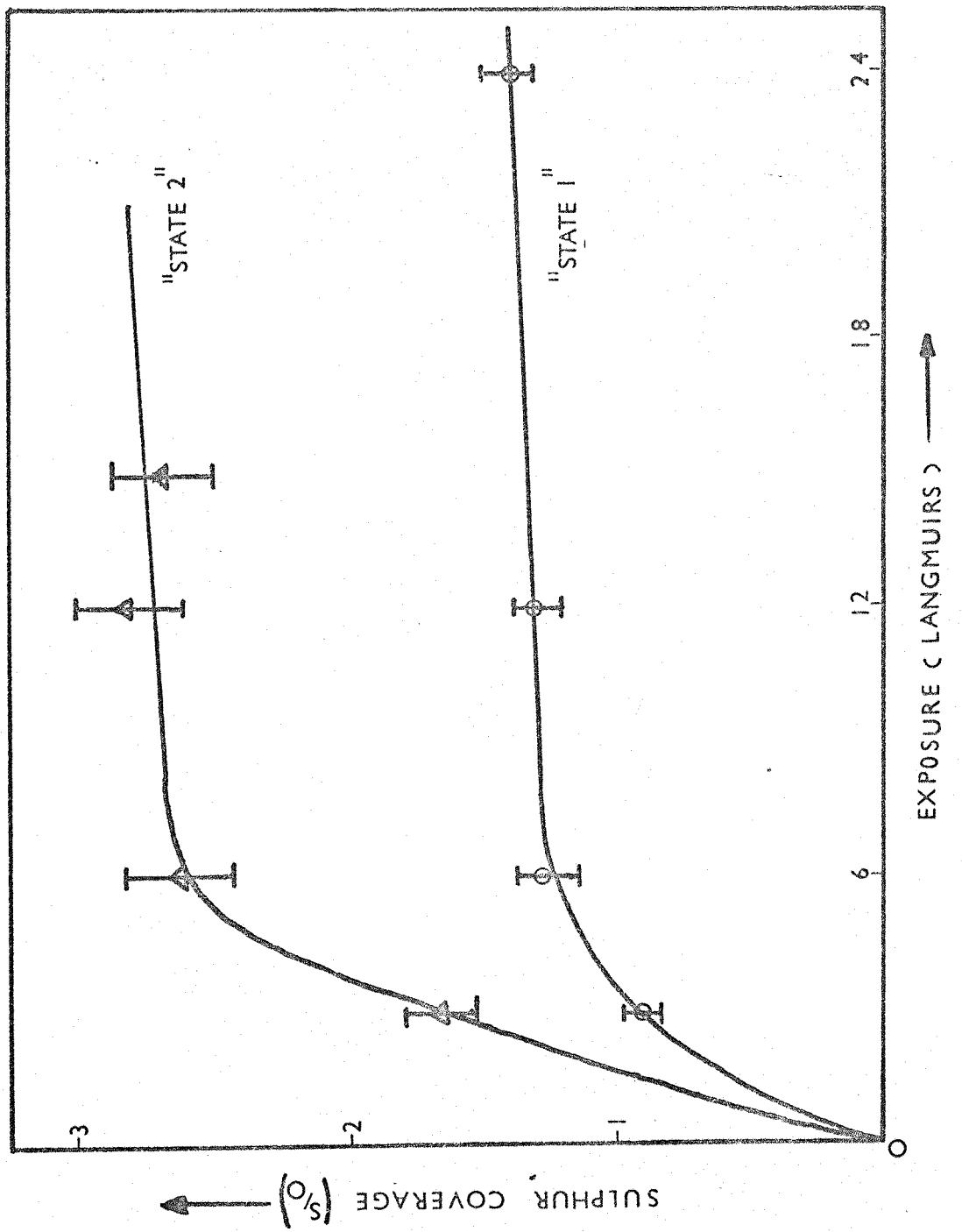

Figure 7.2 H_2S adsorption on Ca-C contaminated $(000\bar{1})$ surfaces.

possible effects of the beam it was switched off during exposure and between successive measurements the previously adsorbed sulphur was removed. (During the course of these experiments the calcium levels remained constant and only slight fluctuations (< 10%) were observed for carbon). Because of electronic drift the sulphur peak was normalised to the 513 eV oxygen transition. Saturation of both "states" occurred after $\sim$ 5 Langmuirs exposure, but the S/O ratio for "state (2)" (2.7 ± 0.3) was more than twice that for "state (1)" (1.2 ± 0.1). The increased adsorption of H_2S on the least contaminated surface may simply be explained by the availability of more "free" surface bonds, however, it was noted during cleaning that the sulphur was also more strongly bound to this surface. Whereas sulphur removal from "state (1)" was achieved merely by exposure to the A.E.S. electron beam for several μA-minutes, mild thermal treatment was required for its removal from "state (2)".

7.2.2 A.E.S. Results - Clean Surface

Exposure of the clean surface to $\sim$ 180 Langmuirs (10^{-7} torr for 30 minutes) resulted in a S/O ratio of 3.0 ± 0.2. This was only $\sim$ 10% above the value found for the least contaminated "state (2)" of the previous section and confirmed that the Ca-C impurity levels were small. It can also be seen that saturation of the clean surface must occur after a similar exposure to that indicated in fig. 7.2, $\sim$ 5 Langmuirs. The above measurement, as with those of the previous section, was made with the A.E.S. electron beam switched off during exposure. The use of an electron beam during adsorption often necessitates a correction of A.E.S. peak heights to account for electron induced desorption. Although beam desorption of sulphur was observed in vacuo, a more dominant effect was present, that of enhanced sulphur deposition, in H_2S. For a H_2S pressure of 5×10^{-9} torr and with the use of two different beam currents, the adsorption profiles of fig. 7.3 were obtained. Saturation again seemed

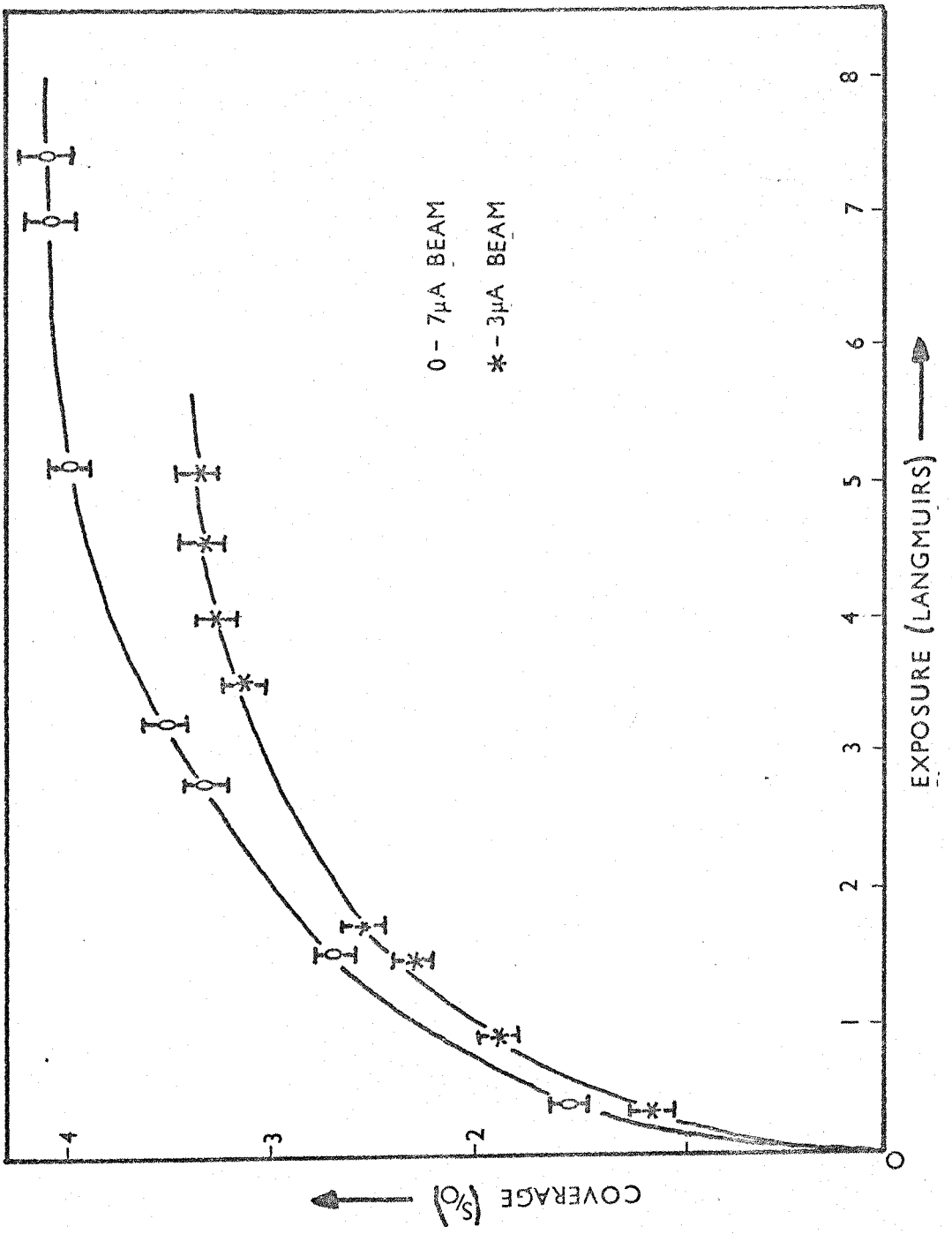

Figure 7.3 Variation of sulphur adsorption with incident beam current.

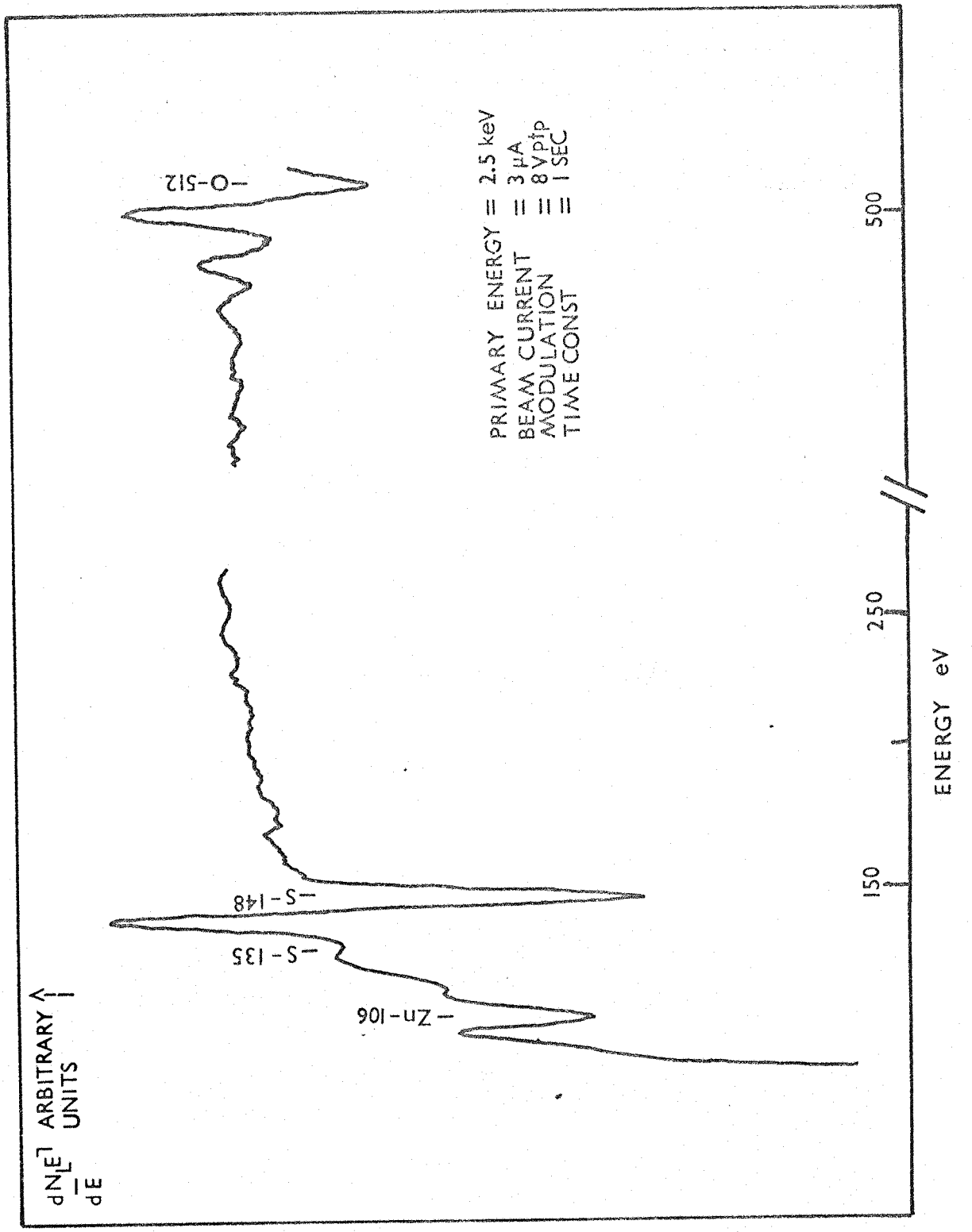

Figure 7.4 A.E. spectrum showing the presence of sulfur on the O-polar surface. A S/O level of 2.2±0.2 is indicated.

occur after an exposure of $\sim$ 5 Langmuirs, but the S/O ratios of 3.3 ± 0.3 and 4.1 ± 0.4, corresponding to the 3 and 7 μA electron beams used, indicated a strong dependence on the incident electron flux density. With a beam current of 3 μA and H_2S pressures of between 2×10^{-8} and 1×10^{-7} torr, the profiles of fig. 7.5 were plotted. Pressure dependence was exhibited and saturation was not achieved. The curves of fig. 7.5 are indistinguishable up to a S/O ratio of $\sim$ 9 from which point the sulphur coverage then increases with pressure.

Following sulphur deposition and evacuation of H_2S from the chamber, continued exposure of the sample to the electron beam resulted in a decrease of the normalised sulphur signal. It was also noted that the rate of desorption was dependent on the initial sulphur level. When adsorption took place in the absence of the electron beam and a saturated sulphur coverage, (S/O = 3.0 ± 0.2), was achieved, the subsequent beam desorption was as summarised in fig. 7.6. The curve exhibits two distinct sections with differing desorption rates. It was possible to calculate the sulphur desorption cross-sections, for electrons, from the equation,

$$N = N_o \exp - (\sigma \phi t) \qquad 7.1$$

where N/N_o is the fractional change in sulphur signal, ϕ is the beam flux, t is the time of beam exposure and σ the total cross-section for the process. The values obtained for fig. 7.6 were, for the first region, $\sigma_m = (3 \pm 2) \times 10^{-23}$ m^2 and for the second, $\sigma_{LS} = (5 \pm 3) \times 10^{-24}$ m^2. (The subscripts assigned to the cross-sections are defined in section 7.3). The first and larger cross-section, σ_m, was not present during beam desorption from sulphur levels deposited under the electron beam. However, for a beam adsorbed sulphur level of 3.4 ± 0.3, a desorption cross-section of $(4 \pm 2) \times 10^{-24}$ m^2 was found, comparable to that of σ_{LS}. Beam

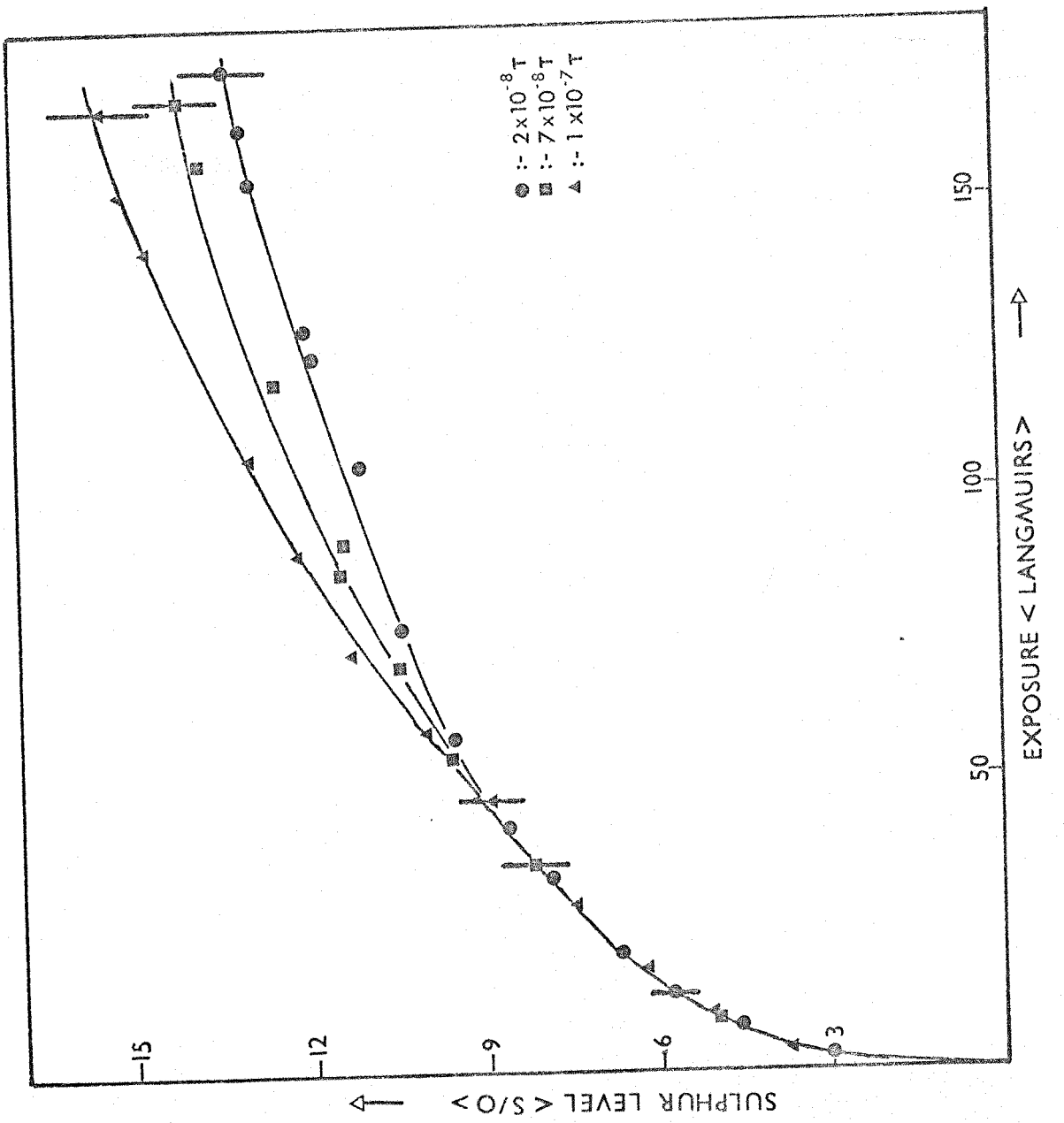

Figure 7.5 Variation of sulphur deposition with pressure, using a constant beam current.

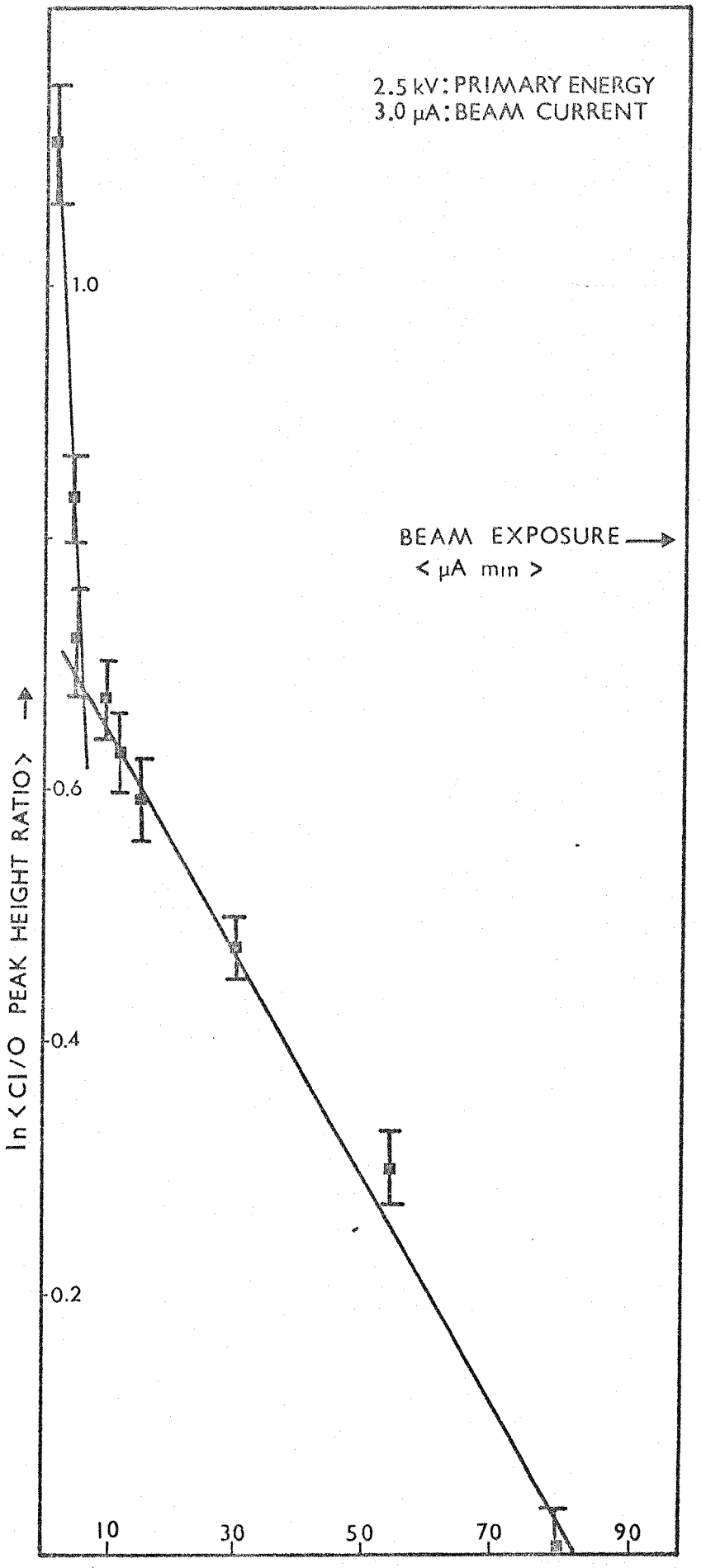

Figure 7.6 Electron-beam desorption curve showing two beam cross-sections.

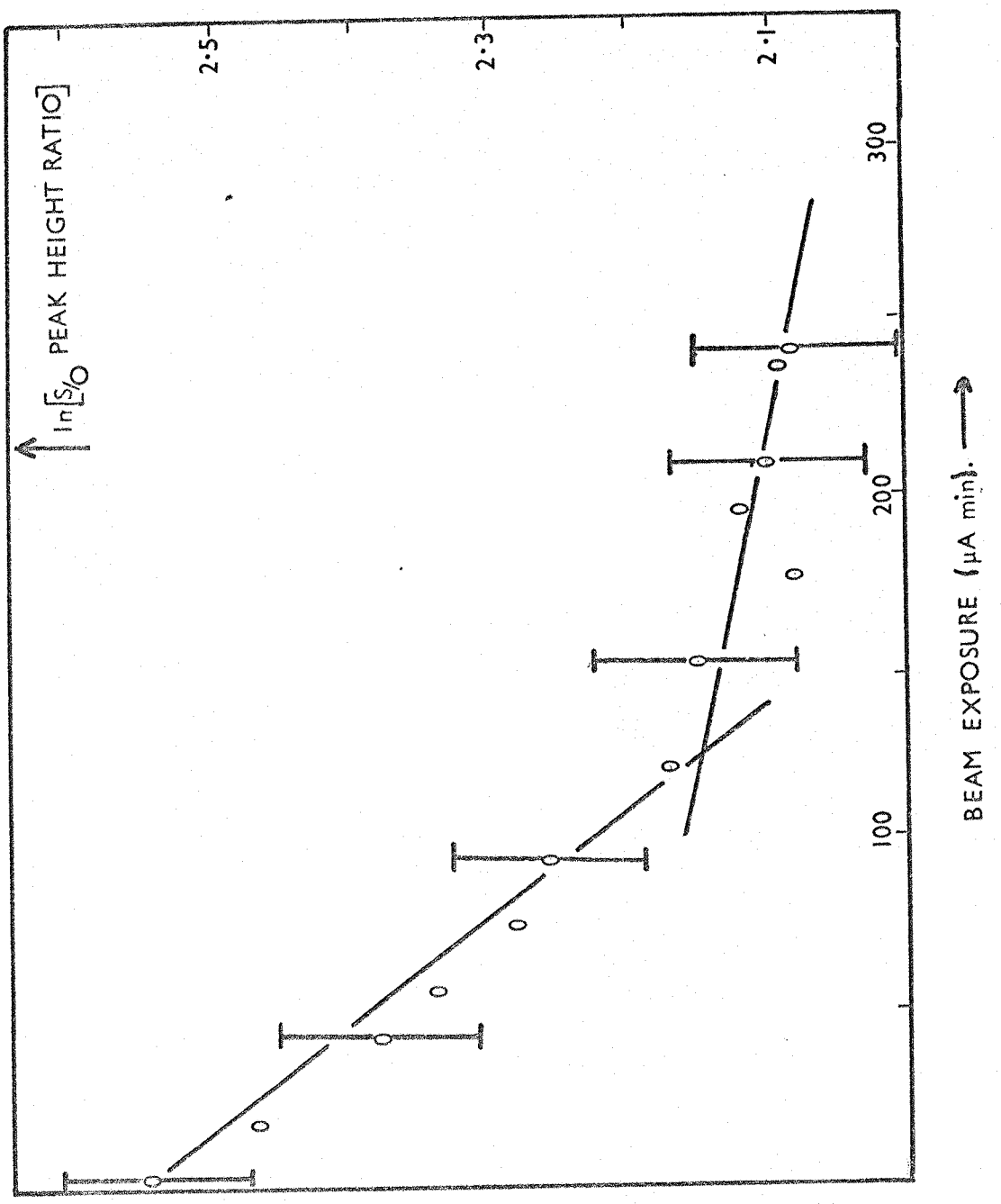

Figure 7.7 Electron-beam desorption curve showing two beam cross-sections.

Initial S/O	Cross-section (m^2)	"Cross-over" S/O	Cross-section (m^2)
14.7 ± 1.2	$\langle 2 \pm 1 \rangle \times 10^{-24}$	8.6 ± 0.7	$\langle 3 \pm 2 \rangle \times 10^{-25}$
4.8 ± 0.4	–	–	$\langle 5 \pm 3 \rangle \times 10^{-25}$
3.4 ± 0.3	–	–	$\langle 4 \pm 2 \rangle \times 10^{-24}$
† 3.0 ± 0.2	$\langle 3 \pm 2 \rangle \times 10^{-23}$	1.9 ± 0.2	$\langle 5 \pm 3 \rangle \times 10^{-24}$

† NO ELECTRON BEAM DURING ADSORPTION.

Table 7.1 Electron beam desorption cross-sections of sulphur from the oxygen polar surface of ZnO.

desorption from higher sulphur coverages was as shown in fig. 7.7. Again two cross-sections were derived, $\sigma_{SS} = (2 \pm 1) \times 10^{-24}$ m^2 and $\sigma_{HS} = (3 \pm 2) \times 10^{-25}$ m^2 and the cross-over point occurred at a S/O ratio of 8.6 ± 0.7. Finally, for an initial sulphur coverage of S/O = 4.8 ± 0.4, a cross-section of $(5 \pm 3) \times 10^{-25}$ m^2 resulted, comparable to that of σ_{HS}. Thus, four sulphur desorption cross-sections, for electrons, were exhibited; firstly, σ_m, present only when sulphur was deposited without the electron beam, secondly, σ_{SS}, corresponding to desorption of sulphur from S/O levels of > 9 and finally, σ_{LS} and σ_{HS}, corresponding to desorption of low sulphur (S/O < ∿ 3.5) and high sulphur (∿ 5 < S/O < ∿ 9) coverages respectively. These results are summarised in table 7.1.

Vacuum desorption was present at very high (S/O > 9) sulphur coverages but at S/O levels of ∿ 9, only ∿ 10% reduction resulted after a 12 hour period in vacuo. This was noted because, due to long anneal times (several hours), a "stable" reference coverage was needed in thermal desorption measurements. To reduce the effect of vacuum desorption, successive points on the thermal desorption curve, fig. 7.8, were made after re-adsorption of sulphur to the "stable" level of S/O = ∿ 9. The curve shows that rapid removal of sulphur in a temperature range of ∿ 70 K took place and that complete removal occurred at ∿ 590 K. During heating, a mass spectrometer was used to monitor hydrogen evolution, fig. 7.9. Only a slight increase in the partial pressure of atomic hydrogen was observed but at ∿ 590 K molecular hydrogen began to evolve, evolution reaching a peak at ∿ 650 K. It has been shown (Mineault and Hansen, 1966) that hydrogen desorbs from tungsten, which was used for the crystal mount, in a similar temperature range. Thus hydrogen evolution from the sample and its support could not be distinguished.

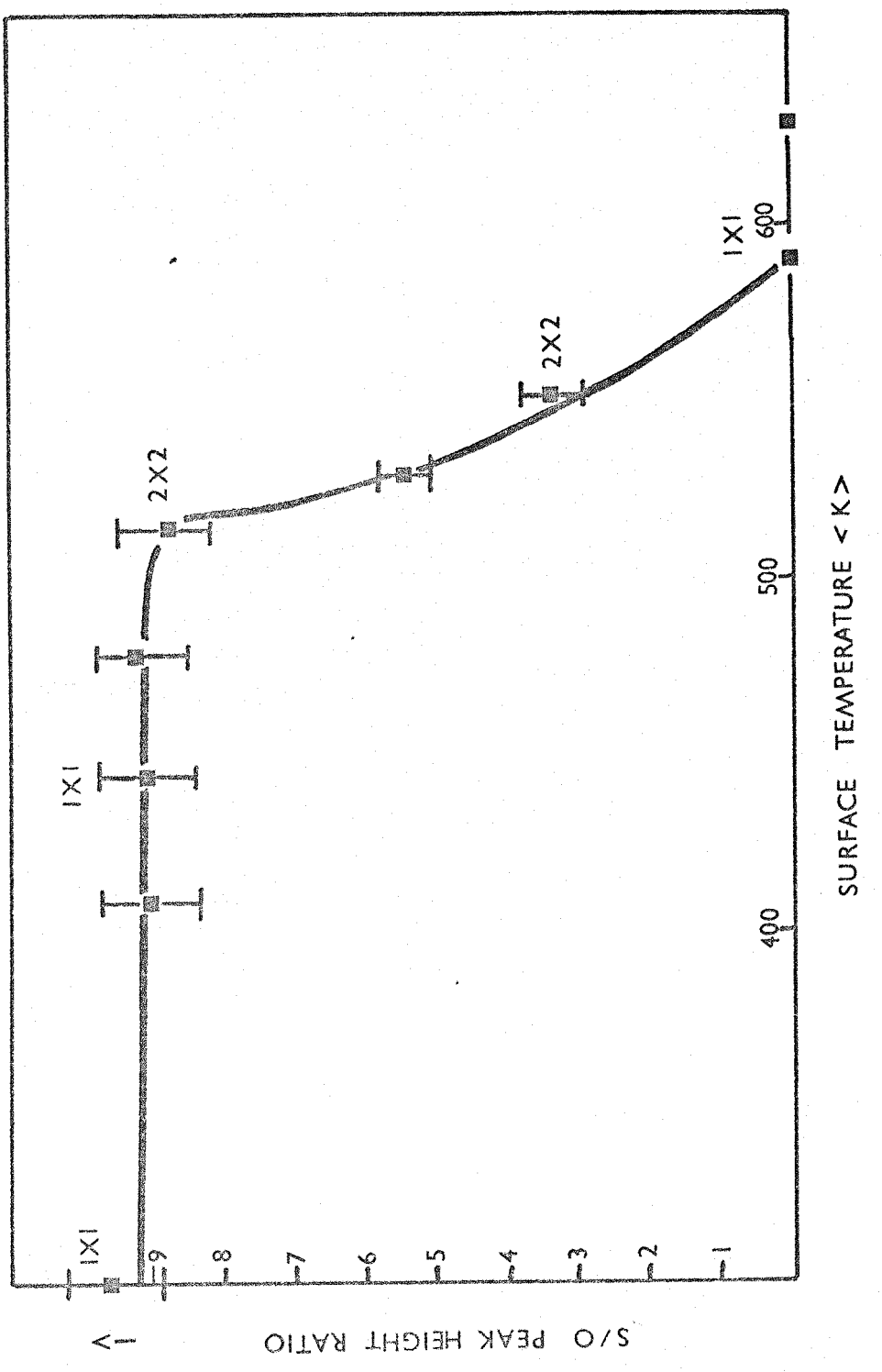

Figure 7.8 Thermal desorption of sulphur, showing the observed LEED structures.

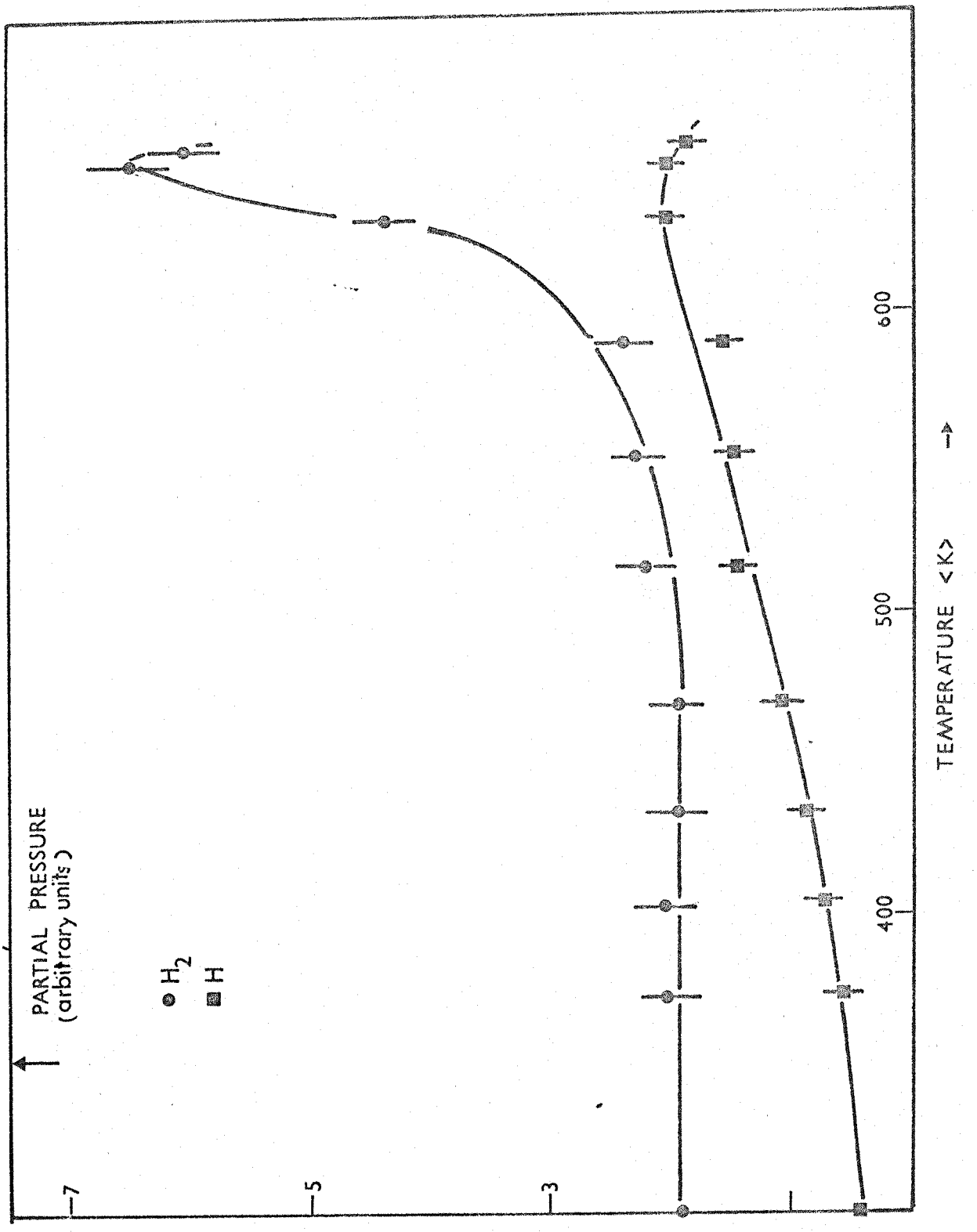

Figure 7.9 Partial pressures of H and H_2 during sample heating.

7.2.3 LEED Results

Absorption of H_2S independent of pressure and with or without the beam, produced no "extra" LEED spots, at 300 K and the (1 x 1) structure remained, fig. 7.10. On heating to a temperature of $\sim$ 500 K, ordering into a (2 x 2) configuration occurred, fig. 7.11. This superstructure persisted to $\sim$ 600 K, see fig. 7.8, at which point complete removal of sulphur took place.

7.2.4 Work Function Results

Exposure to H_2S pressures of $\sim 10^{-7}$ torr resulted in an initial change in work function, $\Delta\phi$, of $\sim$ - 600 meV, after an exposure of $\sim$ 1.5 Langmuirs, fig. 7.12. Although this initial change was generally reproducible, subsequent variations with exposure were not and ranged, in different experiments, from only a slight change, as shown in fig. 7.12, to changes where a gradual return to the origin took place. (Variations in voltage calibration were noted during the course of these experiments, but it was not possible to satisfactorily correlate these with the changes in work function). Following evacuation of H_2S from the chamber a partial reversal of the negative change resulted, but due to the preceding unreproducibility,were not quantified.

7.3 SUMMARY AND DISCUSSION

An obvious limitation of the present study was the inability to detect hydrogen at the crystal surface directly. However, if it is assumed that the H_2S/ZnO interaction can adequately be defined from a study of the sulphur component of the gas then, the A.E.S. results for the clean surface may be summarised as follows. Firstly, without the aid of the electron beam, saturation of the surface occurred after $\sim$ 5 Langmuirs exposure to H_2S which gave as S/O ratio of 3.0 $\pm$ 0.2. Secondly, there were two cross-sections for sulphur desorption by electrons from

7.10 (1X1) LEED pattern of clean polar surface.
80 eV.

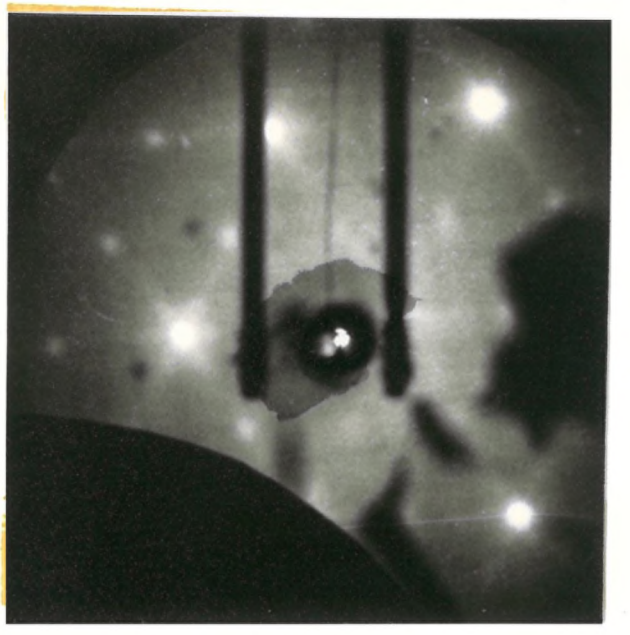

7.11 (2X2) LEED structure $(000\bar{1})$-O + H_2S.
70 eV.

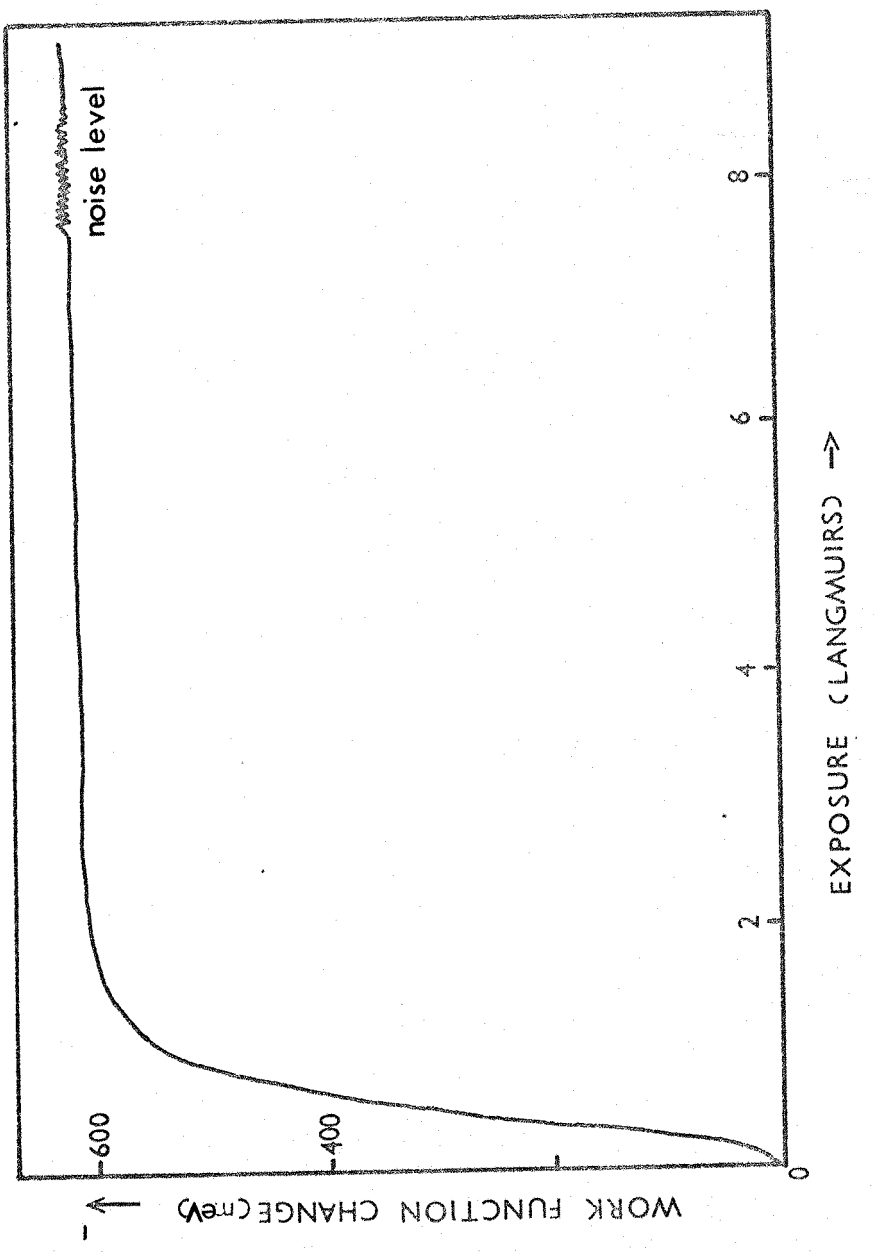

Figure 7.12 Direct trace of work function change (negative) against H_2S exposure for the (000$\bar{1}$) surface.

this coverage. Initially, desorption was rapid with a cross-section, σ_m, of $(3 \pm 2) \times 10^{-23}$ m^2 but after less than 10 μA min exposure, desorption proceded at a slower rate with a cross-section, σ_{LS}, of $(5 \pm 3) \times 10^{-24}$ m^2. Since a cross-section of the order of σ_m was not present in desorption experiments where sulphur was adsorbed under the electron beam and since it is probable that the effect of the beam was to dissociate the incident H_2S molecules, then it would suggest that σ_m corresponds to a weakly bound molecular state. The work on molecular chlorine and oxygen, from which it was proposed that adsorption was dependent on the availability of sufficient surface energy to dissociate the incident molecules, would suggest that a dissociated, sulphur bearing species of H_2S, with desorption cross-section σ_{LS}, was also present. This also implies that "free" hydrogen existed at the surface during adsorption.

The presence of atomic hydrogen at the surface would explain the observed decrease in work function. It was shown (Heiland, 1969) that hydrogen produces an accumulation region resulting in a downward bending of the band structure at the surface (i.e. a decrease in work function). However, molecular adsorption also reduces the work function of a surface and must, in this study, account for at least part of the observed change, particularly since a partial reversal of the work function decrease took place on evacuation of H_2S from the chamber. Adsorption of sulphur, on the other hand, as with chlorine and oxygen would lead to an increase in work function.

LEED, in conjunction with thermal desorption data, showed a connection between a (2 x 2) superstructure and the presence of sulphur, fig. 7.8. A possible arrangement of adatoms which would exhibit a (2 x 2) LEED configuration is shown schematically in fig. 7.13. It is interesting to note that a ¼ of a monolayer of unsaturated surface oxygen bonds remain, which, if saturated with electropositive material would fulfil

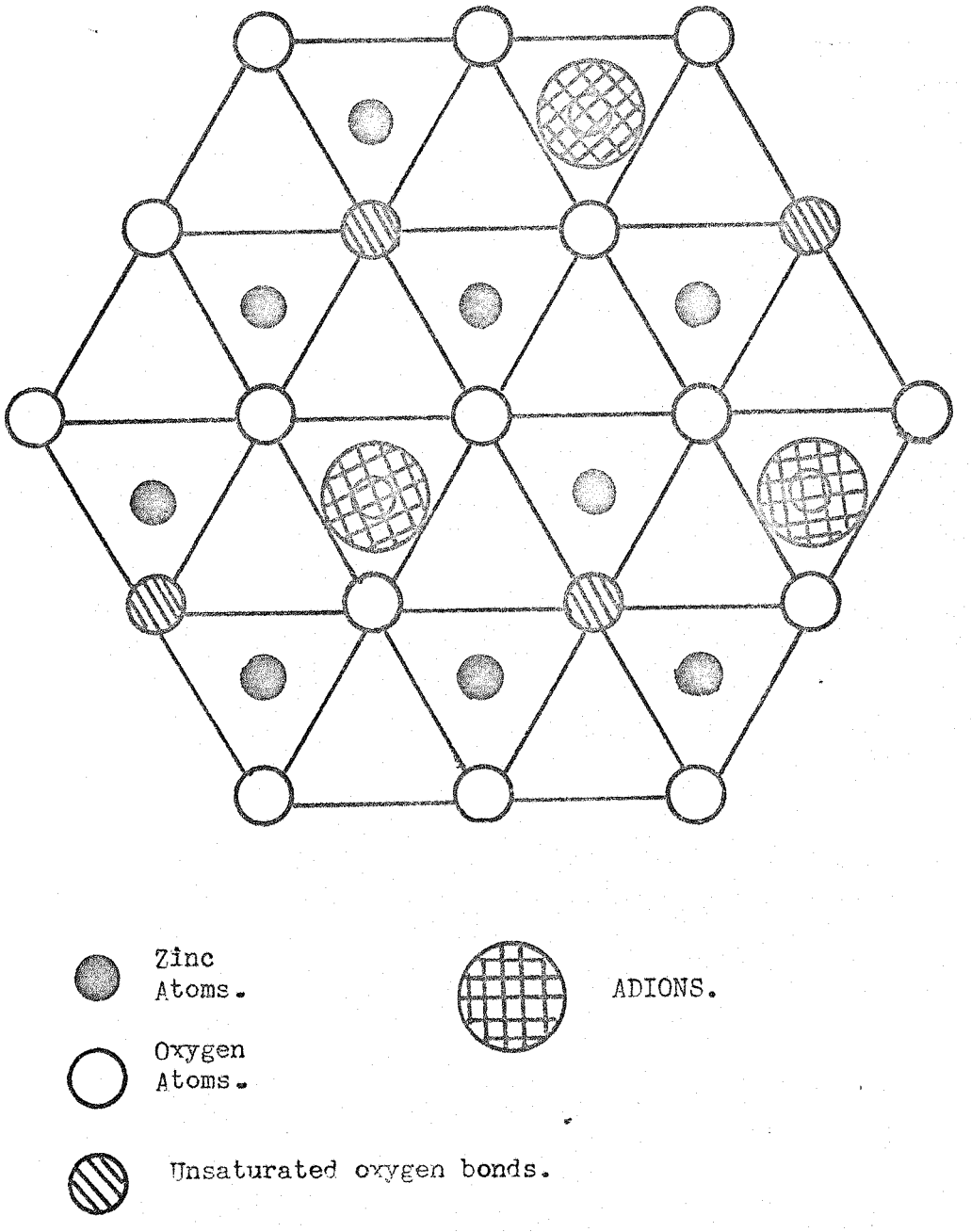

Figure 7.13 Schematic diagram of $(00\bar{1})$ surface showing a possible (2×2) arrangement and the $\frac{1}{4}$ monolayer of unsaturated oxygen bonds.

Nosker's electrostatic requirement. Thus, it is possible for charge compensation to be affected by hydrogen ions, from dissociated H_2S, and also allow the formation of a (2 x 2) sulphur adlayer.

Sulphur deposition, under the electron beam exhibited dependence on both the incident electron flux and the H_2S pressure used. The pressure dependence became most obvious at a sulphur coverage corresponding to S/O $\simeq$ 9. The stability of this sulphur level was indicated by its resistance to vacuum desorption and by the small electron desorption cross-section, σ_{HS}. At higher coverages (S/O > 9) the adsorption process changes, indicated by the larger cross-section (σ_{SS}), and the magnitude of vacuum desorption. That monolayer coverage, or at least a significant sulphur coverage, occurred at S/O = 9 would mean that the subsequent interaction was between H_2S and the sulphur adlayer (hence "SS" in σ_{SS}). There still remains a distinction between "sub-monolayer" coverages exhibited by the differing cross-sections of σ_{LS} (low sulphur coverage) and σ_{HS} (high sulphur coverage). Since σ_{HS} is less than σ_{LS} it implies a stronger interaction with the surface when more sulphur is present. Whether this is due to an interaction between the sulphur adions or by the presence of interstitial hydrogen in the adlayer is not clear.

Thus, adsorption of H_2S on the clean O-polar surface is a competitive process between the two elemental components of the gas. Saturation without the beam occurs after an exposure of $\sim$ 5 Langmuirs which is accompanied by a decrease in work function, probably due to both dissociated hydrogen and molecular adsorption. It is possible that charge stabilisation by dissociated hydrogen and a (2 x 2) sulphur structure can coexist. Beam dissociation of the incident H_2S molecules enhanced sulphur deposition and at S/O ratio of $\sim$ 9 it is suggested that the adsorption process changes from one of H_2S on ZnO to one of H_2S on an adsorbed sulphur-hydrogen adlayer.

Saturation of the contaminated surface of "state (2)" was at a comparable sulphur level to that of the clean surface and it would appear that the contamination of this "state" was only slight. The presence of calcium in the surface of "state (1)" greatly reduced H_2S adsorption and the ease of removal of the adsorbed layer would suggest that it was in the form of a weakly bound molecular state. If charge stabilisation of the surface by calcium was achieved, with a resultant decrease in surface energy, then the incident molecules were not dissociated as in the case of "state (2)" or the clean surface.

H_2S gas pressures were measured using a standard Bayard-Alpert gauge and a gauge factor for H_2S was assumed to be the same as that for nitrogen (i.e. 1). However, an estimated value of 2.2 has been proposed by Summers (1969), but no experimental results were reported.

CHAPTER 8

CHLORINE ADSORPTION ON THE $(000\bar{1})$ POLAR SURFACE OF ZnO

The first section of this chapter reviews previous work, performed in this laboratory (Taylor, 1976) on the adsorption of chlorine on clean $(10\bar{1}0)$ prism and $(000\bar{1})$ polar surfaces. The purpose of the present study was to investigate the adsorption of chlorine on calcium-carbon contaminated $(000\bar{1})$ surface and these results are presented in section 8.2. A comparison between the two sets of results is made in the final section. All the measurements reported in this chapter were made in u.h.v. conditions at $\sim$ 300 K.

8.1 PREVIOUS WORK (CLEAN SURFACE STUDIES)

The presence of chlorine at the crystal surface was characterised by the addition, to the clean A.E. spectra, of peaks at 160, 167 and 182 eV (see for example fig. 8.1). In these experiments (Taylor, 1976) chlorine coverage was monitored from the height of the 182 eV transition which, was normalised to the 512 eV oxygen peak to reduce effects of electronic drift. Saturation of the $(000\bar{1})$-O polar surface, after exposure to 0.85 Langmuirs of Cl_2, resulted in a Cl/O peak height ratio of 4.5 ± 0.3. The reduced reactivity of the halogen with the neutral prism face was indicated by the saturation Cl/O ratio of 1.5 ± 0.1, achieved after exposure to $\sim$ 9 Langmuirs. Electron beam desorption curves for the two surfaces exhibited two states, fig. 8.2 and for the second state, in both cases, the cross-section was of the order of 10^{-25} m^2. Desorption cross-sections for the first state were calculated to be $(1 \pm 0.6) \times 10^{-22}$ m^2 and $(6 \pm 4) \times 10^{-23}$ m^2 for the $(000\bar{1})$ and the $(10\bar{1}0)$ faces respectively. A decrease in work function during adsorption on the $(10\bar{1}0)$ surface suggested that the weakly bound state, indicated by the large desorption

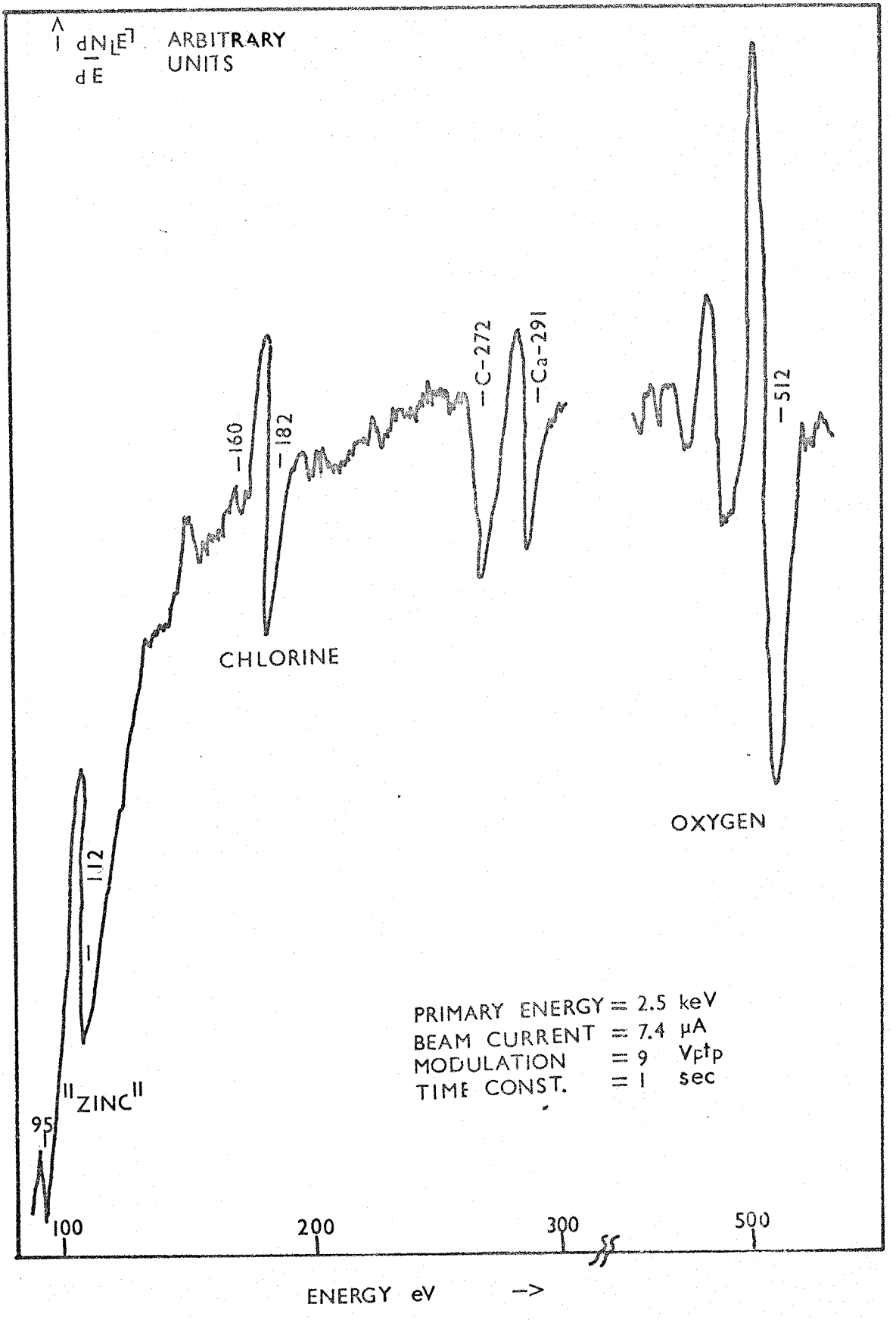

Figure 8.1 A.E. spectrum of the contaminated $(000\bar{1})$ surface, showing the chlorine transitions.

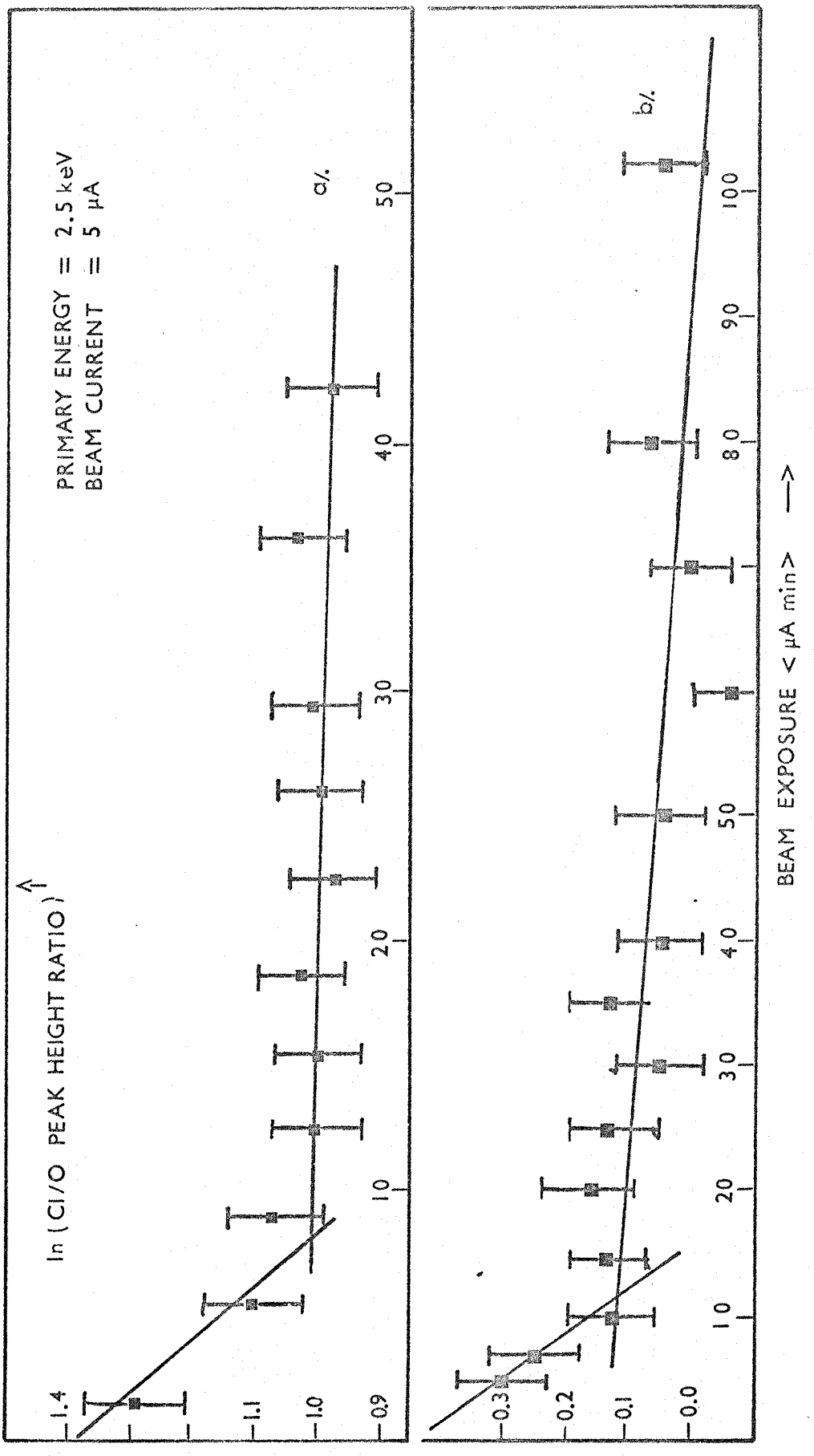

Figure 8.2 Electron-beam desorption curves for
a). O-polar surface
b). prism surface.

cross-section, was molecular. The more tightly bound state, having a relatively small desorption cross-section of $\sim 10^{-25}$ m^2, may have resulted from dissociated chlorine occupying sites created by the thermal desorption of oxygen ions. This is certainly possible physically (i.e. from consideration of size) and may explain the reaction of electronegative chlorine with a surface requiring the addition of positive charge for electrostatic stability.

Pressure measurements were recorded using a standard Bayard-Alpert gauge where the gauge factor was assumed to be the same as for nitrogen (Shaw, 1966).

8.2 PRESENT STUDY (CONTAMINATED SURFACE)

An A.E. spectrum of the contaminated $(000\bar{1})$ surface used in this brief study is shown in fig. 8.1. The carbon and calcium impurity levels were indicated by the C/O and Ca/O peak height ratios of 0.25 and 0.29 respectively (the calcium level was intermediate between those of the two contaminated "states" of section 7.2.1). Initially, admission of chlorine into the chamber resulted in considerable increases of CO and CO_2 partial pressures greatly reducing the purity of the halogen. However, after repeated flushing of the system, the chlorine purity was increased (to $\sim$ 70% at a total pressure of $\sim 5 \times 10^{-8}$ torr). The evolution of CO/CO_2 is attributed to displacement from the chamber walls and internal components by the highly reactive halogen.

Saturation of the $(000\bar{1})$ surface occurred after an exposure to $\sim$10 Langmuirs at a Cl/O ratio of 2.1 ± 0.2. Electron beam desorption of chlorine from this surface was as summarised in fig. 8.3. The curve exhibits two desorption cross-sections which, using equation 7.1, were calculated to be $(5 \pm 3) \times 10^{-23}$ m^2 for the first section and $(7 \pm 4) \times 10^{-24}$ m^2 for the second. These calculations, as with those of chapter 7,

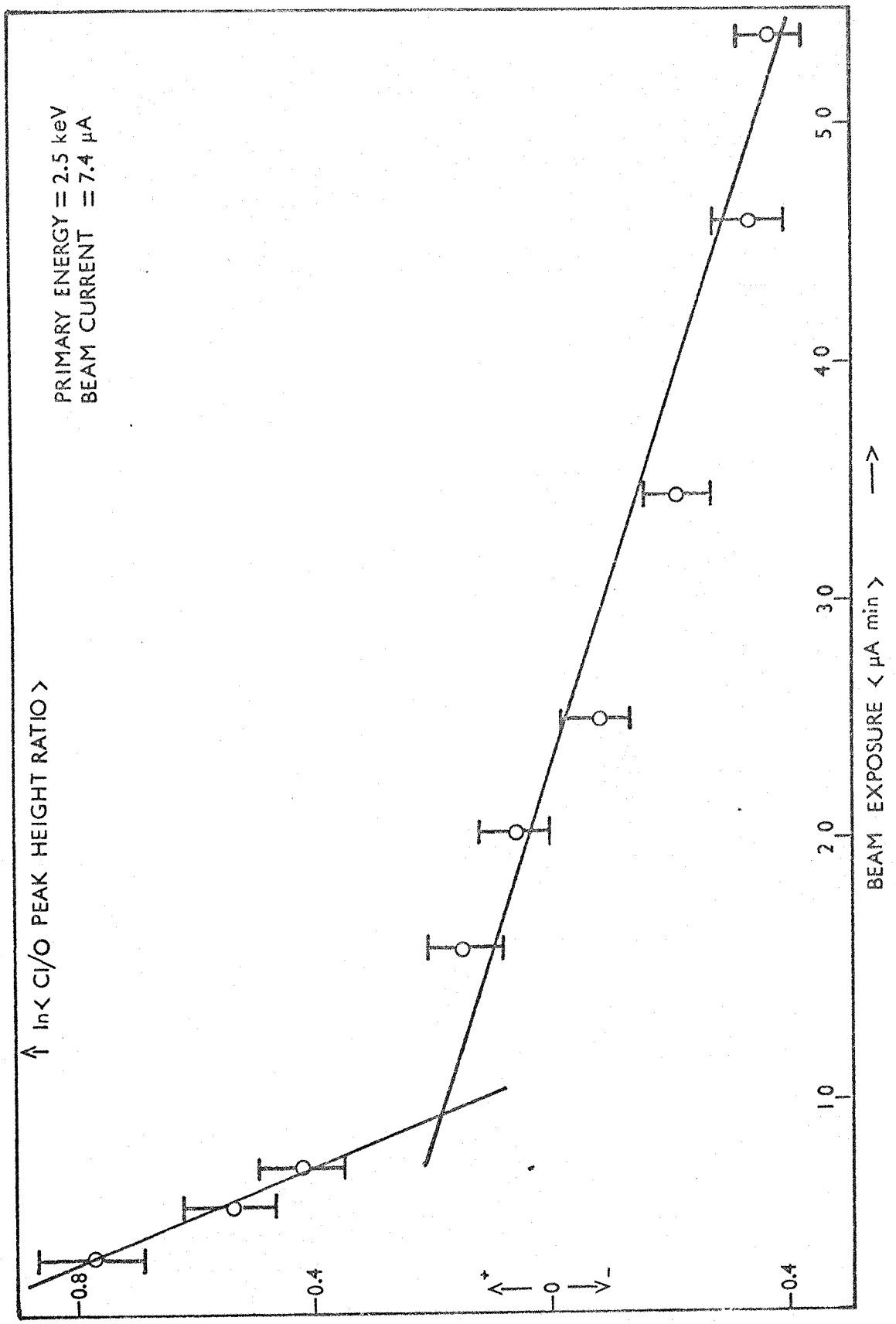

Figure 8.3 Electron-beam desorption curve for the contaminated $(000\bar{1})$ surface.

assumed a beam diameter of 0.5 ± 0.2 mm. This value was based on measurements performed on similar systems in this laboratory, (Jones, 1976).

8.3 DISCUSSION

The results of both the previous clean and the present contaminated surface studies are summarised in Table 8.1. The results for the contaminated O-surface show a marked reduction in the chlorine level over that found for the clean surface. This is presumably a result of the decrease in surface energy due to the presence of calcium which, as discussed in chapter 7, at least partially stabilised this face. Further, the magnitudes of both the desorption cross-sections for the contaminated surface are comparable to those of the proposed molecular state, again indicative of reduced reactivity. The similarity between chlorine adsorption on the contaminated $(000\bar{1})$ and the clean neutral $(10\bar{1}0)$ surfaces is also apparent, again reflecting the effect of surface stabilisation by calcium.

SURFACE	SATURATION CONDITIONS		DESORPTION CROSS SECTION $<m^2>$
	EXPOSURE $<L>$	Cl/O RATIO	
$(000\bar{1})$ CLEAN	0.85	4.5 ± 0.3	1. $(1 \pm .6) \times 10^{-22}$ 2. $(7 \pm 5) \times 10^{-25}$
$(10\bar{1}0)$ CLEAN	~9	1.5 ± 0.1	1. $(6 \pm 4) \times 10^{-23}$ 2. $(7 \pm 5) \times 10^{-25}$
$(000\bar{1})$ + Ca & C	~10	2.1 ± 0.2	1. $(5 \pm 3) \times 10^{-23}$ 2. $(7 \pm 5) \times 10^{-24}$

Table 8.1 Summary of results for the adsorption of chlorine on the $(000\bar{1})$ and $(10\bar{1}0)$ surfaces.

CHAPTER 9

SUMMARY AND DISCUSSION

This thesis contains the results of studies into the behaviour of H_2S on a clean, (1 x 1) $(000\bar{1})$-O polar surface of ZnO. The investigation was made, in part, as a continuation of previous studies into the effect of a layered material on the adsorption characteristics of various mono-atomic gases. The thesis also contains the results of a brief study into the behaviour of a contaminated $(000\bar{1})$ surface following the adsorption of H_2S and Cl_2. These experiments were performed because of the technical interest in ZnO surfaces which, in application, are presumably grossly contaminated.

During initial cleaning, outward diffusion of calcium from the bulk was exhibited and an indication of its role in charge stabilisation of this surface was given by its resistance to removal by heat treatment alone. However, after successive ion bombardment/anneal cycles a clean, (1 x 1) surface was attained. The adsorption of H_2S resulted in a saturation coverage which, from beam desorption data and work function measurements, comprised both molecular and dissociated species. The results suggested, as with previous studies, that adsorption was dependent on dissociation of the incident molecules. Further deposition, to multimonolayer coverages, was achieved by beam dissociation of the gas at the crystal surface. The formation of a (2 x 2) superstructure was attributed to the presence of sulphur, the removal of which coincided with a return to a (1 x 1) pattern. A possible arrangement ad-ions which would give rise to a (2 x 2) LEED pattern leaves the surface with a $\frac{1}{4}$ monolayer of unsaturated surface oxygen bonds. Although there was no direct evidence that these were taken up by "free" hydrogen ions (which would fulfil the charge requirements of this surface) a decrease in work function,

following exposure to H_2S, was attributed to the adsorption of hydrogen (together with a weakly bound molecular state).

A de-activation of the surface, by the presence of calcium-carbon impurities, was reflected in the adsorption characteristics of both hydrogen sulphide and chlorine. Not only were adsorbate levels reduced, compared with those found for the clean surface, but there was evidence that the adsorbate-substrate interaction was much weaker. In an applied context, these results give an indication of one of the difficulties in extrapolation of results of work on clean substrates performed in conditions of u.h.v. to industrial situations. The use of ZnO in the manufacture of gas detector "heads" is a particular example where such work could perhaps provide information on their probable performance. To this end, a more comprehensive and quantitative study of contaminated surfaces is probably required.

The inability to detect hydrogen and the unsatisfactory work function measurements have made quantitative interpretation of the results presented in this thesis difficult. It is suggested that future work should not only repeat work function measurements but also determine the effect of atomic hydrogen adsorption on work function and on H_2S adsorption. A useful modification to the present study would be to convert the present A.E.S. detection system to the technique of Disappearance Potential Spectroscopy (D.A.P.S.) which can be used to detect hydrogen directly (see for example Kirshner and Staib, 1973).

APPENDIX I

ELEMENT	AUGER TRANSITION	ENERGY (eV)
OXYGEN	KL_1L_1	475
	KL_1L_2	493
	KL_2L_2	512
ZINC	$M_{2\,3}M_4M_4$	57
	$M_{2\,3}M_4M_{4\,5}$	82
	$M_1M_{4\,5}M_{4\,5}$	107
	$M_1M_{4\,5}M_{4\,5}$	118
	$L_3M_{2\,3}M_{2\,3}$	833
	$L_3M_{2\,3}M_{4\,5}$	904
	$L_3M_{4\,5}M_{2\,3}$	913
	$L_2M_{2\,3}M_{4\,5}$	928
	$L_3M_{4\,5}M_{4\,5}$	991
	$L_2M_{4\,5}M_{4\,5}$	1014
SULPHUR	$L_{2\,3}M_1M_{2\,3}$	135
	$L_2M_{2\,3}M_{2\,3}$	150
CHLORINE	$L_2M_{2\,3}M_{2\,3}$	182
CARBON	$KL_{2\,3}L_{2\,3}$	272
CALCIUM	$L_3M_{2\,3}M_{2\,3}$	291
POTASSIUM	$L_3M_{2\,3}M_{2\,3}$	250

REFERENCES

Anderson P.A., 1935, Phys. Rev. 47, 958.

Auger P., 1925, J. Phys. Radium 6, 205.

Bloom S. and Ortenburger I., 1973, Phys. Stat. Solidi (b) 58, 561.

Campbell B.D., Haque C.A. and Farnsworth H.E., 1969, The Structure and Chemistry of Solid Surfaces Ed. G.A. Somorjai (Wiley).

Chang C.C., 1971, Surface Sci. 25, 53.

Chang S.C. and Mark P., 1974, Surface Sci. 46, 293.

Chung M.F. and Farnsworth H.E., 1970, Surface Sci. 22, 93.

Dushman S. and Lafferty J.M., 1962, Scientific Foundations of Vacuum Technology (Wiley).

Ehrenberg W., 1934, Phil. Mag. 18, 878.

Fiermans L., Arijs E., Vennik J. and Maenhout-van der Vorst W., 1971, Phys. Stat. Sol. (a) 6, K59.

1973, Surface Sci. 39, 357.

Fowler R.H., 1933, Proc. Roy. Soc. A 141, 56.

Gatos H.C. and Lavine M.C., 1960, J. Electrochem. Soc. 107, 427.

Goodwin E.T., 1939, Proc. Camb. Phil. Soc. 35, 232.

Harris L.A., 1968, J. Appl. Phys. 39, 1419.

Heiland G., 1974, Society of Photographic Scientists and Engineers (Second Int. Conf. on Electrophotography).

Heiland G. and Kunstmann P., 1969, Surface Sci. 13, 72.

Heiland G., Kunstmann P. and Pfister H., 1963, Z. Physik 176, 485.

Heiland G., Mollowo E. and Stockmann F., 1959, Solid State Phys. 8, 191.

Hirsch P.B., Howie A., Nicholson R.B., Pashley D.W. and Whelan M.J., 1965, Electron Microscopy of Thin Crystals (Butterworths).

Hopkins B.J., 1968, Contemp. Phys. 9, 115.

Hopkins B.J., Leysen R. and Taylor P.A., 1975, Surface Sci. 48, 486.

Hopkins B.J. and Taylor P.A., 1976, J. Phys. C. 9, 571.

van Hove H. and Leysen R., 1972, Phys. Stat. Sol. (a) 9, 361.

Jones A.R., 1976, Ph.D. Thesis, University of Southampton

Kohl D., Henzler M. and Heiland G., 1974, Surface Sci. 41, 403.

Kirschner J. and Staib P., 1973, Phys. Letts 42A, No. 5, 335.

Lander J.J., Morrison J. and Unterwald F., 1962, Rev. Sci. Instrum. 33, 782.

Laudise R.A., Kolb E.D. and Caporaso A.J., 1964, J. Am. Ceram. Soc. 47, 9.

Levine J.D. and Mark P., 1966, Phys. Rev. 144, 751.

Levine J.D., Willis A., Bottoms W.R. and Mark P., 1972, Surface Sci. 29, 144.

Leysen R., Hopkins B.J. and Taylor P.A., 1975, J. Phys. C. 8, 907.

Luth H., 1973, Surface Sci. 37, 90.

Luth H. and Heiland G., 1972, Phys. Stat. Sol. (a) 14, 573.

Madey T.E. and Yates Jr., J.T., 1971, J. Vac. Sci. Tech. 8, 40.

Magoninski Y. and Kalman Z.H., 1974, Phys. Lett. 47A, 201.

Magoninski Y. and Kirby R.E., 1975, J. Phys. C. 8, 1516.

Mariano A.N. and Hanneman R.E., 1963, J. Appl. Phys. 34, 384.

Maue A.W., 1935, Z. Physik 94m 717.

Mimeault V.J. and Hansen R.S., 1966, J. Chem. Phys. 45, 2240.

Muller K., 1969, The Structure and Chemistry of Solid Surfaces Ed. G.A. Somorjai (Wiley).

Nathan R. and Hopkins B.J., 1973, J. Phys. E; Sci. Instrum. 6, 1040.

Nathan R. and Hopkins B.J., 1974, J. Phys. E; Sci. Instrum. 7, 851.

Nosker R.W., Mark P. and Levine J.D., 1970, Surface Sci. 19, 291.

Page P.J., 1973, Ph.D. Thesis, University of Southampton.

Palmberg P.W. and Rhodin T.N., 1968, J. Appl. Phys. 39, 2425.

Pendry J.B., 1974, Low Energy Electron Diffraction (Academic Press).

Peria W., 1969, Phys. Rev. Letts. 22, 705.

Powell R.A., Spicer W.E. and McMenamin C.J., 1972, Phys. Rev. B6, 3056.

Redhead P.A., Hobson J.P. and Komelsen E.V., 1968, The Physical Basis of Ultra High Vacuum (Chapman and Hall).

Rijanow S., 1934, Z. Physik 89, 806.

Rivière J.C., 1968, AERA Rept. No. M2110.

Rossler U., 1969, Phys. Rev. 184, 733.

Seitz F., 1940, Theory of Modern Solids (McGraw-Hill).

Shaw M.L., 1966, Rev. Sci. Instrum. 37, 113.

Shockley W., 1939, Phys. Rev. 56, 317.

Sickafus E.N., 1974, J. Vac. Sci. Tech. 11, 299.

Stecklemacher W., 1973, J. Phys E; Sci. Instrum. 6, 1040.

Summers R.L., 1969, NASA Report TND, 5285.

Swank R.K., 1967, Phys. Rev. 153, 844.

Tamm J.E., 1932, Z. Physik 76, 849.

Taylor N.J., 1969, Rev. Sci. Instrum. 40, 792.

Taylor P.A., 1976, Ph.D. Thesis, University of Southampton.

Taylor P.A., Leysen R. and Hopkins B.J., 1975, Solid State Comm. 17, 983.

Wanneberg B., Gelius U. and Siegbahn K., 1974, J. Phys. E; Sci. Instrum. 7, 149.

Watts G.D., 1974, Ph.D. Thesis, University of Southampton.

ACKNOWLEDGEMENTS

I would like to express my sincere thanks to Dr. B.J. Hopkins for his kind support and supervision during this work.

I also wish to express my thanks to:

The members of the Surface Physics Group at Southampton, for their interest and help, particularly Dr. P.A. Taylor for his invaluable assistance.

Professors K.J. Barnes, G.W. Hutchinson and E.W. Lee, for the provision of research facilities.

J.S. Sieger Ltd., Poole, Dorset for provision of a maintenance grant.

Finally, Mrs. J. Jones for typing this thesis so competently.